TECHNICAL REPORT **Report No.: ESSO-INCOIS-MDG-TR-03(2018)**

LETKF-ROMS: An improved predictability system for the Indian Ocean.

by

Balaji B., Deep Sankar Banerjee, Biswamoy Paul, S. Sivareddy & Arya Paul.

Indian National Centre for Ocean Information Services (INCOIS)
Earth System Science Organization (ESSO)
Ministry of Earth Sciences (MoES)
HYDERABAD, INDIA
www.incois.gov.in

24 JULY, 2018

DOCUMENT CONTROL SHEET

Earth System Science Organization (ESSO)
Ministry of Earth Sciences (MoES)
Indian National Centre for Ocean Information Services (INCOIS)

ESSO Document Number: ESSO-INCOIS-MDG-TR-03(2018)

Title of the report: LETKF-ROMS: An improved predictability system for the Indian Ocean.

Author(s) [Last name, First name]:

Balaji B., Deep Sankar Banerjee, Biswamoy Paul, S. Sivareddy & Arya Paul

Originating unit : Ocean Modeling and Data Assimilation Group (MDG), INCOIS.

Type of Document: Technical Report (TR)

Number of pages and figures: 92, 129

Number of references: 27

Keywords: Data Assimilation, Local Ensemble Transform Kalman Filter, Regional Ocean Modeling System, Indian Ocean.

Security classification: Open

Distribution: Open

Date of publication: 24 July, 2018

Abstract (100 words)

We have developed the assimilation scheme Local Ensemble Transform Kalman Filter (LETKF) and interfaced with the present basin-wide operational ROMS set-up (1/12 degree horizontal resolution) that assimilates in-situ temperature and salinity from RAMA moorings, NIOT buoys and Argo floats. The system also assimilate satellite track data of sea-surface temperature from AMSR-E. The speciality of this assimilation system is that it comprises of ensembles that are initialized with different model coefficients like diffusion parameters and the ensemble members also respond to two different mixing schemes - K profile parameterization and Mellor-Yamada. This aids in maintaining the spread of the ensemble intact - which has always been a challenging task. We have also employed a localization radius of ~200 km, i.e., observations influence the prognostic state variables that fall within this range. The assimilation system is also bestowed with better representative error estimates - a method developed in-house along the likes of *Etherton et al.* The ensemble members were forced with ensemble atmospheric fluxes provided by

National Centre for Medium Range Weather Forecast (NCMRWF). Assimilation was performed every five day.

We show that the assimilated system simulates the ocean state better than the present operational basin-wide ROMS. We validate it extensively against multiple observations ranging from RAMA moorings to ADCP observations across both dependent variables like temperature and salinity and independent variables like sea-level anomaly and currents. We show that assimilation improves the overall ocean state except at few isolated locations. It improves the correlation with respect to observations and reduces the root-mean-squared error. We also show that assimilation improves the estimation of mixed layer depth and 20 degree isotherm (which are diagnostic variables) thereby proving that the subsurface conditions are better simulated.

Acknowledgements

The Data Assimilation (DA) team wishes to acknowledge Prof. Eugenia Kalnay and Dr. Steve Penny from University of Maryland, USA for hosting S. Sivareddy and Arya Paul for six months. The present LETKF-ROMS is built on the foundation of LETKF-MOM which Steve had developed for MOM. We are grateful to them for sharing the code of LETKF-MOM and introducing us to rocoto which is an excellent tool for firing parallel jobs. S. Sivareddy and Arya Paul also wishes to thank Ministry of Earth Sciences (MOES) for funding the visit.

The DA team also wishes to thank Dr. Francis Pavanathara, Dr. Kunal Chakraborty, Dr. Abhisek Chatterjee and Dr. Arnab Mookherjee for numerous help ranging from trouble-shooting ROMS to providing boundary conditions. This project was initiated under Dr. Balakrishnan Nair and the team is happy to acknowledge his trust on us. We also thank the OSF team, INCOIS for providing us the ocean state analysis from the present operational ROMS against which LETKF-ROMS is compared with. The team also extend its gratitude to the DMG, INCOIS for providing us with observations without which this program would have been redundant. We also acknowledge the support received from the CWG, INCOIS and the support staff from IITM overseeing the upkeep and maintenance of the high performance computer Aditya and a special thanks to Dr. V.S.Prasad and Dr. Johny C. J from NCMRWF for providing us the atmospheric fluxes. At the end, the team thank our Director, Dr. S.S.C. Shenoi for continuing to have faith in us and extending support in all possible means. Without him, this project would not have seen the light of the day.

Abstract

We have developed the assimilation scheme Local Ensemble Transform Kalman Filter (LETKF) and interfaced with the present basin-wide operational ROMS set-up ($1/12^{\circ}$horizontal resolution) that assimilates in-situ temperature and salinity from RAMA moorings, NIOT buoys and Argo floats. The system also assimilate satellite track data of sea-surface temperature from AMSRE. The speciality of this assimilation system is that it comprises of ensembles that are initialized with different model coefficients like diffusion parameters and the ensemble members also respond to two different mixing schemes - K profile parameterization and Mellor-Yamada. This aids in maintaining the spread of the ensemble intact - which has always been a challenging task. We have also employed a localization radius of 200 km, i.e., observations influence the prognostic state variables that fall within this range. The assimilation system is also bestowed with better representative error estimates - a method developed in-house along the likes of *Etherton et al* [8]. The ensemble members were forced with ensemble atmospheric fluxes provided by National Centre for Medium Range Weather Forecast (NCMRWF). Assimilation was performed every five day.

We show that the assimilated system simulates the ocean state better than the present operational basin-wide ROMS. We validate it extensively against multiple observations ranging from RAMA moorings to ADCP observations across both dependent variables like temperature and salinity and independent variables like sea-level anomaly and currents. We show that assimilation improves the overall ocean state except at few isolated locations. It improves the correlation with respect to observations and reduces the root-mean-squared error. We also show that assimilation improves the estimation of mixed layer depth and 20° isotherm (which are diagnostic variables) thereby proving that the subsurface conditions are better simulated.

Contents

Acknowledgements **iii**

Abstract **iv**

1 The System **3**
1.1 Introduction 3
1.2 Model 4
1.3 Observation 6
1.4 Data Assimilation - LETKF 8

2 Sea Surface Temperature **11**
2.1 Introduction 11
2.2 Comparison with AVHRR 11
2.3 Comparison with RAMA moorings 14
2.4 Comparison with NIOT Buoys 17
2.5 Conclusion 18

3 Temperature **20**
3.1 Introduction 20
3.2 Comparison with RAMA moorings 20
3.3 Comparison with NIOT Buoys 27
3.4 Comparison with Argo floats 30
3.5 Conclusion 34

4 Salinity **36**
4.1 Introduction 36
4.2 Comparison with RAMA moorings 36
4.3 Comparison with NIOT Buoys 43
4.4 Comparison with Argo floats 45
4.5 Conclusion 49

5 Mixed Layer Depth and 20 Degree Isotherm **51**
5.1 Introduction 51
5.2 Comparison with RAMA moorings 51
5.3 Conclusion 56

6 Sea Level Anomaly **58**
6.1 Introduction 58
6.2 Comparison with AVISO 58
6.3 Conclusion 60

7 Currents **62**
7.1 Introduction 62
7.2 Comparison with OSCAR 62
7.2.1 u current 62
7.2.2 v current 66
7.3 Comparison with ADCP 68
7.3.1 Deep Ocean 68
7.3.2 Shallow Ocean 77
7.4 Conclusion 79

8 Discussion & Summary **81**

References **86**

1 The System

1.1 Introduction

Improving forecast of ocean state in the Indian Ocean has been a priority for Indian National Centre for Ocean Information Services (INCOIS) from the day of its inception. This is necessary because a good proportion of the population, roughly about a quarter, resides along the Indian coastline and quite a few of them venture out into the sea for fishing and other activities. Any error in ocean state forecast is likely to adversely affect them. The errors in the model forecasts tend to grow with forward propagation of model due to various reasons like empirically derived parameterizations, inaccurate fluxes and boundary conditions, inaccurate initial conditions, inherent inability to resolve finer scales of motion due to grid resolution and partial knowledge of state parameters. These errors tend to diverge the model state from reality thereby rendering the forecasts far from being in sync with reality. There are multiple ways in which the forecast may be improved. One of the approach is to implement a high resolution general circulation model that can resolve finer length scales and hence simulate processes that were coarse-grained in low resolution models. Under the project High-resolution Operational Ocean Forecast and reanalysis System (HOOFS), these high-resolution ocean model setups provide operational forecast of various oceanographic parameters for the coastal waters around the country. Regional Ocean Modeling System (ROMS), which is a state-of-the art ocean circulation model [1–4] is used as the general circulation model for the HOOFS setups [5]. However it is still some distance away from reality. One of the leading reason is the uncertainty in the initial condition. Periodically corrected initial condition will likely restrain the model trajectory from diverging from the truth. The most prominent way to periodically adjust the initial condition is through the technique of data assimilation (DA). DA is a method that imbibes informations from both the model state and observation, statistically churns them to reduce the cost function (errors) and spits out an initial condition (commonly known as analysis) that is closer to the truth than either the input prior model state or the input observation both in terms of uncertainty and root-mean-squared error. Since the knowledge of truth is elusive, analyses are validated against observations that were not assimilated, i.e., independent observations.

Keeping all these requirements in mind, an advanced data assimilation system has been developed in-house using Local Ensemble Transform Kalman Filter (LETKF) algorithm [6]. LETKF is

interfaced (offline) with the ROMS model for Indian Ocean region to improve the accuracy of the model forecast. Results from the LETKF framework for the ROMS is presented in this work. It is to be acknowledged that the LETKF routine was developed originally by Penny et. al [7] for Modular Ocean Model (MOM). ROMS has a different coordinate system than MOM and we had to modify most of the code to suit for ROMS, keeping the template unaltered. The in-situ temperature and salinity profiles and satellite observed sea surface temperature (SST) are assimilated with a provision to assimilate sea-level anomaly (SLA) and sea surface salinity (SSS). The improvements in state estimation of prognostic variables and some diagnostic variables using the assimilation over an assimilation-free model estimate (henceforth called FREE ROMS) and over the present first day forecast of the operational model estimate (henceforth called O-ROMS) are presented here. Representation error (RE), which occurs due to the deficiency of the model to accurately project its state on to the observation space, is estimated using an high resolution model simulation based on algorithm described in [8]. RE is included as a component of observation error along with the instrument error to represent the uncertainty of observations. It is to be noted that observations are not error-free and hence does not represent the truth. The performance of our assimilation system improves once we include RE into the observation error statistics.

In section 2, we describe the model set-up followed by a description of the observation that went into the assimilation system in section 3. Finally at the end of this chapter, we briefly describe the data assimilation scheme in section 4.

1.2 Model

The model used for the Indian Ocean is the Regional Ocean Modeling System (ROMS, version 3.7), developed by Rutgers University, New Jersey, USA. ROMS is a free surface, terrain following general circulation model which solves a set of primitive equations in an orthogonal curvilinear coordinate system [1–4]. The domain and bathymetry in the model domain for the IO-HOOFS setup is shown in Fig.1.1. The domain extends from 30°E to 120°E in the east-west direction and from 30°S to 30°N in the north-south direction. The horizontal resolution of IO-HOOFS, henceforth termed as O-ROMS, is 1/12 °(approximately 9 km) and it has 40 sigma levels in the vertical. A detailed description of IO-HOOFS setup is provided in [5]. The vertical stretching parameters are chosen such that the vertical scales are finely resolved in the upper part of the ocean. This is important because the baroclinic effects are most prominent in the upper layers of the ocean and should be judiciously resolved. The lateral boundary in the east is connected to the Pacific Ocean through the Indonesian throughflow while the southern boundary is interfaced with the Southern Ocean. On the other hand, the northern and western boundaries are guarded by coastlines and no-slip conditions are employed. The model exchanges information

with the boundary every 5 days. The tracer and momentum fields are nudged to 10-day delayed ocean reanalysis derived from the INCOIS-GODAS analysis [10]. It is to be noted that fast moving barotropic waves that originates outside the stated IO domain will not be captured at the boundaries and remote effects due to these modes will be ignored leading to escalation in errors in ocean state estimate. This may be significant at times - particularly during the boreal winter when Madden-Julian Oscillation is known to generate strong wind stress anomalies (and hence large barotropic fluctuations) close to the north-west coast of Australia. The model uses, unless otherwise mentioned, the K-profile Parameterization (KPP) mixing scheme [11] to parameterize the vertical mixing. Smagorinsky type bi-harmonic diffusion and viscosity schemes [12] are chosen for horizontal mixing and a bulk parameterization scheme [13, 14] is chosen for the computation of air-sea fluxes of heat. Atmospheric fields from high resolution (N768L70) global NCMRWF unified model (NCUM), obtained from NCMRWF (http://www.ncmrwf.gov.in/t254-model/t254_des.pdf), are used for forcing O-ROMS. On the other hand, an ensemble of 80 fluxes obtained from GFS model (used in NCMRWF) was used to force the model in LETKF-ROMS. In addition, the model is incorporated with the tidal forcing from TPX07.2 model in the southern and western open boundaries. The model however does not account for river runoff. Instead, the model states are relaxed to monthly climatology of sea-surface salinity [15, 16]. The chief characteristics of the model configuration of O-ROMS and LETKF-ROMS is enumerated in the table below:

Model	**Resolution**	**Atm Flux**	**Initial Condition**	**Bound Condition**	**Model Parameters**
O-ROMS	9 km horizontal; 40 vertical σ levels	HIgh resolution NCUM flux (6-hourly).	N.A	INCOIS-GODAS.	Diff. Const=50 m^2s^{-1} Visc Const=300 m^2s^{-1}
LETKF-ROMS	9 km horizontal; 40 vertical σ levels	80-member NCMRWF ensemble flux from ensemble GFS model (6-hourly).	Perturbed O-ROMS initial condition to produce 80 ensembles.	INCOIS-GODAS.	Same as O-ROMS except a spread in diffusion & viscosity constant and mixing scheme across ensembles.

1.3 Observation

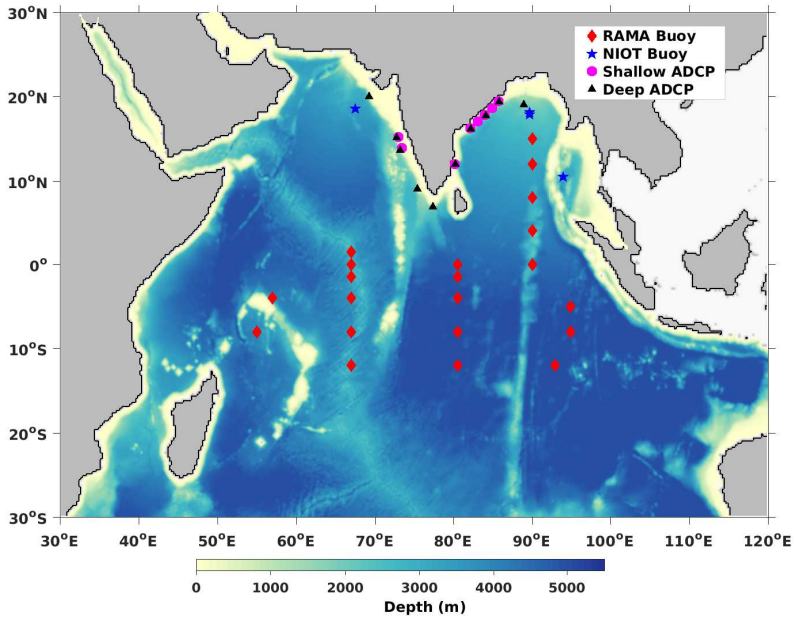

Figure 1.1: Picture of the Indian Ocean domain along with the bathymetry. The location of in-situ RAMA moorings, NIOT buoys and ADCPs are also pointed out.

We assimilate in-situ temperature and salinity profiles from observation networks that include Argo and moored buoys within the Indian Ocean domain. We however discard assimilating observations that are too close to the domain boundaries or too close to any landmass. We also assimilate satellite track data of sea-surface temperature (SST) obtained from Advance Microwave Scanning Radiometer for EOS (AMSR-E). However, since the data along the track is very dense, we coarse-grain the data over a length-scale of 50 km before feeding it into the assimilation system. This "super-obbing" is routinely done in many assimilation systems [17]. This avoids generation of unwanted subgrid scale processes and also consumes less memory during the assimilation process. Even though our system (LETKF) is capable of assimilating sea-surface salinity (SSS) and sea-level anomaly (SLA), we did not assimilate these observations since SSS is not available during the period of our interest and assimilating SLA will incur error due to absence of long-term ensemble fluxes that would have enabled us in estimating the geoid from the model. SLA assimilation is planned to be inducted into the system in near future.
In Fig 1.1, we show the location of fixed in-situ instruments that record temperature, salinity and currents. In Fig 1.2 and Fig 1.3, the availability of temperature and salinity data from Research Moored Array for African-Asian-Australian Monsoon Analysis and Prediction (RAMA) and NIOT buoys are shown during the period of interest i.e., August 2016 - August 2017. In Fig. 1.5, the

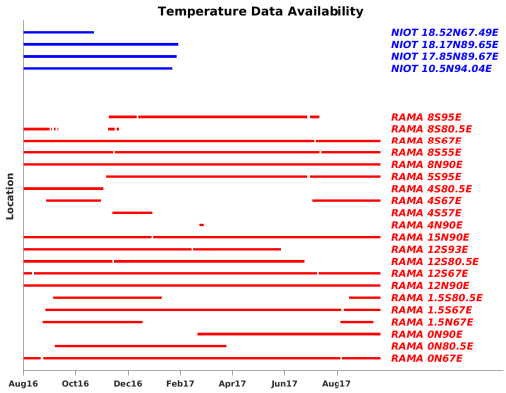

FIGURE 1.2: Availability of temperature data from RAMA moorings (red) and NIOT buoys (blue) in the Indian Ocean during August 2016 - September 2017.

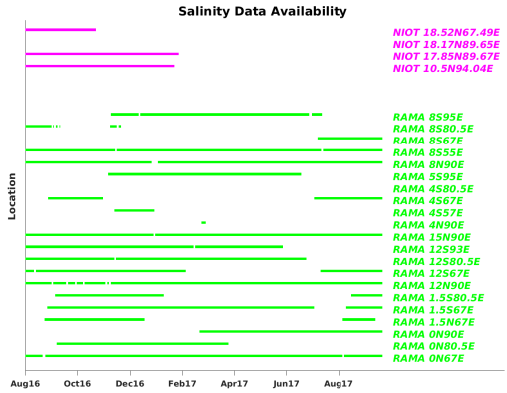

FIGURE 1.3: Availability of salinity data from RAMA moorings (green) and NIOT buoys (pink) in the Indian Ocean during August 2016 - September 2017.

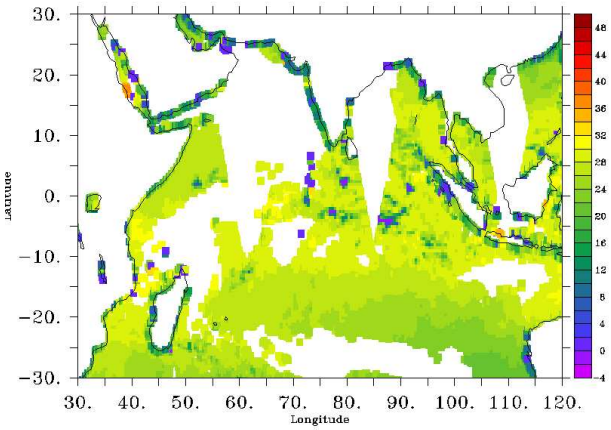

FIGURE 1.4: Sample satellite track (after superobbing) capturing SST over Indian Ocean.

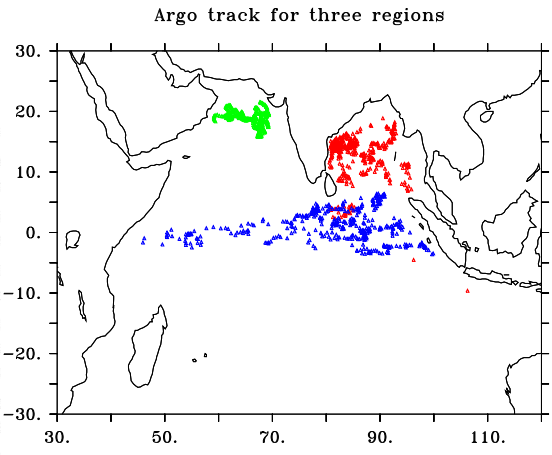

FIGURE 1.5: Daily pop-up of Argo floats in the Indian Ocean - primarily in the Northern Indian Ocean - is plotted which were used for validation. Daily pop-up were segregated according to the location of their pop-ups - green in Arabian Sea, red in Bay of Bengal and blue in Equatorial Indian Ocean.

location of daily pop-up of Argo floats is plotted in the Arabian Sea, Bay of Bengal and Indian Ocean which were used later for validating the results. In Fig.1.4, we show a typical SST L2 level track data (after being coarse-grained) that enters into the assimilation system. In Fig.1.6, we plot the time series of normalized number of observations of temperature, salinity and SST that is assimilated each day. The normalization is done with respect to the maximum of observation that has been assimilated on any particular day during the period of our study. Typically around 10^4 observations were assimilated at each assimilation cycle.

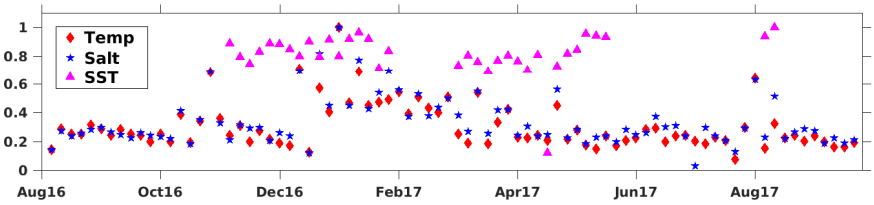

Figure 1.6: Normalized number of observations of temperature (red), salinity (blue) and SST (pink) that were assimilated each day. The maximum number of SST observatios were 10771 whereas for temperature and salinity, the maximum numbers were 4564 and 4822 respectively.

1.4 Data Assimilation - LETKF

We employ Local Ensemble Transform Kalman Filter [6] as the data assimilation technique. LETKF has its origin to the Local Ensemble Kalman Filter (LEKF) [18] and the Ensemble Transform Kalman Filter (ETKF) [19] and is an insightful amalgamation of these two techniques. The major advantage of LETKF is that it can produce analysis that is qualitatively similar to LEKF whereas the efficiency is as good as ETKF thereby exploiting the virtues of both the systems. Nevertheless, it is a variant of Ensemble Kalman Filter wherein the model error covariance is approximated as a sample covariance derived from the ensemble members and whose rank is roughly equal to the number of ensemble members (k) used in the study when the ensemble size is large. For infinite number of ensemble members, this reduces exactly to model error covariance. We have used 80 ensemble members and hence the rank of the model error covariance matrix is 79. The inaccuracy introduced due to this approximation is traded off with the sharp decrease in computational resources and runtime. We prepare the initial ensemble from an ocean state derived from the present operational ROMS. The ocean state is perturbed with a Gaussian random number whose mean is zero and standard deviation derived from a set of 56 ensemble members of ocean states obtained through an ensemble run of ROMS forced with NCEP ensemble fluxes. The ensemble spread from the 56-ensemble run was along the growing modes of the model and

hence was desirable. We employed the same spread into the present ensembles with a hope that the ensembles, so generated, will not collapse in time. We also divide the ensembles into two equal halves - one half uses KPP mixing scheme [11] while the other uses Mellor-Yamada mixing scheme [20]. This is done to ensure that the advantages of both the mixing schemes can be exploited. We also arbitrarily spread the value of coefficients like tracer diffusion constant and horizontal viscosity coefficients about the value used in O-ROMS across the ensembles. This division in mixing schemes and using a range of coefficients aids further in keeping the ensemble spread intact [21, 22]. To further safeguard ensemble collapse, we inflate the ensembles after each analysis by 10%. We keep the localization radius at 200 km i.e., observations can influence the model prognostic variables that falls within a radius of roughly 200 km from the observation location. This is important to ward off spurious correlations that might arise due to observations influencing model state at large distances. The multi-variate covariance error matrix allows the observation of any particular sort to influence all the prognostic variables unless specifically designed to restrict the influence. In Fig.1.7, we show a plot of innovation in SST, i.e., the difference of analysis and background ocean state in SST, from our LETKF-ROMS system in an arbitrary day that illustrates the effect of localization.

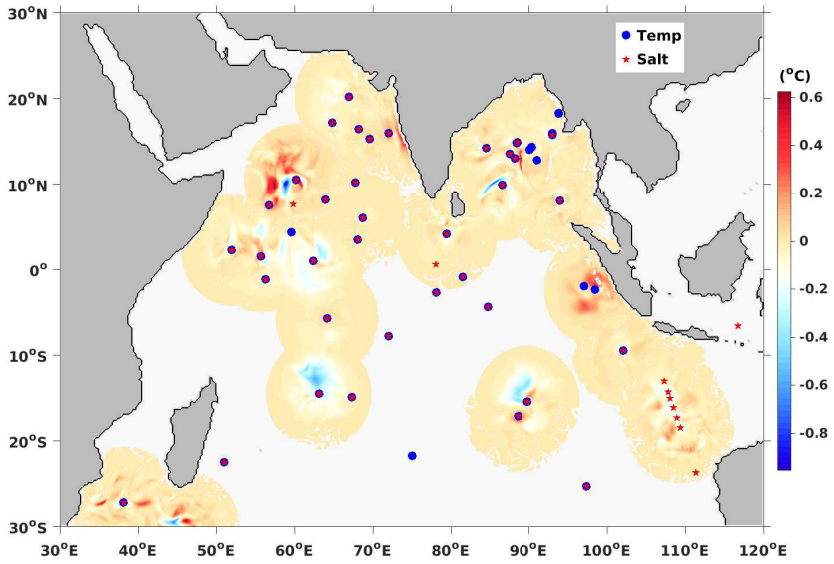

Figure 1.7: **Effect of localization**. Innovation in SST on a typical day. The blue and red star shows the location of observations of temperature and salinity respectively that went into the assimilation system on that particular day. The plot shows that the observations influence only a region around it.

In many assimilation systems [7], a constant representation error (RE) is supplied to the observation error covariance. We however estimate RE following the method suggested by [8] wherein

a high dimensional model is used to estimate the errors due to unresolved scales and processes thereby introducing spatio-temporal variations in RE. The estimated RE is then added to the instrumental error to get the observation error, the square of which are the diagonal elements of the observation error covariance matrix. The off-diagonal elements are assumed to be zero, i.e., the observations do not influence each other. This is a reasonable approximation, particularly for in-situ observations. However, it is to be noted that this approximation is questionable for satellite observations. In spite of this, we include this approximation for SST due to lack of definite method in estimating the off-diagonal elements and also to exploit the diagonal nature of the matrix.

We assimilate observations every 5 days - which is similar to the assimilation frequency of many operational systems [9]. The model runs unhindered for 5 days and is assimilated on the fifth day. The advantage is that assimilation does not affect the ocean state frequently and allows the ocean to respond to the fluxes unhindered. Unlike many other assimilation systems [10], we do not accumulate all the observations over the time-window of 5 days and pass it on to be assimilated on the 5^{th} day. Instead, whatever observations are available on the 5^{th} day is fed into the assimilation systm and the observations pertaining to the previous four days are ignored. Ignoring the observations for four days amounts to loss of information. But the advantage is that past observations do not influence the present state - particularly important for regions which are dynamic. This is a trade-off. The time series of daily output of LETKF-ROMS thus comprises of a sequence of background ocean state of four days followed by an analysis on the fifth day. This modus operandi however might not be best suited while providing forecast because of the small number of available real-time observations.

The performance of LETKF-ROMS is pitted against O-ROMS[5] and INCOIS-GODAS, a gobal ocean data assimilation system[10]. The resolution of INCOIS-GODAS is much coarser compared to O-ROMS or LETKF-ROMS. The horizontal resolution of INCOIS-GODAS is around 25 km in the Equatorial region while the resolution coarsens to about 50 km close to the poles. INCOIS-GODAS is forced with 6-hourly NCMRWF winds. In INCOIS-GODAS, SST is strongly relaxed to Reynolds SST (5 day relaxation period). Monthly climatological river run-off is included in the set-up of INCOIS-GODAS unlike O-ROMS or LETKF-ROMS. Also SSS is not relaxed to any climatology in INCOIS-GODAS unlike O-ROMS and LETKF-ROMS which has a 30 day relaxation to WOA monthly climatology. More details about the configuration of INCOIS-GODAS is present in [10].

In the next few chapters, we will present comparisons of LETKF-ROMS, O-ROMS and INCOIS-GODAS with a variety of observation networks of various state variables like SST, temperature and salinity, mixed layer depth and depth of 20° isotherm, SLA and currents.

2 Sea Surface Temperature

2.1 Introduction

We validate Sea Surface Temperature (SST) with respect to observations from multiple sources - RAMA moorings, NIOT buoys and Advanced Very High Resolution Radiometer (AVHRR) satellite. It is to be noted that ROMS does not relax its SST to any climatological field. This has the advantage that SST obtained during analysis will likely not drift away during forecating when relaxation fields of SST (reanalysis) are unavailable. We will compare the quality of states obtained from LETKF-ROMS with respect to INCOIS-GODAS and O-ROMS. There were no data availability of O-ROMS during the month of May 2016. We emphasize that SST is not an independent variable.

2.2 Comparison with AVHRR

We present here the comparison of the LETKF-ROMS and other unassimilated systems with respect to gridded SST obtained from AVHRR during the period August 2016 - September 2017. AVHRR provides daily SST over a resolution of about 25 km. The model states were projected on to the observation state and compared.

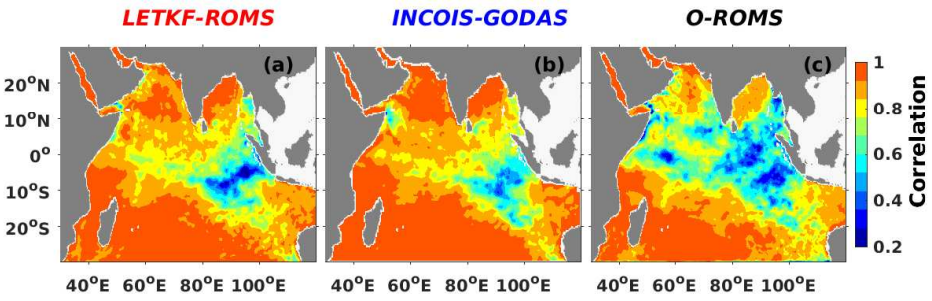

FIGURE 2.1: Spatial plot of correlation with respect to AVHRR for (a) LETKF-ROMS, (b) INCOIS-GODAS and (c) O-ROMS. Assimilation significantly increases the correlation at all places.

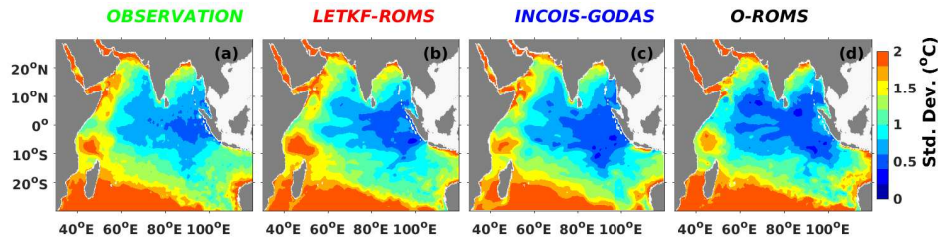

Figure 2.2: Spatial plot of standard deviation for (a) AVHRR, (b) LETKF-ROMS, (c) INCOIS-GODAS and (d) O-ROMS.

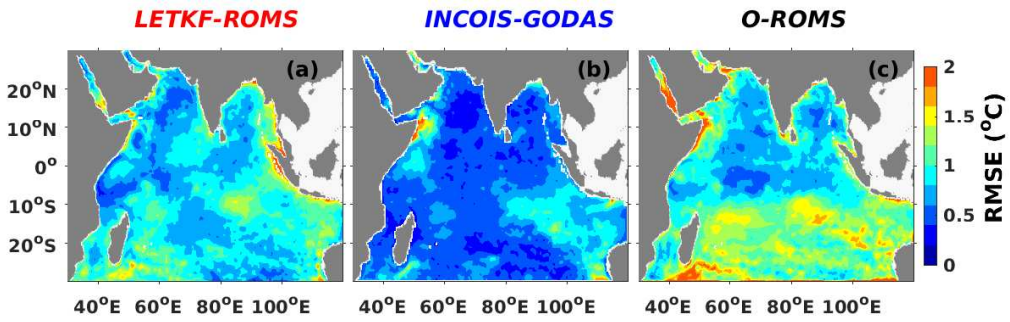

Figure 2.3: Spatial plot of root-mean-squared error (rmse) with respect to AVHRR for (a) LETKF-ROMS, (b) INCOIS-GODAS and (c) O-ROMS. Assimilation significantly brings down the rmse at all places.

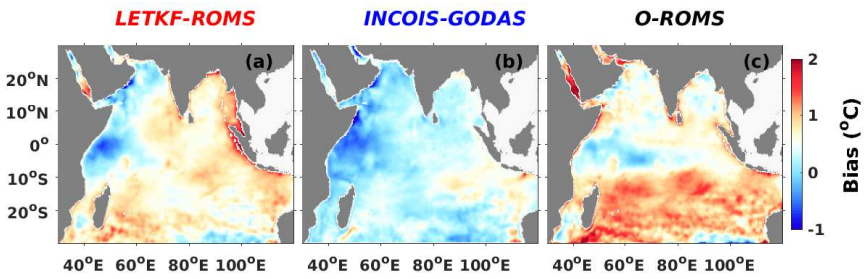

Figure 2.4: Spatial plot of bias with respect to AVHRR for (a) LETKF-ROMS, (b) INCOIS-GODAS and (c) O-ROMS. Assimilation significantly reduces the bias at all places except at the west coast of Kenya and Tanzania and eastern Bay of Bengal.

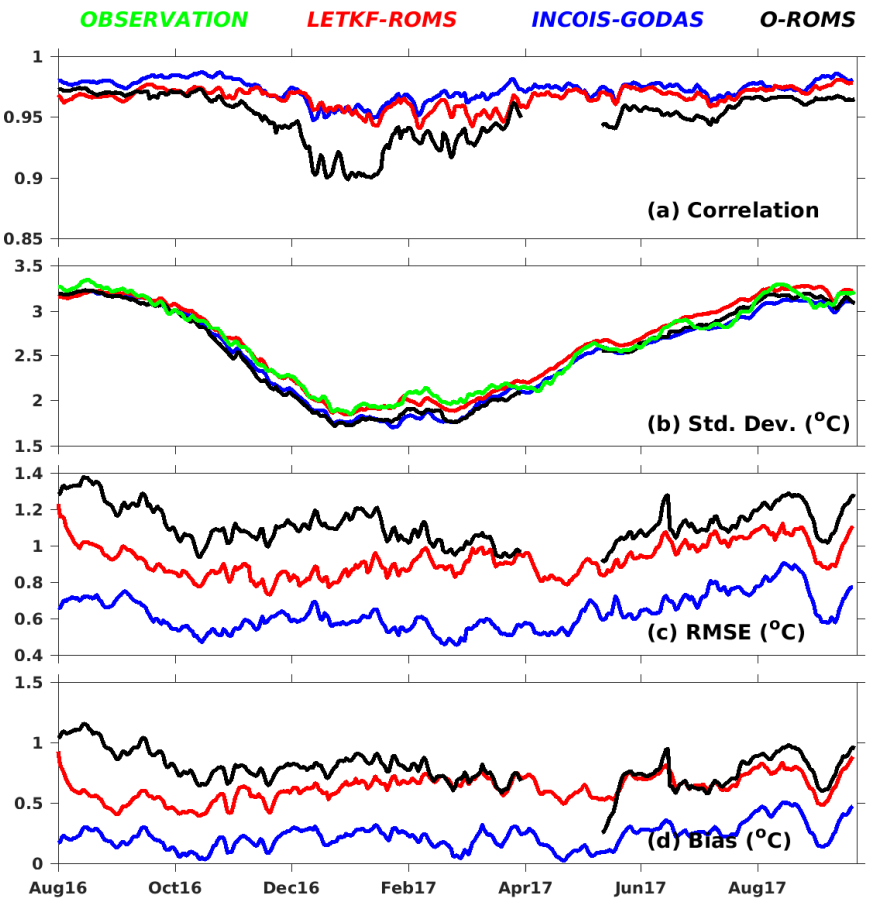

Figure 2.5: Temporal plot of (a) correlation, (b) standard deviation, (c) rmse and (d) bias from LETKF-ROMS (red), INCOIS-GODAS(blue) and O-ROMS (black). Assimilation significantly improves the sea-surface temperature of the Indian Ocean. The standard deviation of observation in (b) is shown in green.

2.3 Comparison with RAMA moorings

We present here the comparison of SST obtained from LETKF-ROMS, INCOIS-GODAS and O-ROMS with observations from RAMA moorings.

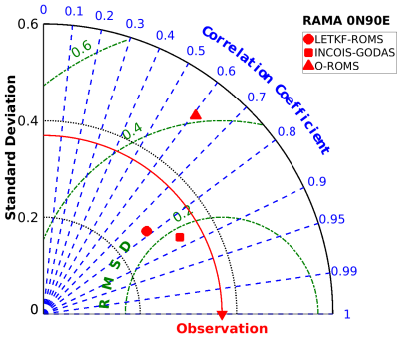

FIGURE 2.6: Taylor Diagram of SST from LETKF-ROMS, INCOIS-GODAS and O-ROMS with respect to RAMA mooring at 0° N & 90° E.

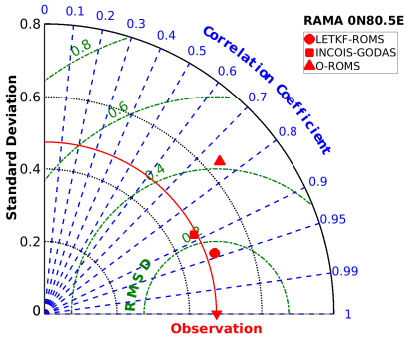

FIGURE 2.7: Taylor Diagram of SST from LETKF-ROMS, INCOIS-GODAS and O-ROMS with respect to RAMA mooring at 0° N & 80.5° E.

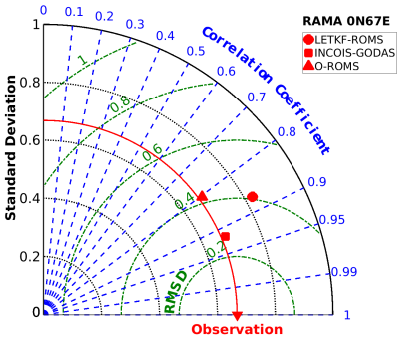

FIGURE 2.8: Taylor Diagram of SST from LETKF-ROMS, INCOIS-GODAS and O-ROMS with respect to RAMA mooring at 0° N & 67° E.

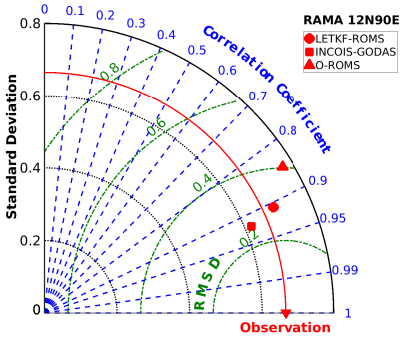

FIGURE 2.9: Taylor Diagram of SST from LETKF-ROMS, INCOIS-GODAS and O-ROMS with respect to RAMA mooring at 12° N & 90° E.

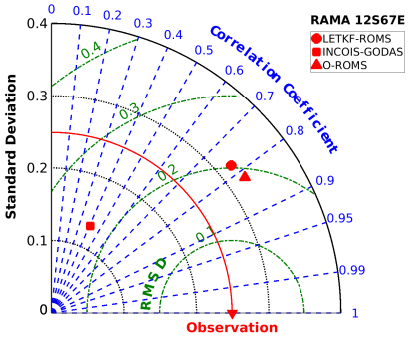

FIGURE 2.10: Taylor Diagram of SST from LETKF-ROMS, INCOIS-GODAS and O-ROMS with respect to RAMA mooring at 12° S & 67° E.

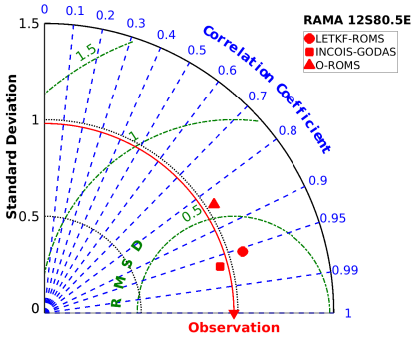

FIGURE 2.11: Taylor Diagram of SST from LETKF-ROMS, INCOIS-GODAS and O-ROMS with respect to RAMA mooring at 12° S & 80.5° E.

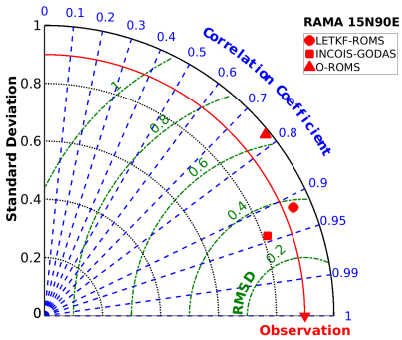

FIGURE 2.12: Taylor Diagram of SST from LETKF-ROMS, INCOIS-GODAS and O-ROMS with respect to RAMA mooring at 15° N & 90° E.

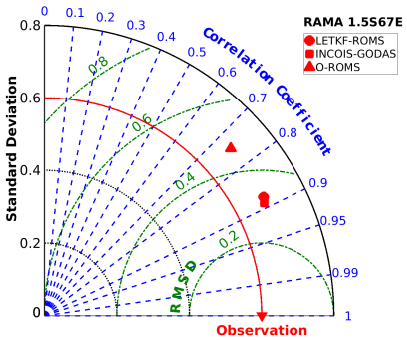

FIGURE 2.13: Taylor Diagram of SST from LETKF-ROMS, INCOIS-GODAS and O-ROMS with respect to RAMA mooring at 1.5° S & 67° E.

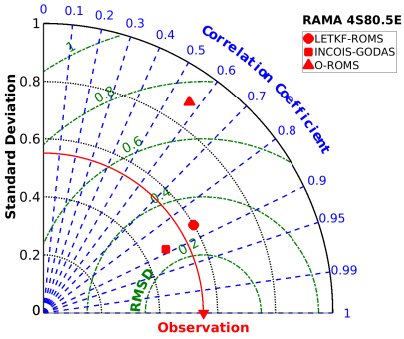

Figure 2.14: Taylor Diagram of SST from LETKF-ROMS, INCOIS-GODAS and O-ROMS with respect to RAMA mooring at 4° S & 80.5° E.

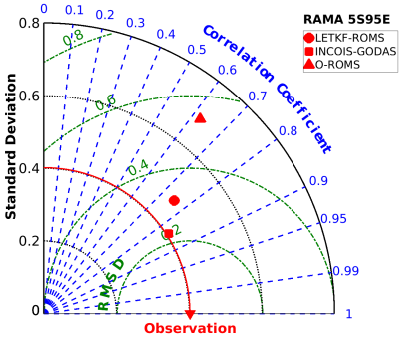

Figure 2.15: Taylor Diagram of SST from LETKF-ROMS, INCOIS-GODAS and O-ROMS with respect to RAMA mooring at 5° S & 95° E.

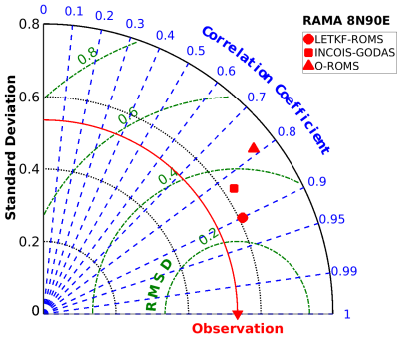

Figure 2.16: Taylor Diagram of SST from LETKF-ROMS, INCOIS-GODAS and O-ROMS with respect to RAMA mooring at 8° N & 90° E.

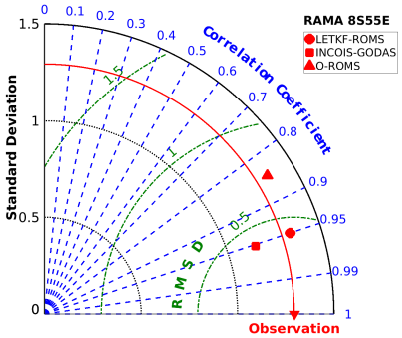

Figure 2.17: Taylor Diagram of SST from LETKF-ROMS, INCOIS-GODAS and O-ROMS with respect to RAMA mooring at 8° S & 55° E.

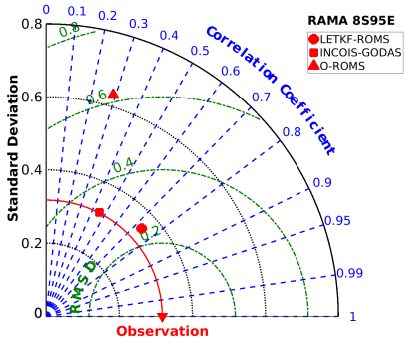

FIGURE 2.18: Taylor diagram of SST from LETKF-ROMS, INCOIS-GODAS and O-ROMS with respect to the RAMA Mooring located at 8° S & 95° E.

2.4 Comparison with NIOT Buoys

The performance of LETKF-ROMS is pitted against buoys deployed and maintained by National Institute of Ocean Technology (NIOT). We call it NIOT buoys for convenience. We plot their Taylor diagrams in Fig.2.19 to Fig.2.22.

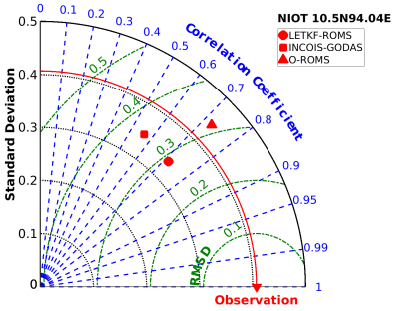

FIGURE 2.19: Taylor diagram of SST for the LETKF-ROMS, INCOIS-GODAS and O-ROMS with respect to NIOT buoy located at 10.5° N and 94.04° E

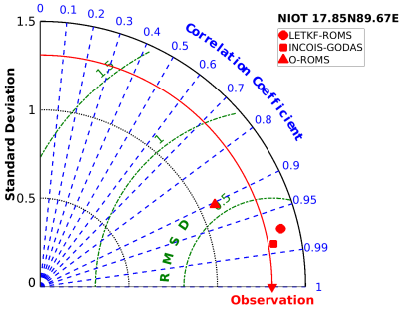

FIGURE 2.20: Taylor Diagram of SST from the LETKF-ROMS, INCOIS-GODAS and O-ROMS with respect to NIOT buoy at 17.85° N & 89.67° E.

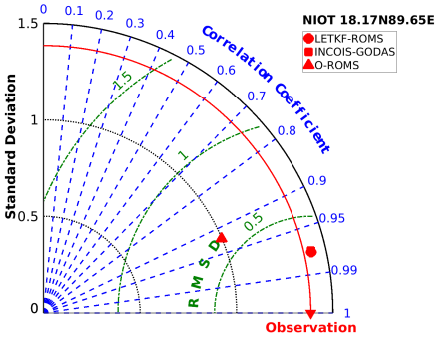

FIGURE 2.21: Taylor diagram of SST for the LETKF-ROMS, INCOIS-GODAS and O-ROMS with respect to NIOT buoy located at 18.17° N and 89.65° E

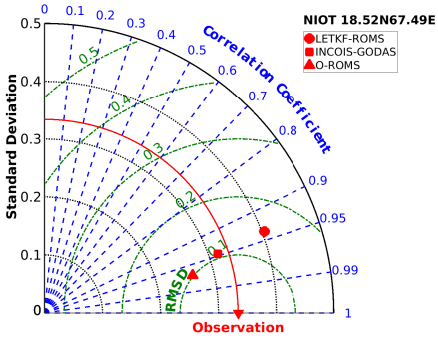

FIGURE 2.22: Taylor Diagram of SST from the LETKF-ROMS, INCOIS-GODAS and O-ROMS with respect to NIOT buoy at 18.52° N & 67.49° E.

2.5 Conclusion

We see that there is a notable improvement in ocean SST due to assimilation introduced through LETKF in ROMS. There has been an overall decrease in global RMSE by 0.2-0.4°(Fig.2.3 & Fig.2.5c), an improved spatial correlation with AVHRR SST (Fig.2.1) and an improved representation of standard deviation throughout the domain (Fig.2.5b) with respect to O-ROMS. In Fig.2.4, we see that the O-ROMS suffer from a large positive bias in the Indian Ocean south of equator. This suggests that the NCUM radiation fluxes possibly suffer from biases. However, LETKF manages to reduce the bias and perform better than O-ROMS in the southern part of Indian Ocean. This may be because of the positive effects of assimilation or because of absence of bias in the ensemble fluxes. But when ROMS is forced with an average of NCMRWF ensemble fluxes, it produces bias not only in the Southern Indian Ocean but also in the Eastern Indian Ocean (Fig.2.23) thereby confirming that the reduction in bias in LETKF-ROMS is a work of assimilation. The large bias seen in equatorial Indian Ocean and Bay of Bengal in FREE-ROMS is considerably reduced in LETKF-ROMS (Fig.2.23). Nevertheless, INCOIS-GODAS performs best in simulating the SST in the Indian Ocean. It has the highest correlation (Fig.2.1) and least rmse (Fig.2.3) with AVHRR SST. However, LETKF-ROMS looks like the best in reproducing the observed standard deviation (Fig.2.2).

We have also compared the performance against 17 in-situ observations. Only those in-situ observations were chosen that has relatively longer availability of data during the period of our interest. When compared against in-situ observations, we find an improvement in the statistics with respect to O-ROMS due to assimilation at all places except at four locations - $(0°N, 67°E), (12°S, 67°E), (1.5°S, 67°E)$ and $(18.52°N, 67.49°E)$. It seems that apparently there is an issue in the vicinity of $67°E$ longitude. The reason needs to be ascertained and fixed.

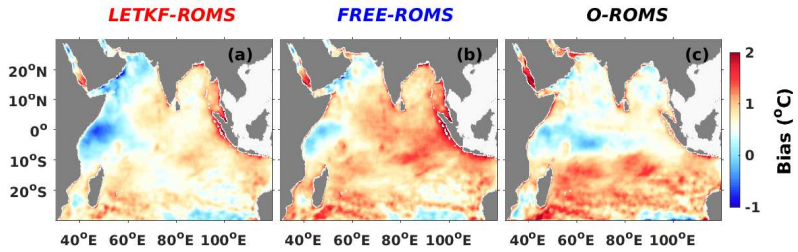

Figure 2.23: Bias in SST in (a) LETKF-ROMS, (b) FREE-ROMS and (c) O-ROMS with respect to AVHRR SST.

Overall, INCOIS-GODAS performs better in reproducing the SST. However, it is to be noted that SST is strongly relaxed in INCOIS-GODAS.

3 Temperature

3.1 Introduction

We validate temperature profiles obtained from LETKF-ROMS with respect to observations from multiple sources - RAMA moorings, NIOT buoys and Argo floats. There were no data availability of O-ROMS during the month of May 2016.

3.2 Comparison with RAMA moorings

We present here the comparison of temperature from LETKF-ROMS, O-ROMS and INCOIS-GODAS with respect to RAMA moorings during the period August 2016 - September 2017.

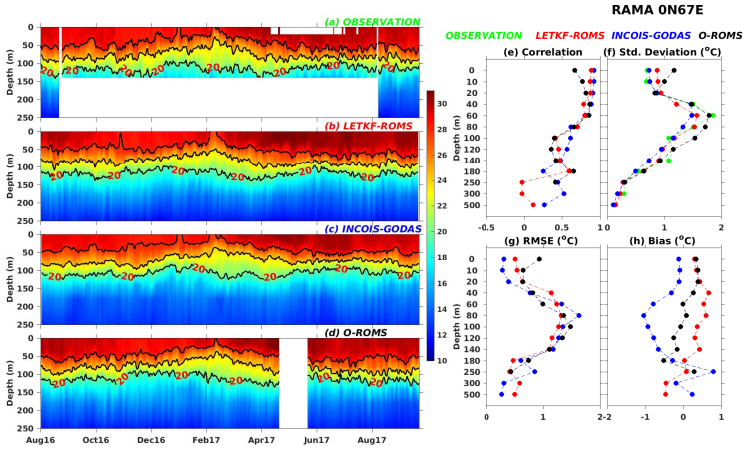

FIGURE 3.1: Time-depth section of temperature at $0°N, 67°E$ from (a) RAMA, (b) LETKF-ROMS, (c) INCOIS-GODAS and (d) O-ROMS. (e) Correlation of RAMA with LETKF-ROMS (red), INCOIS-GODAS (blue) and O-ROMS (black). (f) Standard deviation of RAMA (green), LETKF-ROMS (red), INCOIS-GODAS (blue) and O-ROMS (black). (g) RMSE with respect to RAMA for LETKF-ROMS (red), INCOIS-GODAS (blue) and O-ROMS (black). (h) Bias of LETKF-ROMS (red), INCOIS-GODAS (blue) and O-ROMS (black) with respect to RAMA. The white shades represent data unavailability.

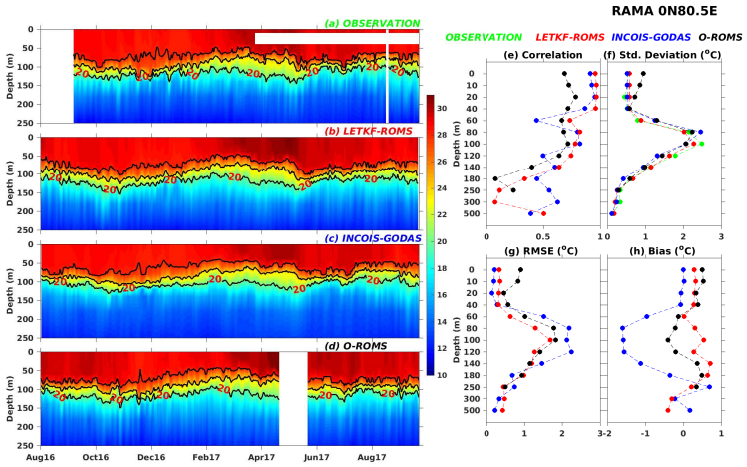

FIGURE 3.2: Time-depth section of temperature at $0°N, 80.5°E$ from (a) RAMA, (b) LETKF-ROMS, (c) INCOIS-GODAS and (d) O-ROMS. (e) Correlation of RAMA with LETKF-ROMS (red), INCOIS-GODAS (blue) and O-ROMS (black). (f) Standard deviation of RAMA (green), LETKF-ROMS (red), INCOIS-GODAS (blue) and O-ROMS (black). (g) RMSE with respect to RAMA for LETKF-ROMS (red), INCOIS-GODAS (blue) and O-ROMS (black). (h) Bias of LETKF-ROMS (red), INCOIS-GODAS (blue) and O-ROMS (black) with respect to RAMA. The white shades represent data unavailability.

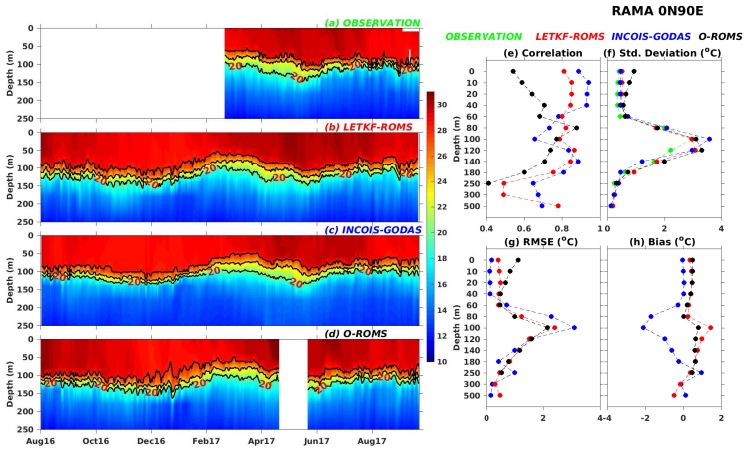

FIGURE 3.3: Time-depth section of temperature at $0°N, 90°E$ from (a) RAMA, (b) LETKF-ROMS, (c) INCOIS-GODAS and (d) O-ROMS. (e) Correlation of RAMA with LETKF-ROMS (red), INCOIS-GODAS (blue) and O-ROMS (black). (f) Standard deviation of RAMA (green), LETKF-ROMS (red), INCOIS-GODAS (blue) and O-ROMS (black). (g) RMSE with respect to RAMA for LETKF-ROMS (red), INCOIS-GODAS (blue) and O-ROMS (black). (h) Bias of LETKF-ROMS (red), INCOIS-GODAS (blue) and O-ROMS (black) with respect to RAMA. The white shades represent data unavailability.

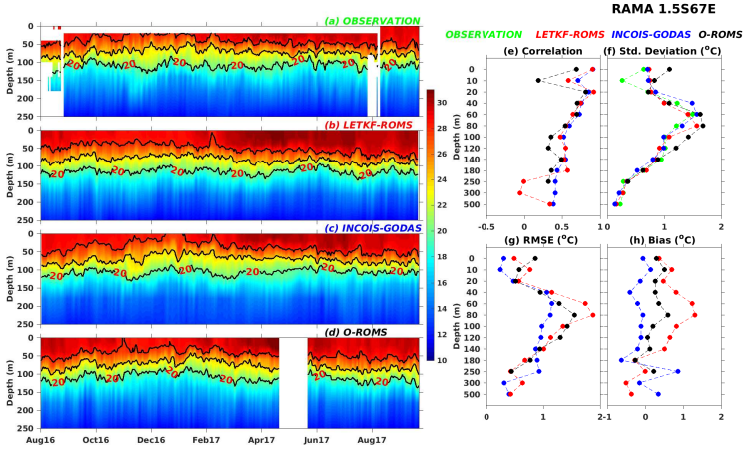

FIGURE 3.4: Time-depth section of temperature at $1.5°S, 67°E$ from (a) RAMA, (b) LETKF-ROMS, (c) INCOIS-GODAS and (d) O-ROMS. (e) Correlation of RAMA with LETKF-ROMS (red), INCOIS-GODAS (blue) and O-ROMS (black). (f) Standard deviation of RAMA (green), LETKF-ROMS (red), INCOIS-GODAS (blue) and O-ROMS (black). (g) RMSE with respect to RAMA for LETKF-ROMS (red), INCOIS-GODAS (blue) and O-ROMS (black). (h) Bias of LETKF-ROMS (red), INCOIS-GODAS (blue) and O-ROMS (black) with respect to RAMA. The white shades represent data unavailability.

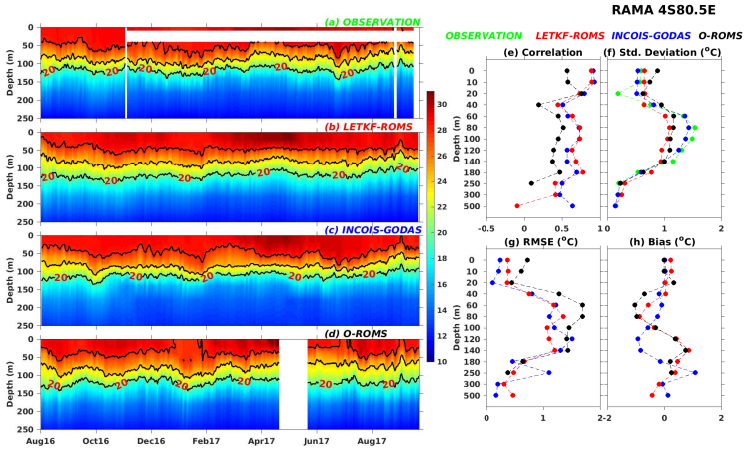

FIGURE 3.5: Time-depth section of temperature at $4°S, 80.5°E$ from (a) RAMA, (b) LETKF-ROMS, (c) INCOIS-GODAS and (d) O-ROMS. (e) Correlation of RAMA with LETKF-ROMS (red), INCOIS-GODAS (blue) and O-ROMS (black). (f) Standard deviation of RAMA (green), LETKF-ROMS (red), INCOIS-GODAS (blue) and O-ROMS (black). (g) RMSE with respect to RAMA for LETKF-ROMS (red), INCOIS-GODAS (blue) and O-ROMS (black). (h) Bias of LETKF-ROMS (red), INCOIS-GODAS (blue) and O-ROMS (black) with respect to RAMA.

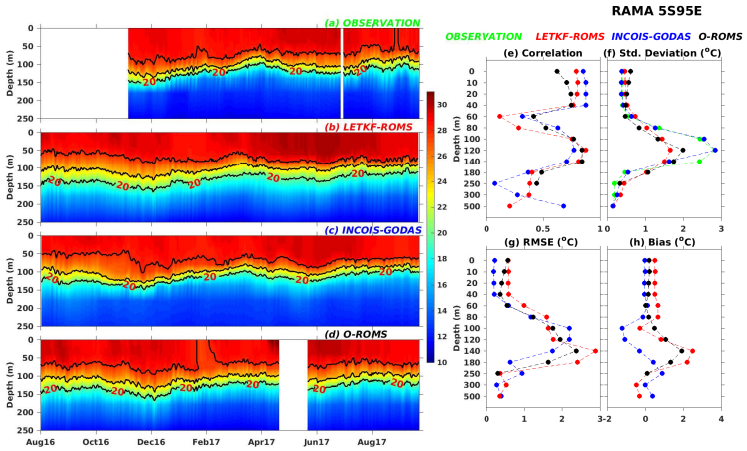

FIGURE 3.6: Time-depth section of temperature at $5°S, 95°E$ from (a) RAMA, (b) LETKF-ROMS, (c) INCOIS-GODAS and (d) O-ROMS. (e) Correlation of RAMA with LETKF-ROMS (red), INCOIS-GODAS (blue) and O-ROMS (black). (f) Standard deviation of RAMA (green), LETKF-ROMS (red), INCOIS-GODAS (blue) and O-ROMS (black). (g) RMSE with respect to RAMA for LETKF-ROMS (red), INCOIS-GODAS (blue) and O-ROMS (black). (h) Bias of LETKF-ROMS (red), INCOIS-GODAS (blue) and O-ROMS (black) with respect to RAMA. The white shades represent data unavailability.

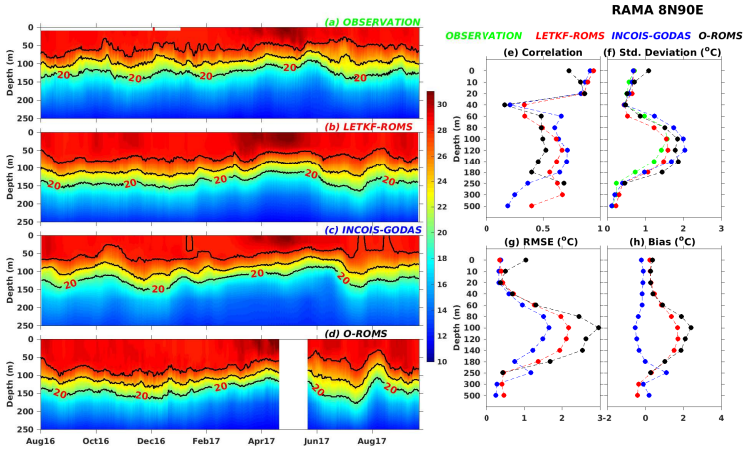

FIGURE 3.7: Time-depth section of temperature at $8°N, 90°E$ from (a) RAMA, (b) LETKF-ROMS, (c) INCOIS-GODAS and (d) O-ROMS. (e) Correlation of RAMA with LETKF-ROMS (red), INCOIS-GODAS (blue) and O-ROMS (black). (f) Standard deviation of RAMA (green), LETKF-ROMS (red), INCOIS-GODAS (blue) and O-ROMS (black). (g) RMSE with respect to RAMA for LETKF-ROMS (red), INCOIS-GODAS (blue) and O-ROMS (black). (h) Bias of LETKF-ROMS (red), INCOIS-GODAS (blue) and O-ROMS (black) with respect to RAMA. The white shades represent data unavailability.

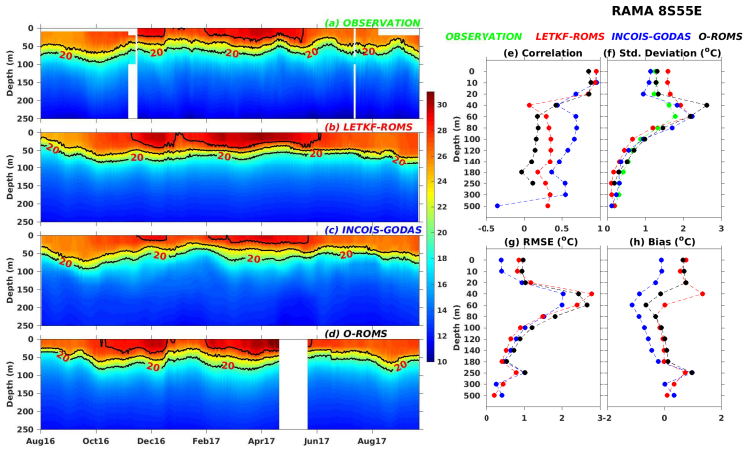

FIGURE 3.8: Time-depth section of temperature at $8°S, 55°E$ from (a) RAMA, (b) LETKF-ROMS, (c) INCOIS-GODAS and (d) O-ROMS. (e) Correlation of RAMA with LETKF-ROMS (red), INCOIS-GODAS (blue) and O-ROMS (black). (f) Standard deviation of RAMA (green), LETKF-ROMS (red), INCOIS-GODAS (blue) and O-ROMS (black). (g) RMSE with respect to RAMA for LETKF-ROMS (red), INCOIS-GODAS (blue) and O-ROMS (black). (h) Bias of LETKF-ROMS (red), INCOIS-GODAS (blue) and O-ROMS (black) with respect to RAMA. The white shades represent data unavailability.

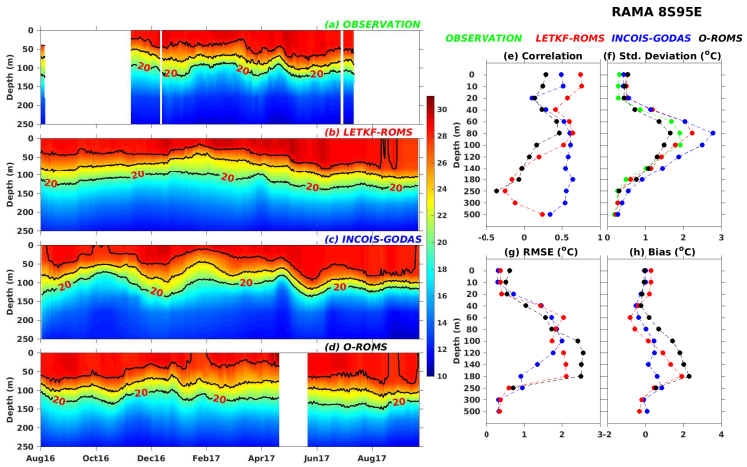

FIGURE 3.9: Time-depth section of temperature at $8°S, 95°E$ from (a) RAMA, (b) LETKF-ROMS, (c) INCOIS-GODAS and (d) O-ROMS. (e) Correlation of RAMA with LETKF-ROMS (red), INCOIS-GODAS (blue) and O-ROMS (black). (f) Standard deviation of RAMA (green), LETKF-ROMS (red), INCOIS-GODAS (blue) and O-ROMS (black). (g) RMSE with respect to RAMA for LETKF-ROMS (red), INCOIS-GODAS (blue) and O-ROMS (black). (h) Bias of LETKF-ROMS (red), INCOIS-GODAS (blue) and O-ROMS (black) with respect to RAMA. The white shades represent data unavailability.

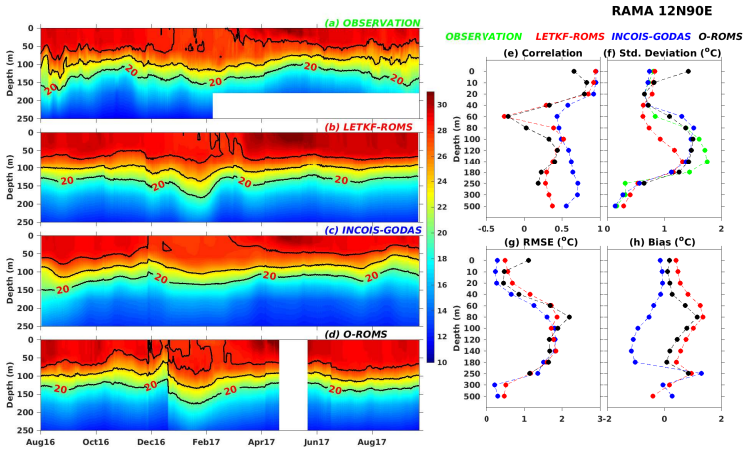

FIGURE 3.10: Time-depth section of temperature at $12°N, 90°E$ from (a) RAMA, (b) LETKF-ROMS, (c) INCOIS-GODAS and (d) O-ROMS. (e) Correlation of RAMA with LETKF-ROMS (red), INCOIS-GODAS (blue) and O-ROMS (black). (f) Standard deviation of RAMA (green), LETKF-ROMS (red), INCOIS-GODAS (blue) and O-ROMS (black). (g) RMSE with respect to RAMA for LETKF-ROMS (red), INCOIS-GODAS (blue) and O-ROMS (black). (h) Bias of LETKF-ROMS (red), INCOIS-GODAS (blue) and O-ROMS (black) with respect to RAMA. The white shades represent data unavailability.

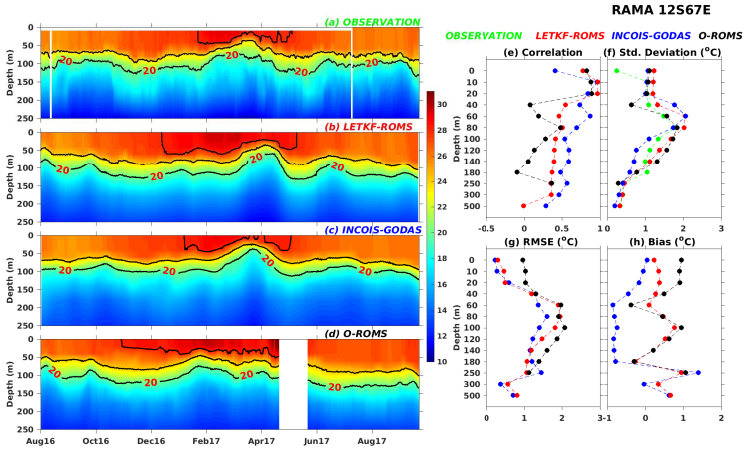

FIGURE 3.11: Time-depth section of temperature at $12°S, 67°E$ from (a) RAMA, (b) LETKF-ROMS, (c) INCOIS-GODAS and (d) O-ROMS. (e) Correlation of RAMA with LETKF-ROMS (red), INCOIS-GODAS (blue) and O-ROMS (black). (f) Standard deviation of RAMA (green), LETKF-ROMS (red), INCOIS-GODAS (blue) and O-ROMS (black). (g) RMSE with respect to RAMA for LETKF-ROMS (red), INCOIS-GODAS (blue) and O-ROMS (black). (h) Bias of LETKF-ROMS (red), INCOIS-GODAS (blue) and O-ROMS (black) with respect to RAMA. The white shades represent data unavailability.

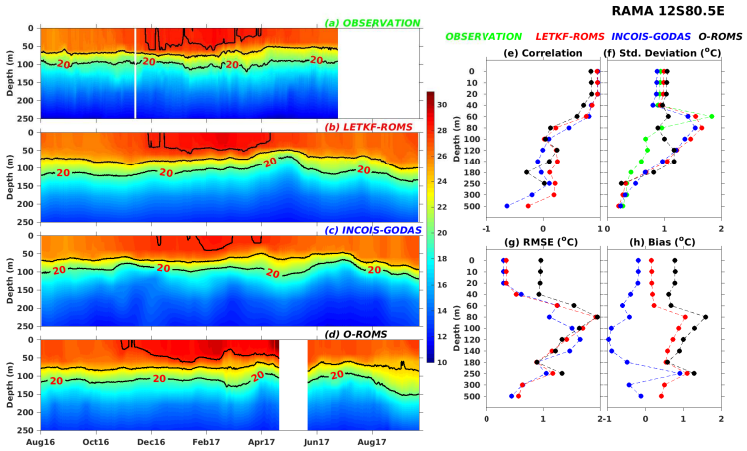

FIGURE 3.12: Time-depth section of temperature at $12°S, 80.5°E$ from (a) RAMA, (b) LETKF-ROMS, (c) INCOIS-GODAS and (d) O-ROMS. (e) Correlation of RAMA with LETKF-ROMS (red), INCOIS-GODAS (blue) and O-ROMS (black). (f) Standard deviation of RAMA (green), LETKF-ROMS (red), INCOIS-GODAS (blue) and O-ROMS (black). (g) RMSE with respect to RAMA for LETKF-ROMS (red), INCOIS-GODAS (blue) and O-ROMS (black). (h) Bias of LETKF-ROMS (red), INCOIS-GODAS (blue) and O-ROMS (black) with respect to RAMA. The white shades represent data unavailability.

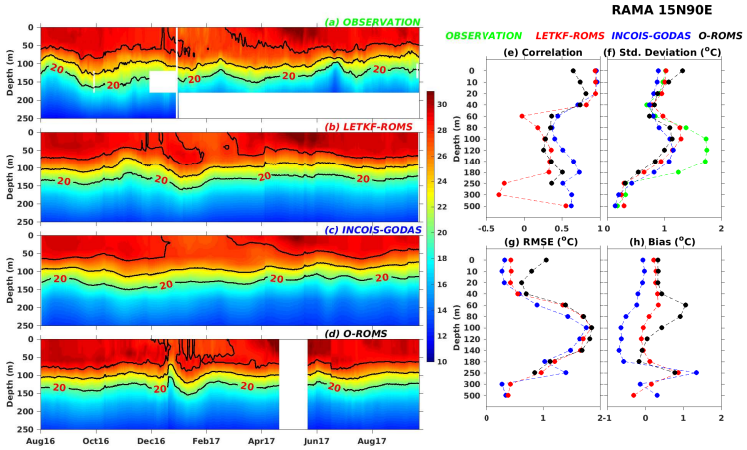

FIGURE 3.13: Time-depth section of temperature at $15°N, 90°E$ from (a) RAMA, (b) LETKF-ROMS, (c) INCOIS-GODAS and (d) O-ROMS. (e) Correlation of RAMA with LETKF-ROMS (red), INCOIS-GODAS (blue) and O-ROMS (black). (f) Standard deviation of RAMA (green), LETKF-ROMS (red), INCOIS-GODAS (blue) and O-ROMS (black). (g) RMSE with respect to RAMA for LETKF-ROMS (red), INCOIS-GODAS (blue) and O-ROMS (black). (h) Bias of LETKF-ROMS (red), INCOIS-GODAS (blue) and O-ROMS (black) with respect to RAMA. The white shades represent data unavailability.

3.3 Comparison with NIOT Buoys

The performance of temperature from LETKF-ROMS is pitted against NIOT buoys. The below figures showcases its merit.

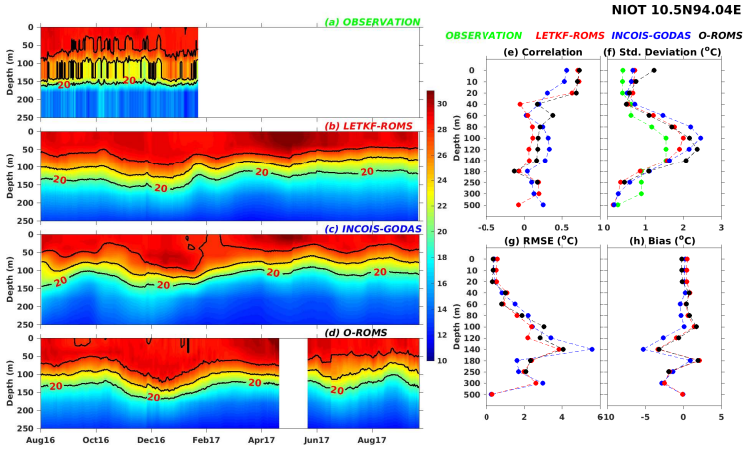

FIGURE 3.14: Time-depth section of temperature at $10.5°N, 94.04°E$ from (a) NIOT buoy, (b) LETKF-ROMS, (c) INCOIS-GODAS and (d) O-ROMS. (e) Correlation of NIOT buoy with LETKF-ROMS (red), INCOIS-GODAS (blue) and O-ROMS (black). (f) Standard deviation of NIOT buoy (green), LETKF-ROMS (red), INCOIS-GODAS (blue) and O-ROMS (black). (g) RMSE with respect to NIOT buoy for LETKF-ROMS (red), INCOIS-GODAS (blue) and O-ROMS (black). (h) Bias of LETKF-ROMS (red), INCOIS-GODAS (blue) and O-ROMS (black) with respect to NIOT buoy. The white shades represent data unavailability.

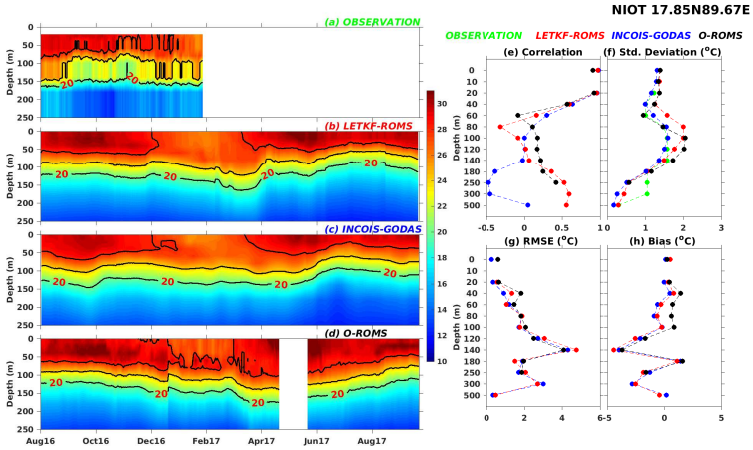

FIGURE 3.15: Time-depth section of temperature at $17.85°N, 89.67°E$ from (a) NIOT buoy, (b) LETKF-ROMS, (c) INCOIS-GODAS and (d) O-ROMS. (e) Correlation of NIOT buoy with LETKF-ROMS (red), INCOIS-GODAS (blue) and O-ROMS (black). (f) Standard deviation of NIOT buoy (green), LETKF-ROMS (red), INCOIS-GODAS (blue) and O-ROMS (black). (g) RMSE with respect to NIOT buoy for LETKF-ROMS (red), INCOIS-GODAS (blue) and O-ROMS (black). (h) Bias of LETKF-ROMS (red), INCOIS-GODAS (blue) and O-ROMS (black) with respect to NIOT buoy. The white shades represent data unavailability.

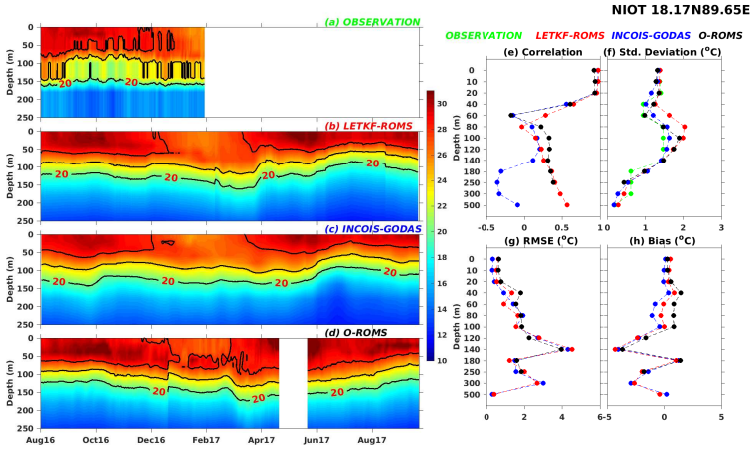

FIGURE 3.16: Time-depth section of temperature at $18.17°N, 89.65°E$ from (a) NIOT buoy, (b) LETKF-ROMS, (c) INCOIS-GODAS and (d) O-ROMS. (e) Correlation of NIOT buoy with LETKF-ROMS (red), INCOIS-GODAS (blue) and O-ROMS (black). (f) Standard deviation of NIOT buoy (green), LETKF-ROMS (red), INCOIS-GODAS (blue) and O-ROMS (black). (g) RMSE with respect to NIOT buoy for LETKF-ROMS (red), INCOIS-GODAS (blue) and O-ROMS (black). (h) Bias of LETKF-ROMS (red), INCOIS-GODAS (blue) and O-ROMS (black) with respect to NIOT buoy. The white shades represent data unavailability.

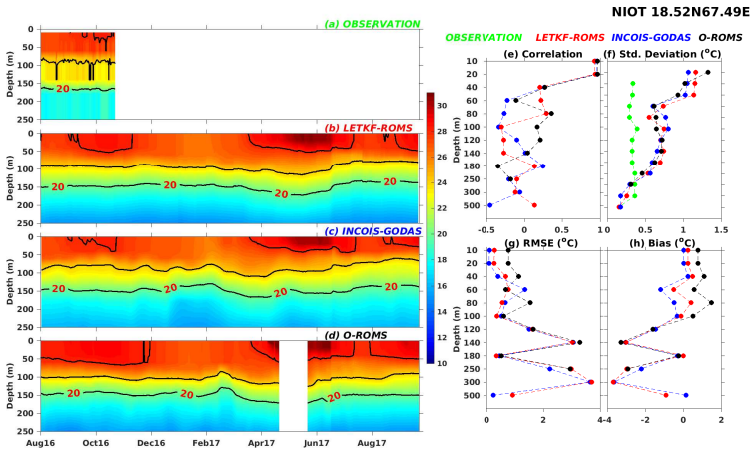

FIGURE 3.17: Time-depth section of temperature at $18.52°N, 67.49°E$ from (a) NIOT buoy, (b) LETKF-ROMS, (c) INCOIS-GODAS and (d) O-ROMS. (e) Correlation of NIOT buoy with LETKF-ROMS (red), INCOIS-GODAS (blue) and O-ROMS (black). (f) Standard deviation of NIOT buoy (green), LETKF-ROMS (red), INCOIS-GODAS (blue) and O-ROMS (black). (g) RMSE with respect to NIOT buoy for LETKF-ROMS (red), INCOIS-GODAS (blue) and O-ROMS (black). (h) Bias of LETKF-ROMS (red), INCOIS-GODAS (blue) and O-ROMS (black) with respect to NIOT buoy. The white shades represent data unavailability.

3.4 Comparison with Argo floats

Here we quantify the performance of all the three systems with respect to Argo floats in simulating the temperature of the oceans. Since Argo floats traverse in time, we divide the Indian Ocean into three broad regions - Arabian Sea, Bay of Bengal and Equatorial Indian Ocean and perform a collective analysis on the performance. Data from each region is concatenated and a daily Argo observation is obtained for each of the region. In Fig.1.5, we plot the location of pop-up of Argo floats in the Northern and Equatorial Indian Ocean that were taken into consideration for this validation exercise.

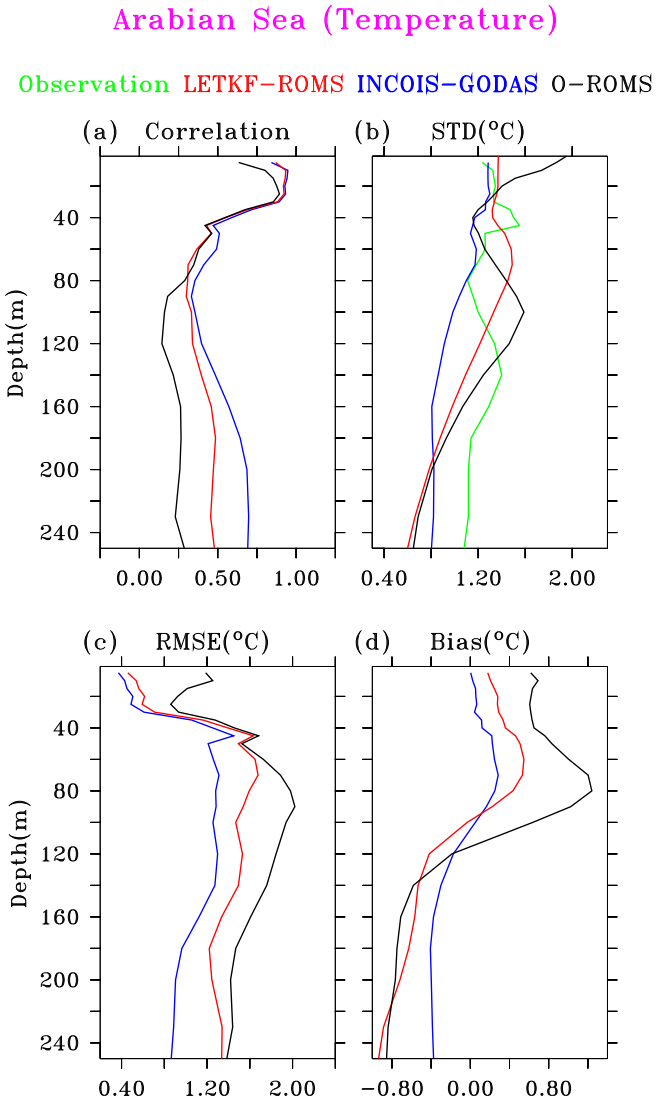

Figure 3.18: (a) Correlation of Argo floats with LETKF-ROMS (red), INCOIS-GODAS (blue) and O-ROMS (black) at vertical levels till $260m$. (b) Standard deviation of Argo floats (green), LETKF-ROMS (red), INCOIS-GODAS (blue) and O-ROMS (black). (c) RMSE with respect to Argo floats for LETKF-ROMS (red), INCOIS-GODAS (blue) and O-ROMS (black) at vertical levels till $260m$. (d) Bias of LETKF-ROMS (red), INCOIS-GODAS (blue) and O-ROMS (black) at vertical levels till $260m$ with respect to Argo floats.

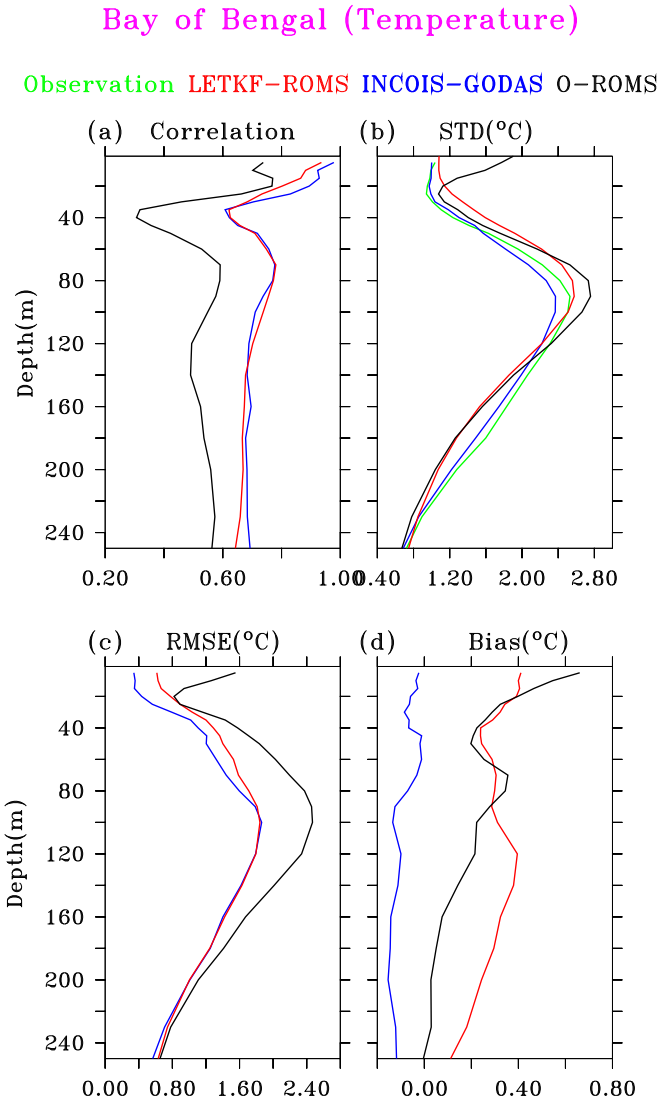

Figure 3.19: (a) Correlation of Argo floats with LETKF-ROMS (red), INCOIS-GODAS (blue) and O-ROMS (black) at vertical levels till $260m$. (b) Standard deviation of Argo floats (green), LETKF-ROMS (red), INCOIS-GODAS (blue) and O-ROMS (black). (c) RMSE with respect to Argo floats for LETKF-ROMS (red), INCOIS-GODAS (blue) and O-ROMS (black) at vertical levels till $260m$. (d) Bias of LETKF-ROMS (red), INCOIS-GODAS (blue) and O-ROMS (black) at vertical levels till $260m$ with respect to Argo floats.

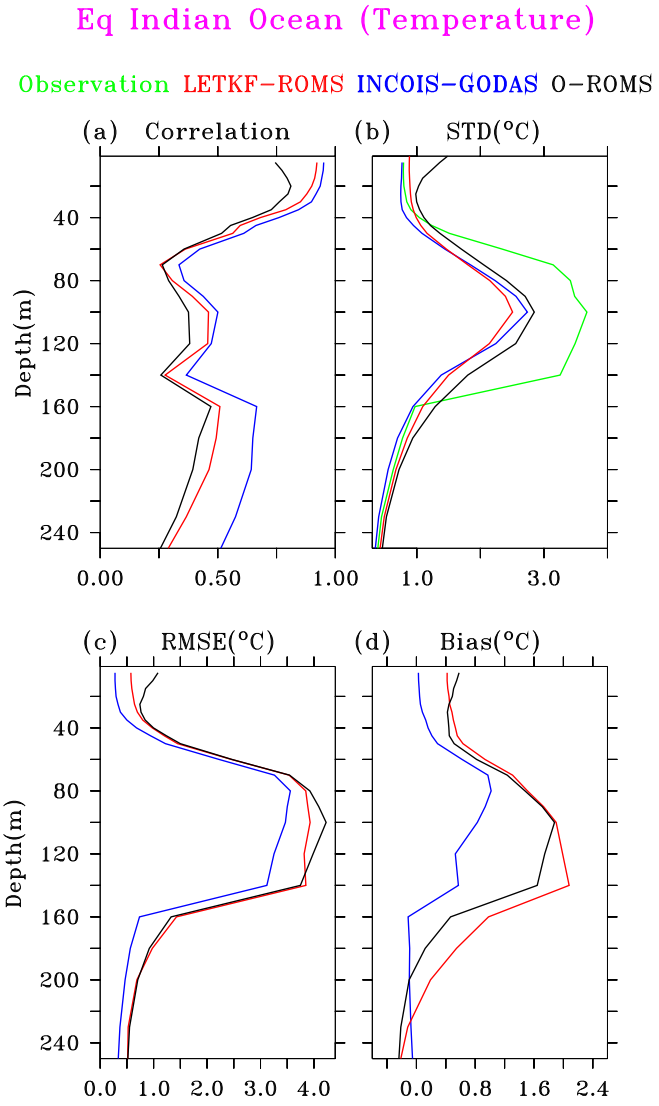

FIGURE 3.20: (a) Correlation of Argo floats with LETKF-ROMS (red), INCOIS-GODAS (blue) and O-ROMS (black) at vertical levels till $260m$. (b) Standard deviation of Argo floats (green), LETKF-ROMS (red), INCOIS-GODAS (blue) and O-ROMS (black). (c) RMSE with respect to Argo floats for LETKF-ROMS (red), INCOIS-GODAS (blue) and O-ROMS (black) at vertical levels till $260m$. (d) Bias of LETKF-ROMS (red), INCOIS-GODAS (blue) and O-ROMS (black) at vertical levels till $260m$ with respect to Argo floats.

We have also specifically looked at the performance of the LETKF-ROMS at 5 m depth. The corresponding Taylor diagrams with respect to Argo floats are shown below :

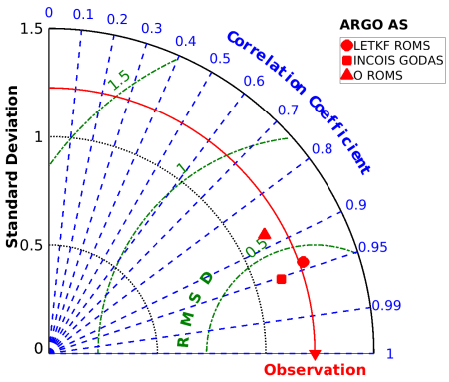

FIGURE 3.21: Taylor Diagram at 5 m depth from Argo floats at Arabian Sea.

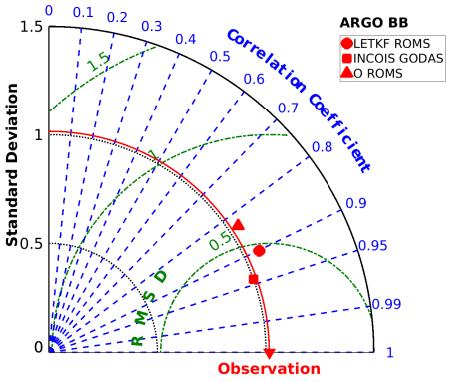

FIGURE 3.22: Taylor Diagram at 5 m depth from Argo floats at Bay of Bengal.

3.5 Conclusion

We see that there is a notable improvement in the vertical temperature profile due to assimilation introduced through LETKF in ROMS. We have compared the performance against 17 in-situ observations and multiple Argo floats congregated into three broad regions. However this is to

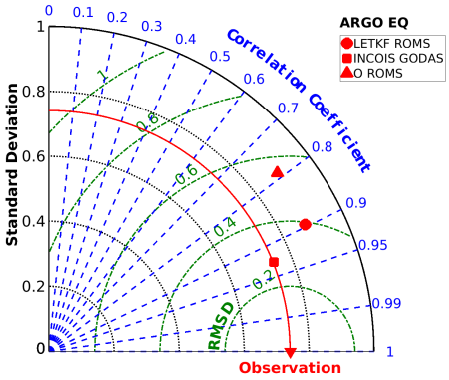

Figure 3.23: Taylor Diagram at 5 m depth from Argo floats at Equatorial Indian Ocean.

be remembered that all the observations, against which comparisons are made, were assimilated and hence are not independent observations. In most of the cases, the states are better correlated with the observations and we see a reduction in rmse as well. In case of Argo floats, we see an improvement in all the three regions - Arabian Sea, Bay of Bengal and Equatorial Indian Ocean. The time-depth section of Argo floats at all the three regions is noisy (and hence not shown) because there is large variability introduced due to changing locations of the Argo. The statistics at 5m depth shown in Fig.3.21,3.22 and 3.23 shows that LETKF-ROMS performs better than O-ROMS leading to larger correlation and smaller rmse in all the three regions. However, INCOIS-GODAS seems to be the best in reproducing the observation at 5 m depth. Also, INCOIS-GODAS reproduces observations from Argo floats best as is seen in Fig.3.18, Fig.3.19 and Fig.3.20. But it is clear that LETKF-ROMS outperforms O-ROMS in reproducing the 3D-temperature in the Indian Ocean.

4 Salinity

4.1 Introduction

We validate salinity profiles obtained from LETKF-ROMS with respect to observations from multiple sources - RAMA moorings, NIOT buoys and Argo floats. There were no data availability of O-ROMS during the month of May 2016. It is to be noted that the numerical model ROMS do not include effects of river discharge and tides and hence sea-surface salinity is weakly relaxed to World Ocean Atlas monthly salinity climatology in ROMS (30 day rekaxation time). On the other hand, INCOIS-GODAS includes cimatological river-runoff and do not relax its SSS.

4.2 Comparison with RAMA moorings

We present here the comparison of salinity from LETKF-ROMS, O-ROMS and INCOIS-GODAS with respect to RAMA moorings during the period August 2016 - September 2017. Only those moorings were chosen which has 50% or more data availability during this period.

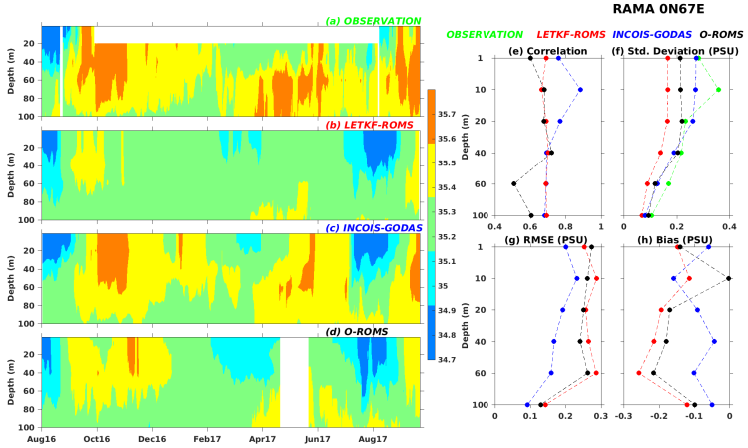

FIGURE 4.1: Time-depth section of salinity at $0°N, 67°E$ from (a) RAMA, (b) LETKF-ROMS, (c) INCOIS-GODAS and (d) O-ROMS. (e) Correlation of RAMA with LETKF-ROMS (red), INCOIS-GODAS (blue) and O-ROMS (black) at vertical levels till $100m$. (f) Standard deviation of RAMA (green), LETKF-ROMS (red), INCOIS-GODAS (blue) and O-ROMS (black). (g) RMSE with respect to RAMA for LETKF-ROMS (red), INCOIS-GODAS (blue) and O-ROMS (black) at vertical levels till $100m$. (h) Bias of LETKF-ROMS (red), INCOIS-GODAS (blue) and O-ROMS (black) at vertical levels till $100m$ with respect to RAMA. The white shades represent data unavailability.

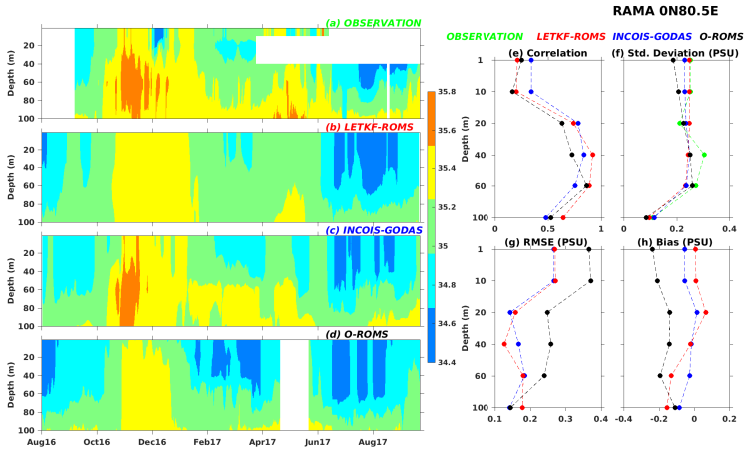

FIGURE 4.2: Time-depth section of salinity at $0°N, 80.5°E$ from (a) RAMA, (b) LETKF-ROMS, (c) INCOIS-GODAS and (d) O-ROMS. (e) Correlation of RAMA with LETKF-ROMS (red), INCOIS-GODAS (blue) and O-ROMS (black) at vertical levels till $100m$. (f) Standard deviation of RAMA (green), LETKF-ROMS (red), INCOIS-GODAS (blue) and O-ROMS (black). (g) RMSE with respect to RAMA for LETKF-ROMS (red), INCOIS-GODAS (blue) and O-ROMS (black) at vertical levels till $100m$. (h) Bias of LETKF-ROMS (red), INCOIS-GODAS (blue) and O-ROMS (black) at vertical levels till $100m$ with respect to RAMA.

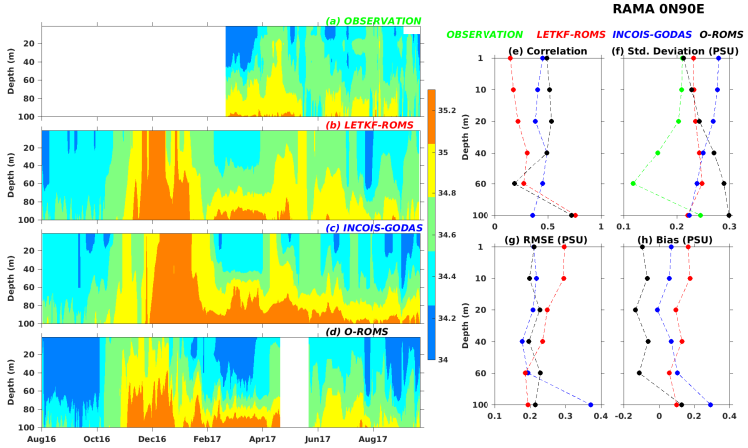

FIGURE 4.3: Time-depth section of salinity at $0°N, 90°E$ from (a) RAMA, (b) LETKF-ROMS, (c) INCOIS-GODAS and (d) O-ROMS. (e) Correlation of RAMA with LETKF-ROMS (red), INCOIS-GODAS (blue) and O-ROMS (black) at vertical levels till $100m$. (f) Standard deviation of RAMA (green), LETKF-ROMS (red), INCOIS-GODAS (blue) and O-ROMS (black). (g) RMSE with respect to RAMA for LETKF-ROMS (red), INCOIS-GODAS (blue) and O-ROMS (black) at vertical levels till $100m$. (h) Bias of LETKF-ROMS (red), INCOIS-GODAS (blue) and O-ROMS (black) at vertical levels till $100m$ with respect to RAMA.

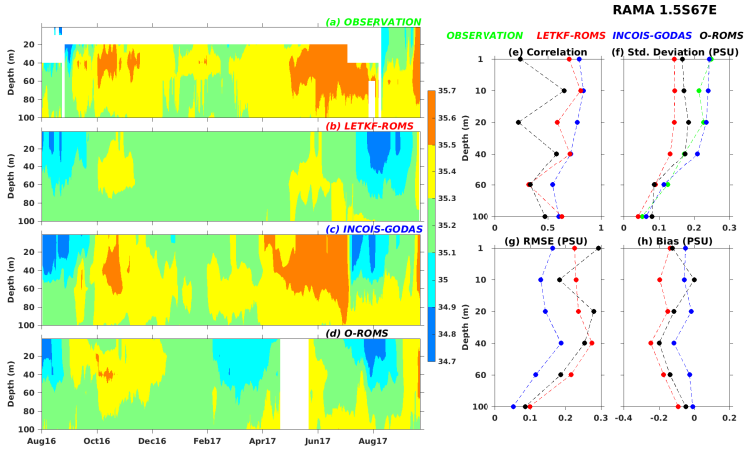

FIGURE 4.4: Time-depth section of salinity at $1.5°S, 67°E$ from (a) RAMA, (b) LETKF-ROMS, (c) INCOIS-GODAS and (d) O-ROMS. (e) Correlation of RAMA with LETKF-ROMS (red), INCOIS-GODAS (blue) and O-ROMS (black) at vertical levels till $100m$. (f) Standard deviation of RAMA (green), LETKF-ROMS (red), INCOIS-GODAS (blue) and O-ROMS (black). (g) RMSE with respect to RAMA for LETKF-ROMS (red), INCOIS-GODAS (blue) and O-ROMS (black) at vertical levels till $100m$. (h) Bias of LETKF-ROMS (red), INCOIS-GODAS (blue) and O-ROMS (black) at vertical levels till $100m$ with respect to RAMA. The white shades represent data unavailability.

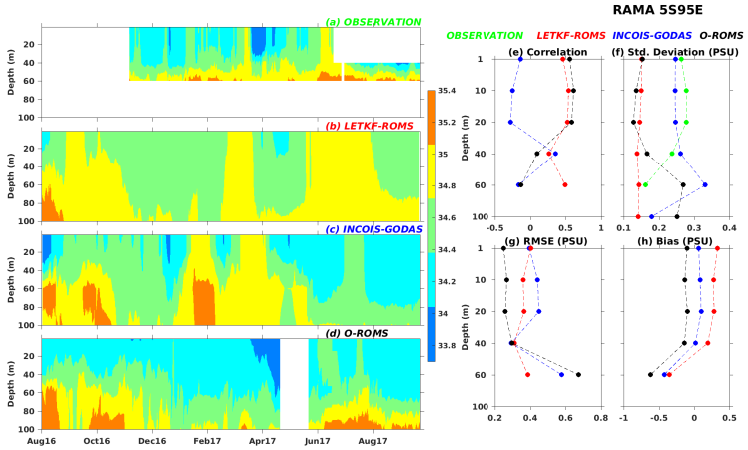

FIGURE 4.5: Time-depth section of salinity at $5°S, 95°E$ from (a) RAMA, (b) LETKF-ROMS, (c) INCOIS-GODAS and (d) O-ROMS. (e) Correlation of RAMA with LETKF-ROMS (red), INCOIS-GODAS (blue) and O-ROMS (black) at vertical levels till $100m$. (f) Standard deviation of RAMA (green), LETKF-ROMS (red), INCOIS-GODAS (blue) and O-ROMS (black). (g) RMSE with respect to RAMA for LETKF-ROMS (red), INCOIS-GODAS (blue) and O-ROMS (black) at vertical levels till $100m$. (h) Bias of LETKF-ROMS (red), INCOIS-GODAS (blue) and O-ROMS (black) at vertical levels till $100m$ with respect to RAMA. The white shades represent data unavailability.

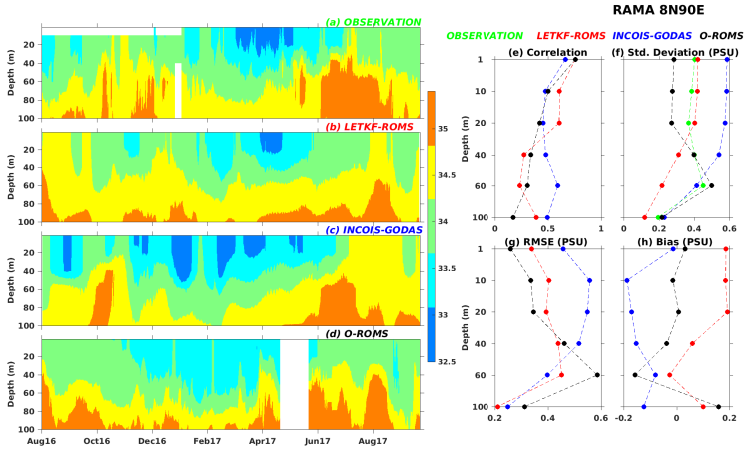

FIGURE 4.6: Time-depth section of salinity at $8°N, 90°E$ from (a) RAMA, (b) LETKF-ROMS, (c) INCOIS-GODAS and (d) O-ROMS. (e) Correlation of RAMA with LETKF-ROMS (red), INCOIS-GODAS (blue) and O-ROMS (black) at vertical levels till $100m$. (f) Standard deviation of RAMA (green), LETKF-ROMS (red), INCOIS-GODAS (blue) and O-ROMS (black). (g) RMSE with respect to RAMA for LETKF-ROMS (red), INCOIS-GODAS (blue) and O-ROMS (black) at vertical levels till $100m$. (h) Bias of LETKF-ROMS (red), INCOIS-GODAS (blue) and O-ROMS (black) at vertical levels till $100m$ with respect to RAMA. The white shades represent data unavailability.

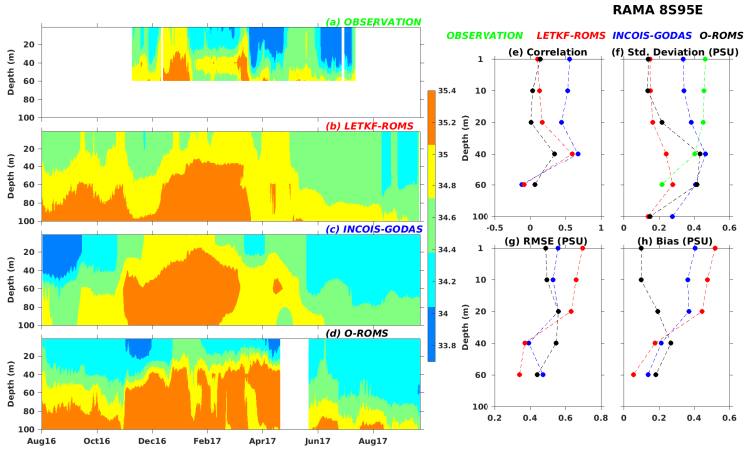

FIGURE 4.7: Time-depth section of salinity at $8°S, 95°E$ from (a) RAMA, (b) LETKF-ROMS, (c) INCOIS-GODAS and (d) O-ROMS. (e) Correlation of RAMA with LETKF-ROMS (red), INCOIS-GODAS (blue) and O-ROMS (black) at vertical levels till $100m$. (f) Standard deviation of RAMA (green), LETKF-ROMS (red), INCOIS-GODAS (blue) and O-ROMS (black). (g) RMSE with respect to RAMA for LETKF-ROMS (red), INCOIS-GODAS (blue) and O-ROMS (black) at vertical levels till $100m$. (h) Bias of LETKF-ROMS (red), INCOIS-GODAS (blue) and O-ROMS (black) at vertical levels till $100m$ with respect to RAMA. The white shades represent data unavailability.

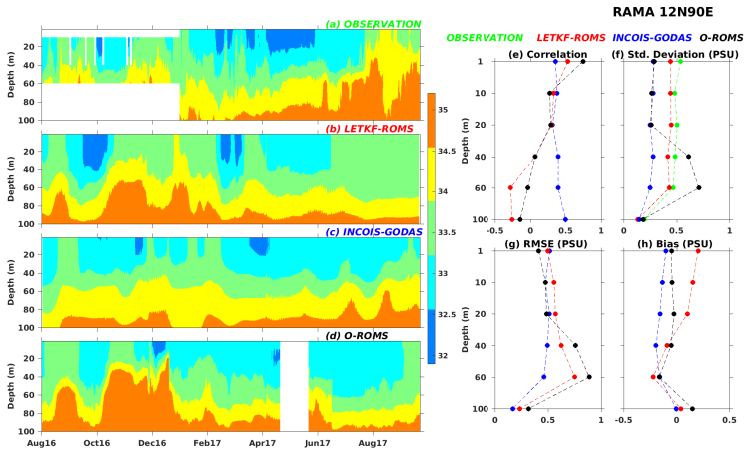

FIGURE 4.8: Time-depth section of salinity at $12°N, 90°E$ from (a) RAMA, (b) LETKF-ROMS, (c) INCOIS-GODAS and (d) O-ROMS. (e) Correlation of RAMA with LETKF-ROMS (red), INCOIS-GODAS (blue) and O-ROMS (black) at vertical levels till $100m$. (f) Standard deviation of RAMA (green), LETKF-ROMS (red), INCOIS-GODAS (blue) and O-ROMS (black). (g) RMSE with respect to RAMA for LETKF-ROMS (red), INCOIS-GODAS (blue) and O-ROMS (black) at vertical levels till $100m$. (h) Bias of LETKF-ROMS (red), INCOIS-GODAS (blue) and O-ROMS (black) at vertical levels till $100m$ with respect to RAMA. The white shades represent data unavailability.

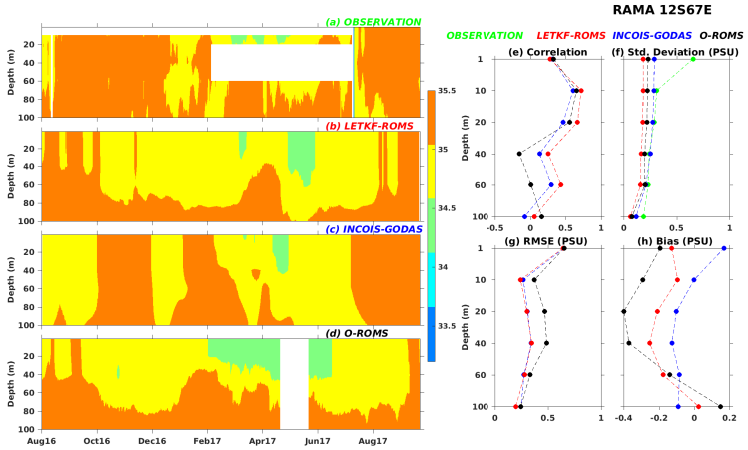

FIGURE 4.9: Time-depth section of salinity at $12°S, 67°E$ from (a) RAMA, (b) LETKF-ROMS, (c) INCOIS-GODAS and (d) O-ROMS. (e) Correlation of RAMA with LETKF-ROMS (red), INCOIS-GODAS (blue) and O-ROMS (black) at vertical levels till $100m$. (f) Standard deviation of RAMA (green), LETKF-ROMS (red), INCOIS-GODAS (blue) and O-ROMS (black). (g) RMSE with respect to RAMA for LETKF-ROMS (red), INCOIS-GODAS (blue) and O-ROMS (black) at vertical levels till $100m$. (h) Bias of LETKF-ROMS (red), INCOIS-GODAS (blue) and O-ROMS (black) at vertical levels till $100m$ with respect to RAMA. The white shades represent data unavailability.

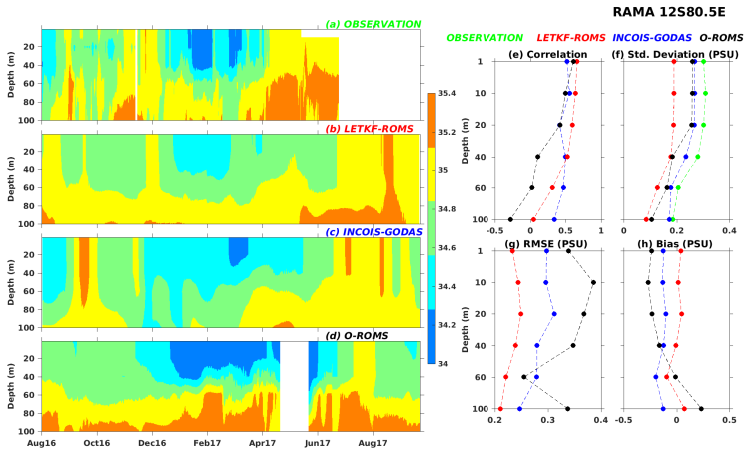

FIGURE 4.10: Time-depth section of salinity at $12°S, 80.5°E$ from (a) RAMA, (b) LETKF-ROMS, (c) INCOIS-GODAS and (d) O-ROMS. (e) Correlation of RAMA with LETKF-ROMS (red), INCOIS-GODAS (blue) and O-ROMS (black) at vertical levels till $100m$. (f) Standard deviation of RAMA (green), LETKF-ROMS (red), INCOIS-GODAS (blue) and O-ROMS (black). (g) RMSE with respect to RAMA for LETKF-ROMS (red), INCOIS-GODAS (blue) and O-ROMS (black) at vertical levels till $100m$. (h) Bias of LETKF-ROMS (red), INCOIS-GODAS (blue) and O-ROMS (black) at vertical levels till $100m$ with respect to RAMA. The white shades represent data unavailability.

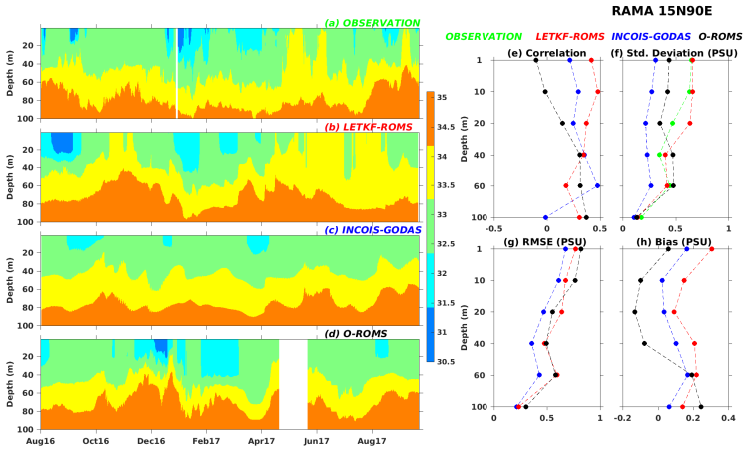

FIGURE 4.11: Time-depth section of salinity at $15°N, 90°E$ from (a) RAMA, (b) LETKF-ROMS, (c) INCOIS-GODAS and (d) O-ROMS. (e) Correlation of RAMA with LETKF-ROMS (red), INCOIS-GODAS (blue) and O-ROMS (black) at vertical levels till $100m$. (f) Standard deviation of RAMA (green), LETKF-ROMS (red), INCOIS-GODAS (blue) and O-ROMS (black). (g) RMSE with respect to RAMA for LETKF-ROMS (red), INCOIS-GODAS (blue) and O-ROMS (black) at vertical levels till $100m$. (h) Bias of LETKF-ROMS (red), INCOIS-GODAS (blue) and O-ROMS (black) at vertical levels till $100m$ with respect to RAMA. The white shades represent data unavailability.

4.3 Comparison with NIOT Buoys

The performance of salinity from LETKF-ROMS, INCOIS-GODAS an O-ROMS is compared with observations from NIOT buoys. The below figures showcases its merit. The other two NIOT buoys have a lot of missing data during our period of interest.

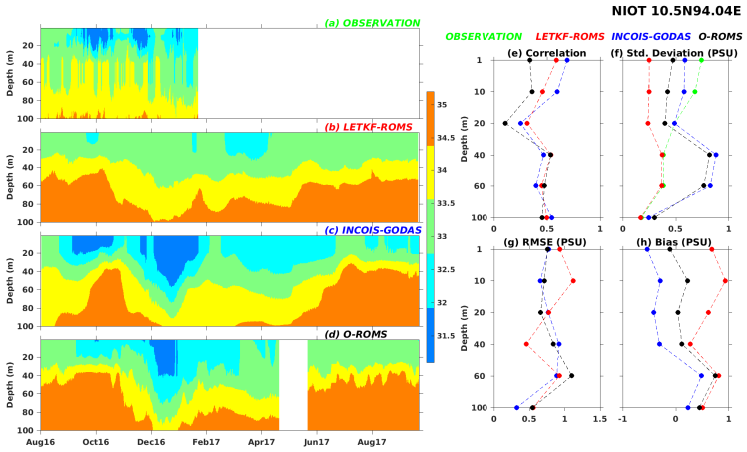

FIGURE 4.12: Time-depth section of salinity at $10.5°N, 94.04°E$ from (a) NIOT buoy, (b) LETKF-ROMS, (c) INCOIS-GODAS and (d) O-ROMS. (e) Correlation of NIOT buoy with LETKF-ROMS (red), INCOIS-GODAS (blue) and O-ROMS (black) at vertical levels till $100m$. (f) Standard deviation of NIOT buoy (green), LETKF-ROMS (red), INCOIS-GODAS (blue) and O-ROMS (black). (g) RMSE with respect to NIOT buoy for LETKF-ROMS (red), INCOIS-GODAS (blue) and O-ROMS (black) at vertical levels till $100m$. (h) Bias of LETKF-ROMS (red), INCOIS-GODAS (blue) and O-ROMS (black) at vertical levels till $100m$ with respect to NIOT buoy. The white shades represent data unavailability.

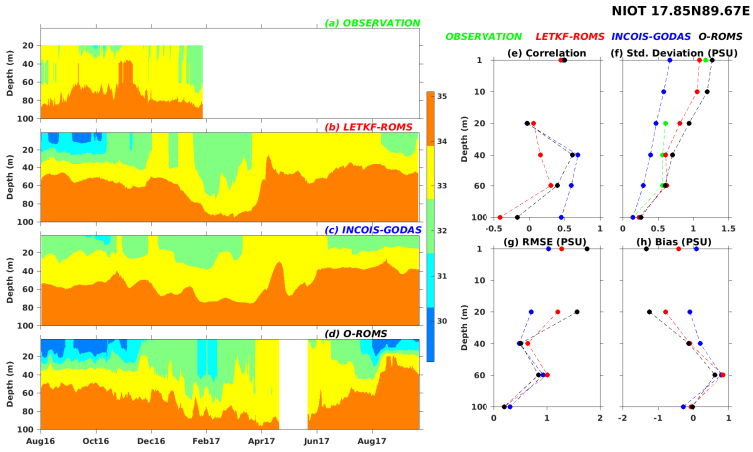

FIGURE 4.13: Time-depth section of salinity at $17.85°N, 89.67°E$ from (a) NIOT buoy, (b) LETKF-ROMS, (c) INCOIS-GODAS and (d) O-ROMS. (e) Correlation of NIOT buoy with LETKF-ROMS (red), INCOIS-GODAS (blue) and O-ROMS (black) at vertical levels till $100m$. (f) Standard deviation of NIOT buoy (green), LETKF-ROMS (red), INCOIS-GODAS (blue) and O-ROMS (black). (g) RMSE with respect to NIOT buoy for LETKF-ROMS (red), INCOIS-GODAS (blue) and O-ROMS (black) at vertical levels till $100m$. (h) Bias of LETKF-ROMS (red), INCOIS-GODAS (blue) and O-ROMS (black) at vertical levels till $100m$ with respect to NIOT buoy. The white shades represent data unavailability.

4.4 Comparison with Argo floats

Here we quantify the performance of all the three systems with respect to Argo floats in simulating the temperature of the oceans. Since Argo floats traverse in time, we divide the Indian Ocean into three broad regions - Arabian Sea, Bay of Bengal and Equatorial Indian Ocean and perform a collective analysis on the performance. Data from each region is concatenated and a daily Argo observation is obtained for each of the region. In Fig.1.5, we plot the location of pop-up of Argo floats in the Northern and Equatorial Indian Ocean that were taken into consideration for this validation exercise.

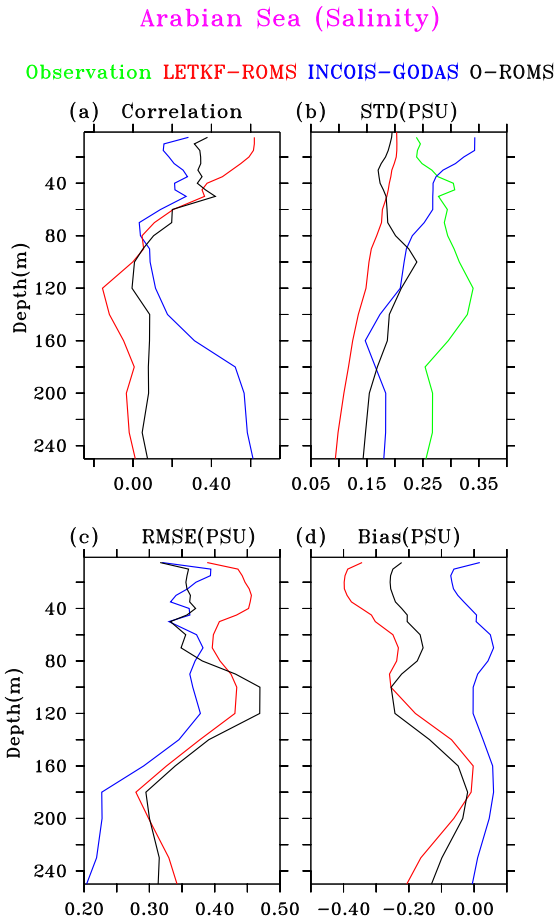

Figure 4.14: Time-depth section of salinity in the Arabian Sea from (a) Argo float, (b) LETKF-ROMS, (c) INCOIS-GODAS and (d) O-ROMS. (e) Correlation of Argo floats with LETKF-ROMS (red), INCOIS-GODAS (blue) and O-ROMS (black) at vertical levels till $260m$. (f) Standard deviation of Argo floats (green), LETKF-ROMS (red), INCOIS-GODAS (blue) and O-ROMS (black). (g) RMSE with respect to Argo floats for LETKF-ROMS (red), INCOIS-GODAS (blue) and O-ROMS (black) at vertical levels till $260m$. (h) Bias of LETKF-ROMS (red), INCOIS-GODAS (blue) and O-ROMS (black) at vertical levels till $260m$ with respect to Argo floats. The white shades represent data unavailability.

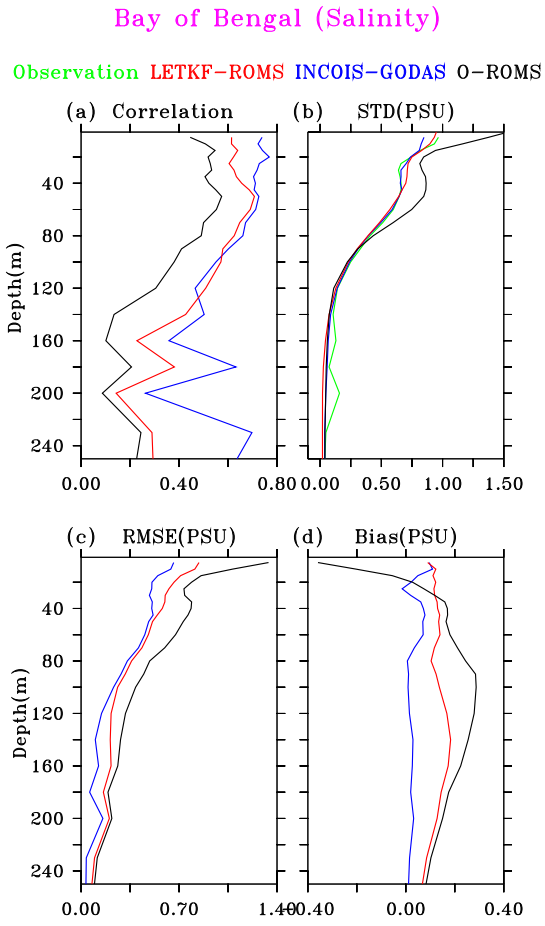

Figure 4.15: Time-depth section of salinity in the Bay of Bengal from (a) Argo float, (b) LETKF-ROMS, (c) INCOIS-GODAS and (d) O-ROMS. (e) Correlation of Argo floats with LETKF-ROMS (red), INCOIS-GODAS (blue) and O-ROMS (black) at vertical levels till $260m$. (f) Standard deviation of Argo floats (green), LETKF-ROMS (red), INCOIS-GODAS (blue) and O-ROMS (black). (g) RMSE with respect to Argo floats for LETKF-ROMS (red), INCOIS-GODAS (blue) and O-ROMS (black) at vertical levels till $260m$. (h) Bias of LETKF-ROMS (red), INCOIS-GODAS (blue) and O-ROMS (black) at vertical levels till $260m$ with respect to Argo floats. The white shades represent data unavailability.

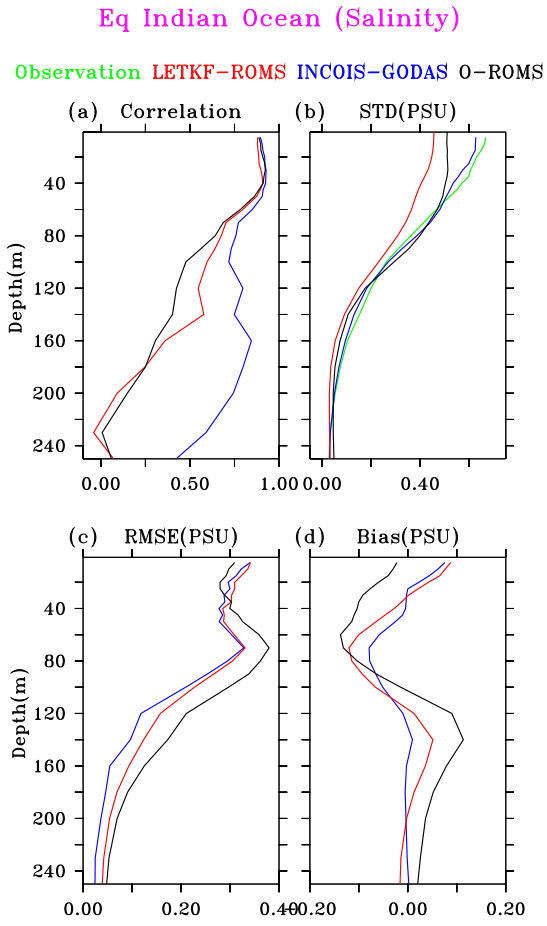

Figure 4.16: Time-depth section of salinity in the Arabian Sea from (a) Argo float, (b) LETKF-ROMS, (c) INCOIS-GODAS and (d) O-ROMS. (e) Correlation of Argo floats with LETKF-ROMS (red), INCOIS-GODAS (blue) and O-ROMS (black) at vertical levels till $260m$. (f) Standard deviation of Argo floats (green), LETKF-ROMS (red), INCOIS-GODAS (blue) and O-ROMS (black). (g) RMSE with respect to Argo floats for LETKF-ROMS (red), INCOIS-GODAS (blue) and O-ROMS (black) at vertical levels till $260m$. (h) Bias of LETKF-ROMS (red), INCOIS-GODAS (blue) and O-ROMS (black) at vertical levels till $260m$ with respect to Argo floats. The white shades represent data unavailability.

We also look at the performance of all the three system through Taylor diagrams at 5m depth.

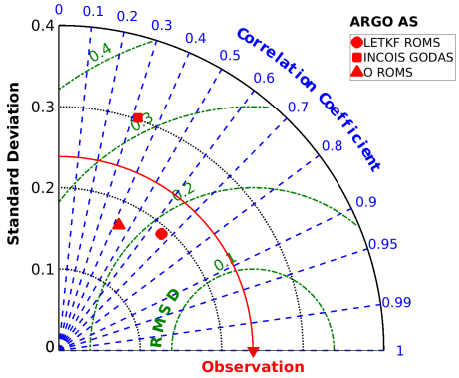

Figure 4.17: Taylor diagram of salt at 5m from Argo floats in Arabian Sea.

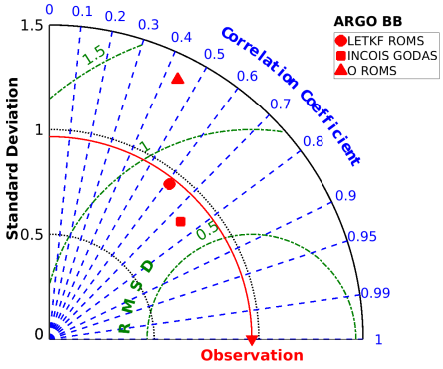

Figure 4.18: Taylor diagram of salt at 5m from Argo floats in Bay of Bengal.

4.5 Conclusion

We see that there is an improvement in the vertical salinity profile due to assimilation introduced through LETKF in ROMS. The features obtained from LETKF-ROMS are smooth compared to the features seen in O-ROMS. This is because the ensemble average in LETKF-ROMS smooths out the sharpness. We have compared the performance against 13 in-situ observations that

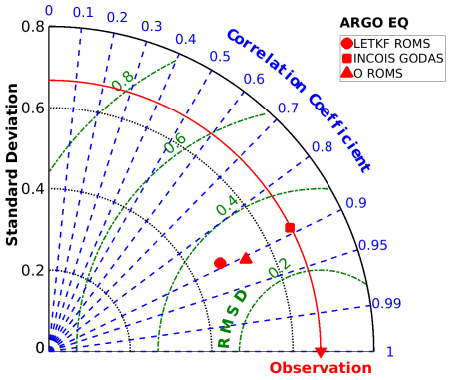

Figure 4.19: Taylor diagram of salt at 5m from Argo floats in Equatorial Indian Ocean.

includes both RAMA moorings and NIOT buoys and multiple Argo floats congregated into three broad regions. It is to be remembered that SSS is relaxed to monthly climatology in both O-ROMS and LETKF-ROMS whereas river-runoff monthly climatology is included in INCOIS-GODAS. The improvements are better reflected with respect to O-ROMS when compared to the Argo floats - in particular to Bay of Bengal region which has been a challenge to simulate due to large influx of fresh water leading to large stratification (see Fig.4.15 and 4.18). The rmse is contained within 0.75 psu even in the top layers while the bias is less that 0.2 psu across all layers compared to much larger rmse and biases particularly in the top layers of the ocean in O-ROMS (see Fig.4.15).

5 Mixed Layer Depth and 20 Degree Isotherm

5.1 Introduction

In this chapter, we look at the performance of LETKF-ROMS in simulating the mixed layer depth (MLD) and the 20 °C isotherm (D20) and compare it with INCOIS-GODAS and O-ROMS. Both MLD and D20 are important diagnostic variables that portray the ability of the model in recreating the mixing processes and hence in recreating the thermocline and halocline. There were no data availability of O-ROMS during the month of May 2016.

5.2 Comparison with RAMA moorings

We present here the comparison of MLD obtained from LETKF-ROMS, INCOIS-GODAS and O-ROMS with observations from RAMA moorings. We only plot for those RAMA moorings that has a continuous set of subsurface data during the period of our interest.

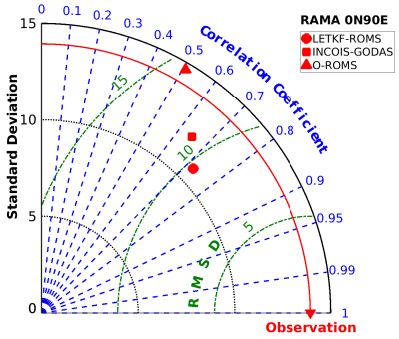

FIGURE 5.1: Taylor Diagram of mixed layer depth from LETKF-ROMS, INCOIS-GODAS and O-ROMS with respect to RAMA mooring at 0° N & 90° E.

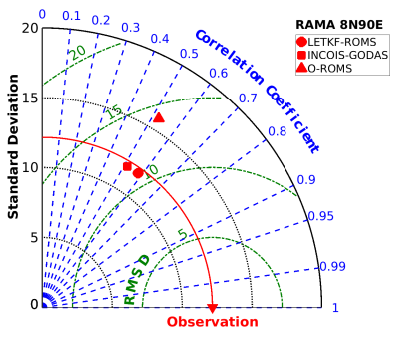

FIGURE 5.2: Taylor Diagram of mixed layer depth from LETKF-ROMS, INCOIS-GODAS and O-ROMS with respect to RAMA mooring at 8° N & 90° E.

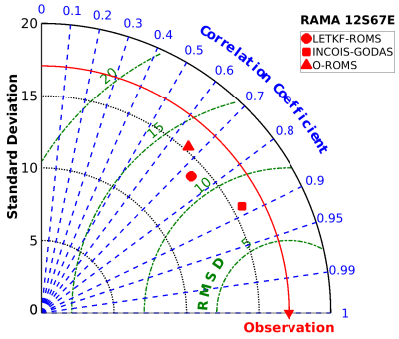

FIGURE 5.3: Taylor Diagram of MLD from LETKF-ROMS, INCOIS-GODAS and O-ROMS with respect to RAMA mooring at 12° S & 67° E.

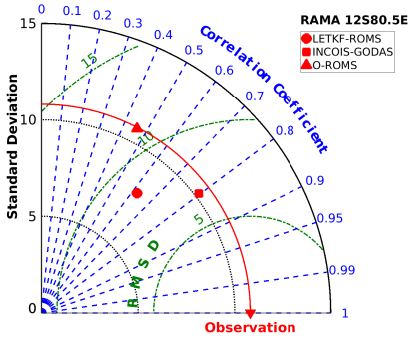

FIGURE 5.4: Taylor Diagram of MLD from LETKF-ROMS, INCOIS-GODAS and O-ROMS with respect to RAMA mooring at 12° S & 80.5° E.

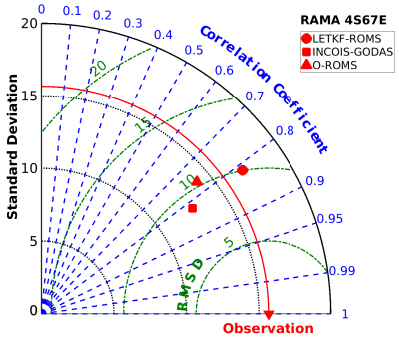

FIGURE 5.5: Taylor Diagram of MLD from LETKF-ROMS, INCOIS-GODAS and O-ROMS with respect to RAMA mooring at 4° S & 67° E.

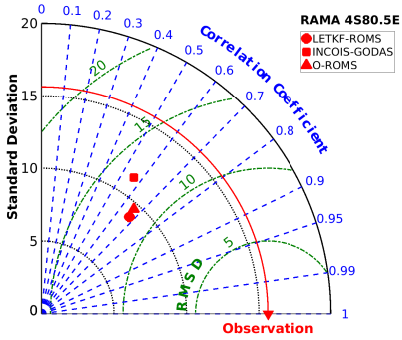

FIGURE 5.6: Taylor Diagram of MLD from LETKF-ROMS, INCOIS-GODAS and O-ROMS with respect to RAMA mooring at 4° S & 80.5° E.

We now show the performance of MLD in LETKF-ROMS in comparison to INCOIS-GODAS and O-ROMS with respect to Argo floats concatenated in three regions - Arabian Sea, Bay of Bengal and Equatorial Indian Ocean.

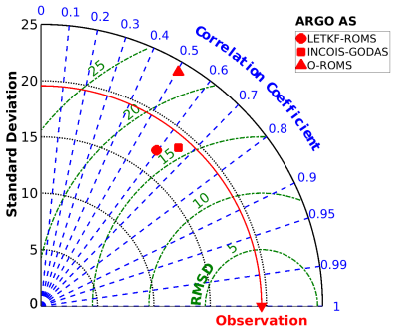

Figure 5.7: Taylor Diagram of MLD from LETKF-ROMS, INCOIS-GODAS and O-ROMS with respect to concatenated Argo floats in Arabian Sea

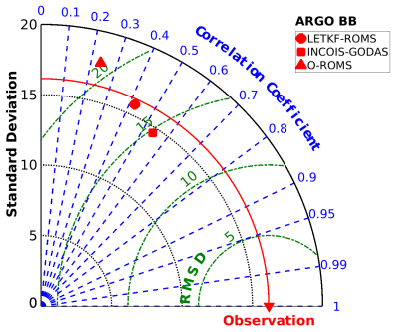

Figure 5.8: Taylor Diagram of MLD from LETKF-ROMS, INCOIS-GODAS and O-ROMS with respect to concatenated Argo floats in Bay of Bengal

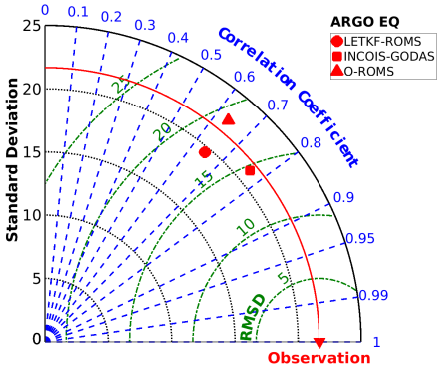

Figure 5.9: Taylor Diagram of MLD from LETKF-ROMS, INCOIS-GODAS and O-ROMS with respect to concatenated Argo floats in Equatorial Indian Ocean.

We now show the performance of D20 in LETKF-ROMS in comparison to INCOIS-GODAS and O-ROMS with respect to in-situ RAMA moorings. Only those RAMA moorings are taken into account whose data is available during the period of our interest.

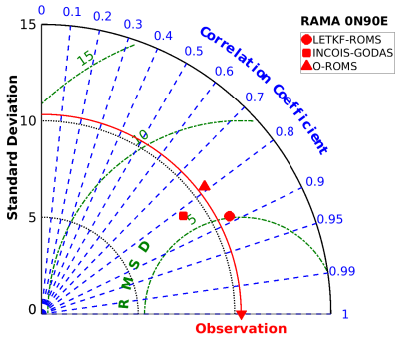

FIGURE 5.10: Taylor Diagram of D20 from LETKF-ROMS, INCOIS-GODAS and O-ROMS with respect to RAMA mooring at 0° N & 90° E.

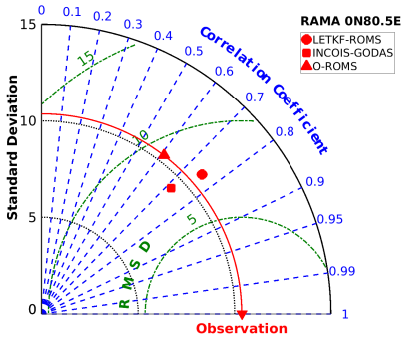

FIGURE 5.11: Taylor Diagram of D20 from LETKF-ROMS, INCOIS-GODAS and O-ROMS with respect to RAMA mooring at 0° N & 80.5° E.

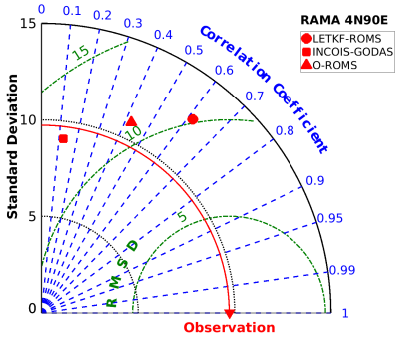

FIGURE 5.12: Taylor Diagram of D20 from LETKF-ROMS, INCOIS-GODAS and O-ROMS with respect to RAMA mooring at 4° N & 90° E.

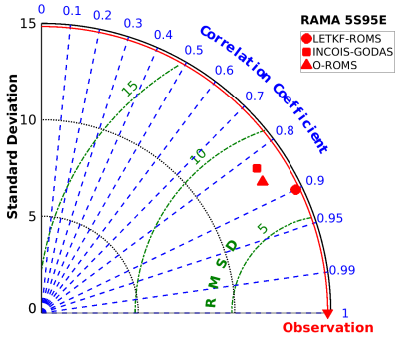

FIGURE 5.13: Taylor Diagram of D20 from LETKF-ROMS, INCOIS-GODAS and O-ROMS with respect to RAMA mooring at 5° S & 95° E.

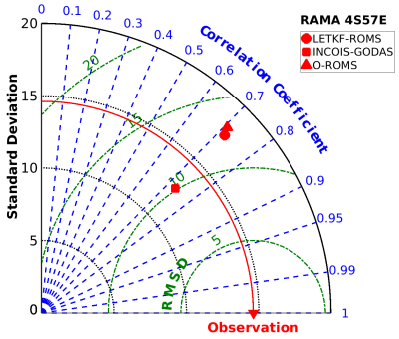

FIGURE 5.14: Taylor Diagram of D20 from LETKF-ROMS, INCOIS-GODAS and O-ROMS with respect to RAMA mooring at 4° S & 57° E.

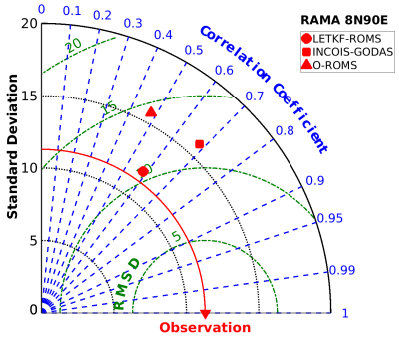

FIGURE 5.15: Taylor Diagram of D20 from LETKF-ROMS, INCOIS-GODAS and O-ROMS with respect to RAMA mooring at 8° N & 90° E.

We now show the performance of D20 in LETKF-ROMS in comparison to INCOIS-GODAS and O-ROMS with respect to Argo floats concatenated in three regions - Arabian Sea, Bay of Bengal and Equatorial Indian Ocean.

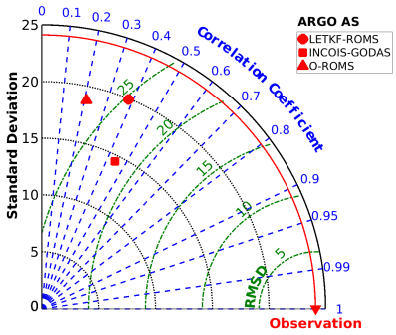

FIGURE 5.16: Taylor Diagram of D20 from LETKF-ROMS, INCOIS-GODAS and O-ROMS with respect to concatenated Argo floats in Arabian Sea

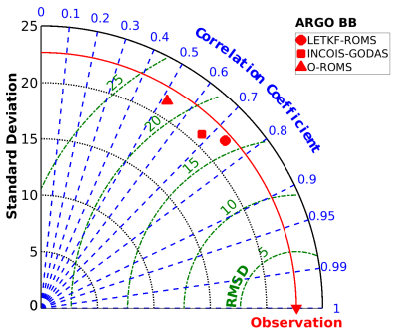

FIGURE 5.17: Taylor Diagram of D20 from LETKF-ROMS, INCOIS-GODAS and O-ROMS with respect to concatenated Argo floats in Bay of Bengal

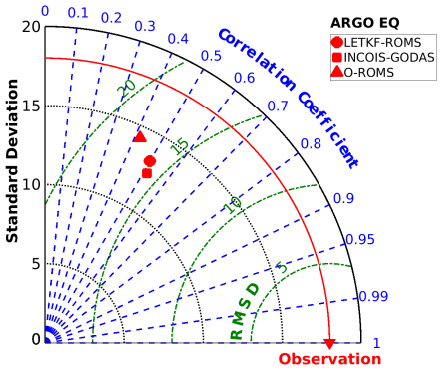

FIGURE 5.18: Taylor Diagram of D20 from LETKF-ROMS, INCOIS-GODAS and O-ROMS with respect to concatenated Argo floats in Equatorial Indian Ocean.

5.3 Conclusion

We see that assimilation improves both the mixed layer depth and the depth of 20 °C isotherm across all the statistical parameters - rmse, correlation and standard deviation. The rmse in all cases, barring one (Fig.5.12), is less than the standard deviation. INCOIS-GODAS looks to be

marginally better in reproducing the MLD whereas LETKF-ROMS outperforms other two systems in reproducing the depth of 20 °C isotherm.

6 Sea Level Anomaly

6.1 Introduction

We validate sea level anomaly (SLA) obtained from LETKF-ROMS, INCOIS-GODAS and O-ROMS with respect to observations from Archiving Validation and Interpretation of Satellite Oceanography (AVISO) Altimetry [23]. There were no data availability of O-ROMS during May 2017. We are interested in validating sea level anomaly and not sea surface height because of the mismatch in the model geoid and satellite derived geoid. It is also to be noted that SLA is an independent variable. No SLA data has been assimilated.

6.2 Comparison with AVISO

We present here the comparison of SLA from LETKF-ROMS, O-ROMS and INCOIS-GODAS with respect to AVISO SLA during the period August 2016 - September 2017. AVISO provides daily-averaged gridded SLA data over a length-scale of about 25 km. The typical error associated with gridded SLA from AVISO is about $4cm$. However, it is to be noted that gridded AVISO SLA removes tidal constituents and all barotropic SLA below 20-day period (Dynamic Atmosphere Correction) using the barotropic model Mog2D [24]. On the contrary, both ROMS and MOM (the ocean engine of INCOIS-GODAS) contain barotropic SLA at all frequencies, i.e., no dynamical atmospheric corrections are made, but does not contain tidal constituents. Also, ROMS exchanges boundary information every day and will therefore smooth out the fast moving barotropic fluctuations at the boundaries, if any. Only when the barotropic SLA in the Indian Ocean is negligible (particularly for periods inferior to 20 days and no significant barotropic wave at the boundaries), ROMS is expected to reproduce gridded AVISO SLA.

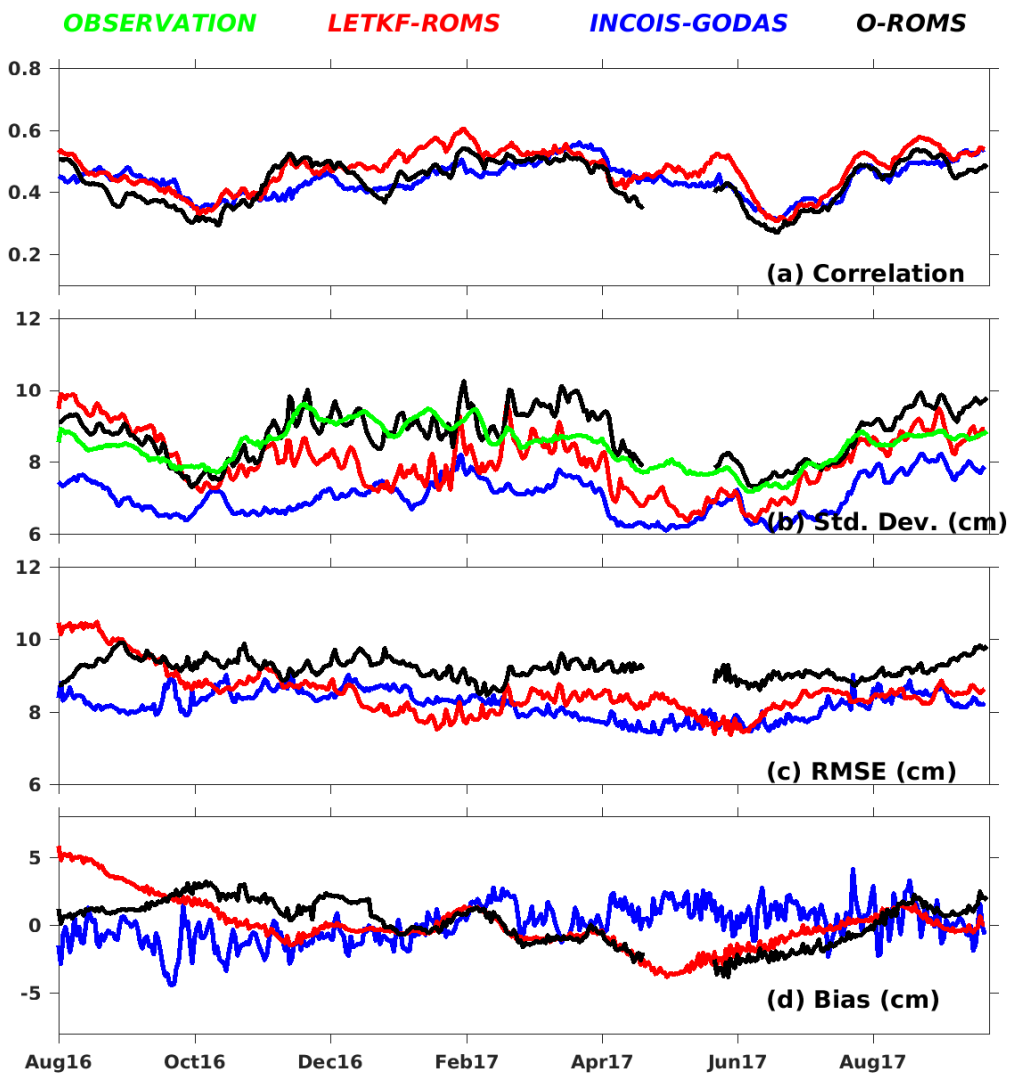

Figure 6.1: (a) Correlation of AVISO SLA with SLA from LETKF-ROMS(red), INCOIS-GODAS (blue) and O-ROMS (black). (b) Standard deviation of SLA from AVISO (green), LETKF-ROMS (red), INCOIS-GODAS (blue) and O-ROMS (black). (c) Rmse of SLA from LETKF-ROMS (red), INCOIS-GODAS (blue) and O-ROMS (black) with respect to SLA from AVISO. (d) Bias of SLA from LETKF-ROMS (red), INCOIS-GODAS (blue) and O-ROMS (black) with respect to SLA from AVISO.

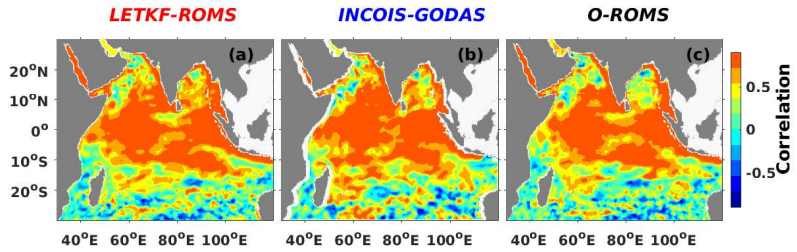

Figure 6.2: Spatial correlation of SLA from AVISO with SLA from (a) LETKF-ROMS, (b) INCOIS-GODAS and (c) O-ROMS. There is a marginal improvement in correlation due to assimilation.

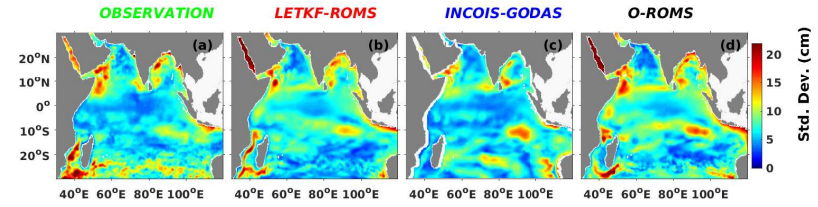

Figure 6.3: Spatial standard deviation of SLA from (a) AVISO, (b) LETKF-ROMS, (c) INCOIS-GODAS and (d) O-ROMS.

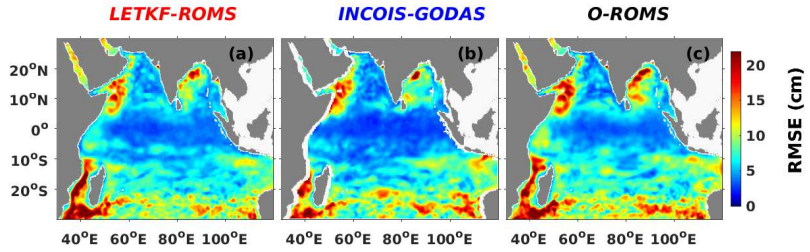

Figure 6.4: Spatial rmse of SLA from AVISO with SLA from (a) LETKF-ROMS, (b) INCOIS-GODAS and (c) O-ROMS. There is an improvement in rmse due to assimilation - particularly in the Bay of Bengal and west coast of Africa.

6.3 Conclusion

We see that there is a notable improvement in the time series of rmse in SLA due to assimilation introduced through LETKF in ROMS. The improvement in global rmse is about $3-5$ cm with respect to O-ROMS (see Fig. 6.1) and it appears that on running the system further, the

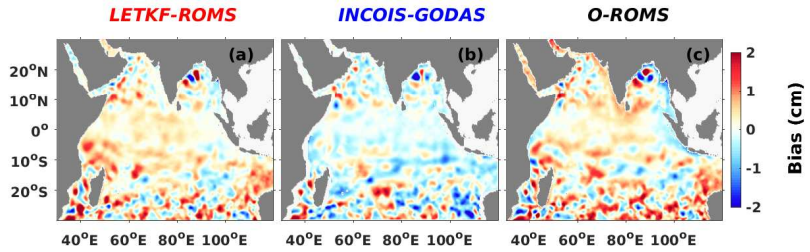

Figure 6.5: Bias of SLA from (a) LETKF-ROMS, (b) INCOIS-GODAS and (c) O-ROMS with respect to AVISO SLA.

improvements may be much better. The correlation also improves marginally and is in the range of about 0.5 - marginally better than O-ROMS. The correlation improve in the western Bay of Bengal (east coast of India) due to assimilation (see Fig.6.2). Spatially, there is a considerable improvement in rmse as seen in Fig.6.4 with respect to O-ROMS. LETKF-ROMS also manages to simulate the variability in SLA better as seen in Fig.6.5 and keeps the rmse smaller than the standard deviation. However, spatial rmse is least in INCOIS-GODAS (Fig.6.4). LETKF-ROMS looks to reproduce the variablity best - particularly along the east coast of India (Fig.6.5). All these results should be seen under the assumption that there is negligible non-tidal barotropic component of SLA in both the regional model SLA. This assumption is questionable because of the large-scale ($> 1000km$) strong wind stress anomalies existing over Indian and Pacific Ocean due to MJO [25] which can potentially trigger barotropic waves. LETKF-ROMS and O-ROMS exchage boundary information with INCOIS-GODAS on a daily scale and hence most of the remote barotric response that originate beyond the Indian Ocean domain will not be captured in either of the ROMS-based system. If these waves significantly modulate SLA, it is not surprising that LETKF-ROMS will tend to underperform even after assimilation.

7 Currents

7.1 Introduction

We look at the performance in simulating ocean currents in LETKF-ROMS and compare it with the assimilation free runs like INCOIS-GODAS and O-ROMS. It is to be remembered that currents were not assimilated and hence are independent variables. We compare the performance against Ocean Surface Current Analysis Real-time (OSCAR) and Acoustic Doppler Current Profilers (ADCP) installed at various locations along the Indian coast (see Fig.1.1). However, it is to be kept in mind that ROMS cannot account for fast moving barotropic waves that enters Indian Ocean through the boundaries - particularly just outside the eastern boundary which is a potential source of barotropic fluctuations produced from baroclinicity [26]. These fluctuations can, in principle, give rise to internal waves upon breaking at the shelf which ROMS will not be able to fully resolve.

We divide the analysis into two sections - for comparison with OSCAR and ADCPs respectively. 5-day OSCAR currents are available at a resolution of about 36 km whereas ADCPs provide in-situ data at a temporal resolution of 30 minutes at shallow regions and 60 minutes at deeper regions. We however used daily averaged ADCP data for comparison at both shallow and deep locations. In Fig. 7.1, we plot the availability of data during the period of our interest.

7.2 Comparison with OSCAR

We validate the performance of LETKF-ROMS against OSCAR currents and compare it with the performance of INCOIS-GODAS and O-ROMS. The model data from all the three systems were projected on to the OSCAR grid and compared.

7.2.1 u current

We first compare the performance of the zonal (u) current.

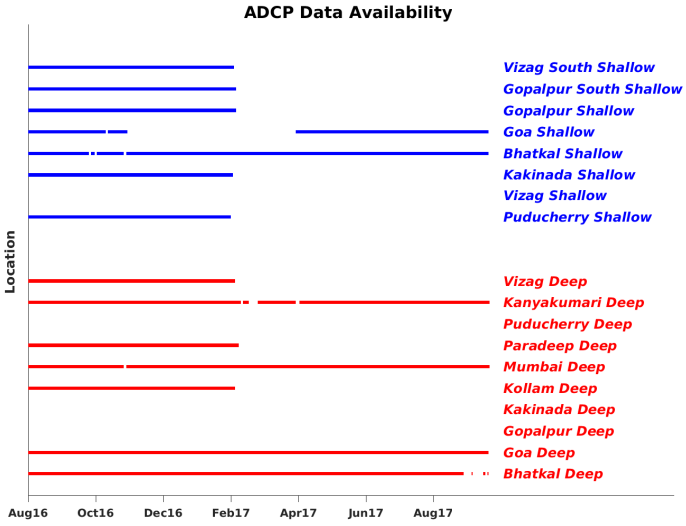

FIGURE 7.1: Availability of ADCP data in the shallow (blue) and the deeper (red) part of the Ocean.

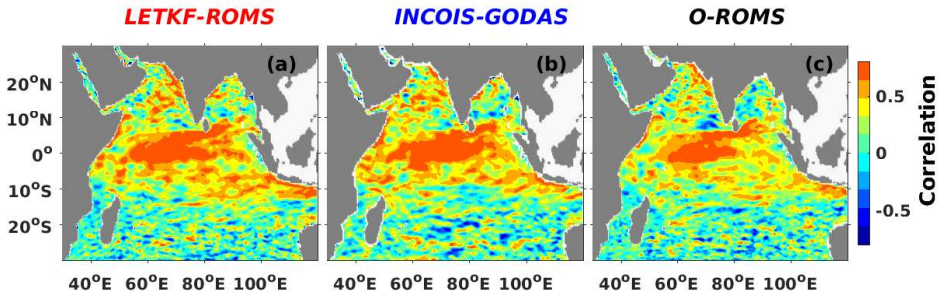

FIGURE 7.2: . Spatial correlation with respect to OSCAR current of u component of the horizontal velocity from (a) LETKF-ROMS, (b) INCOIS-GODAS and (c) O-ROMS.

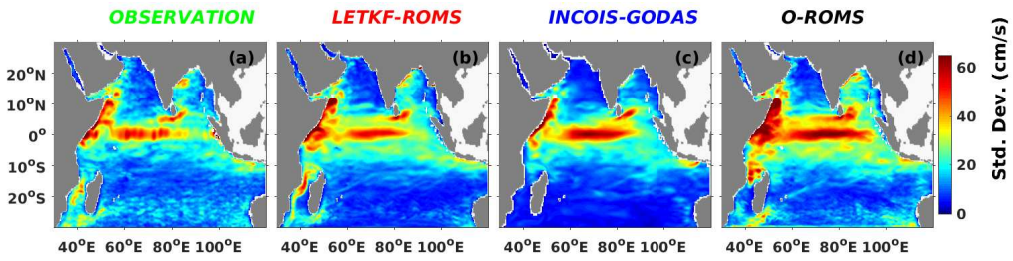

FIGURE 7.3: Spatial plot of standard deviation of u in (a) OSCAR current, (b) LETKF-ROMS, (c) INCOIS-GODAS and (d) O-ROMS.

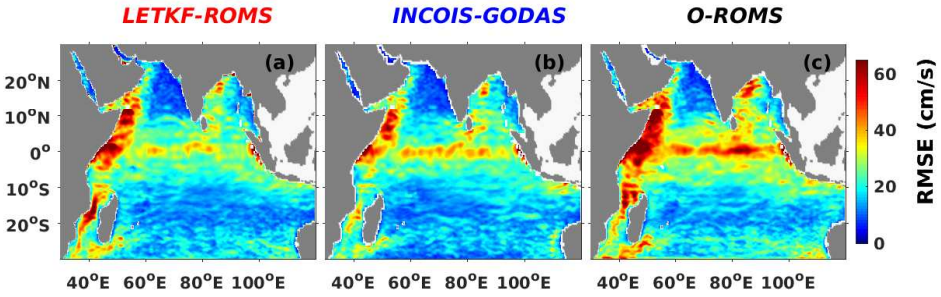

Figure 7.4: . Spatial rmse with respect to OSCAR current of u component of the horizontal velocity from (a) LETKF-ROMS, (b) INCOIS-GODAS and (c) O-ROMS.

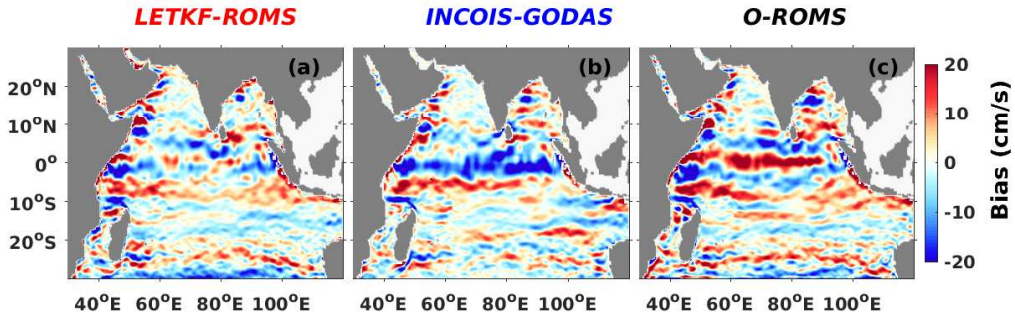

Figure 7.5: . Spatial bias with respect to OSCAR current of u component of the horizontal velocity from (a) LETKF-ROMS, (b) INCOIS-GODAS and (c) O-ROMS.

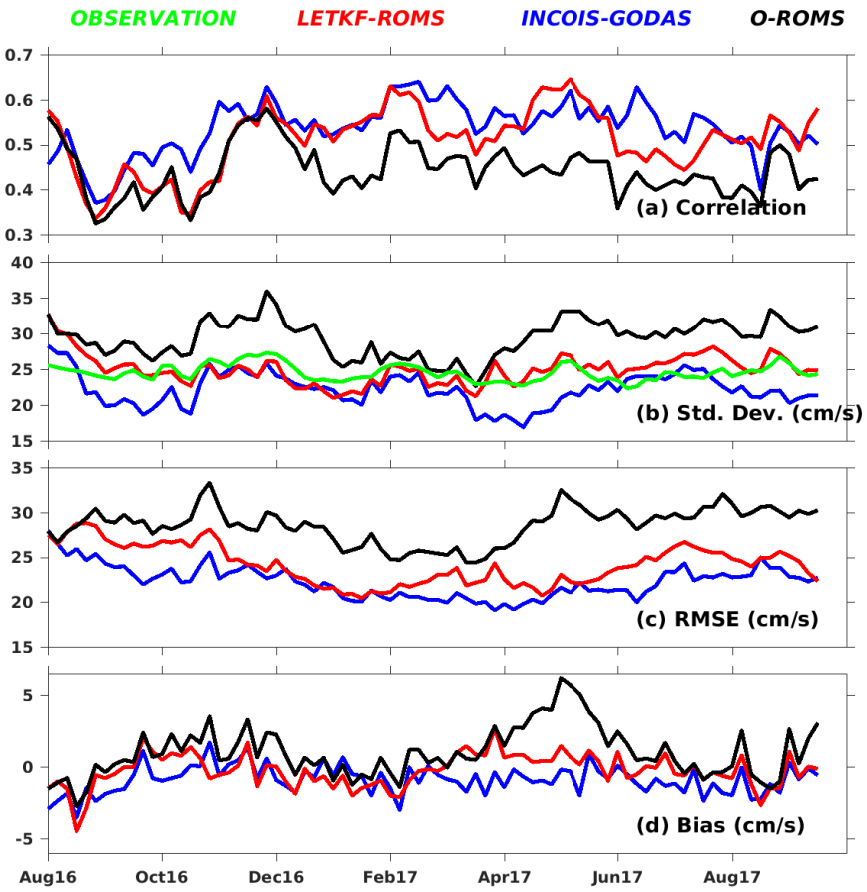

Figure 7.6: Temporal plot of (a) correlation, (b) standard deviation, (c) rmse and (d) bias in u from LETKF-ROMS (red), INCOIS-GODAS (blue) and O-ROMS (black). The standard deviation of u in OSCAR is shown in green.

7.2.2 v current

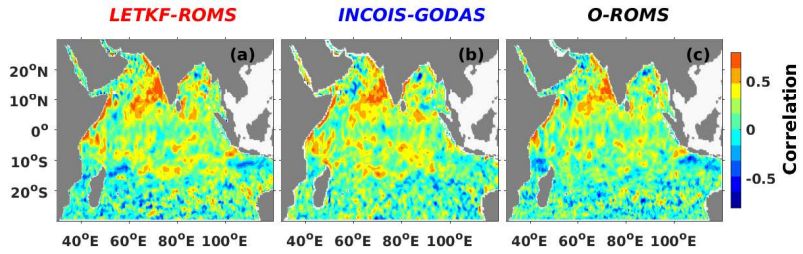

Figure 7.7: . Spatial correlation with respect to OSCAR current of v component of the horizontal velocity from (a) LETKF-ROMS, (b) INCOIS-GODAS and (c) O-ROMS.

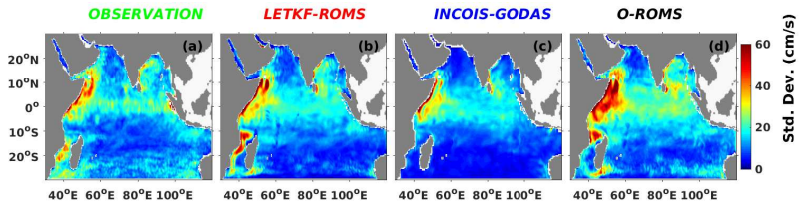

Figure 7.8: Spatial plot of standard deviation of v in (a) OSCAR current, (b) LETKF-ROMS, (c) INCOIS-GODAS and (d) O-ROMS.

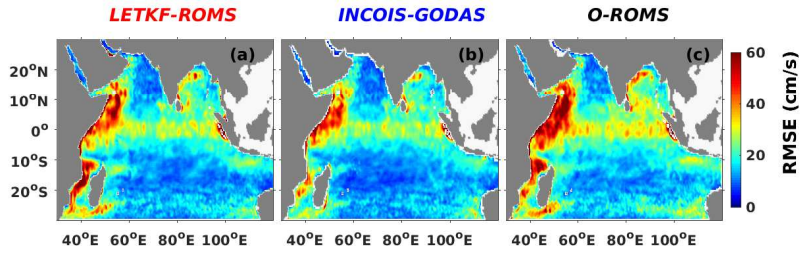

Figure 7.9: . Spatial rmse with respect to OSCAR current of v component of the horizontal velocity from (a) LETKF-ROMS, (b) INCOIS-GODAS and (c) O-ROMS.

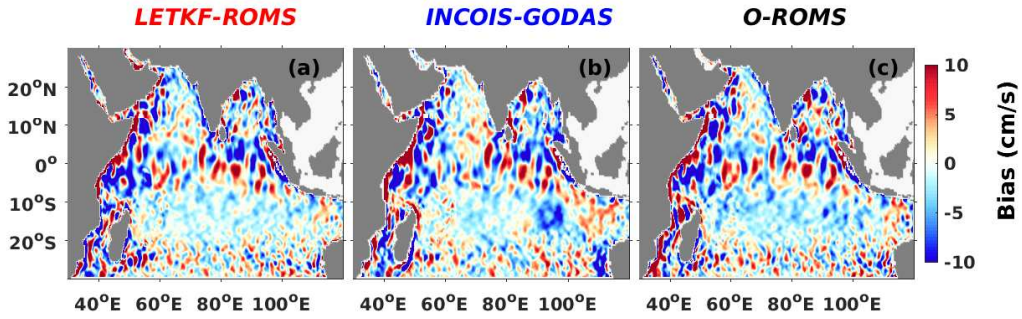

Figure 7.10: . Spatial bias with respect to OSCAR current of v component of the horizontal velocity from (a) LETKF-ROMS, (b) INCOIS-GODAS and (c) O-ROMS.

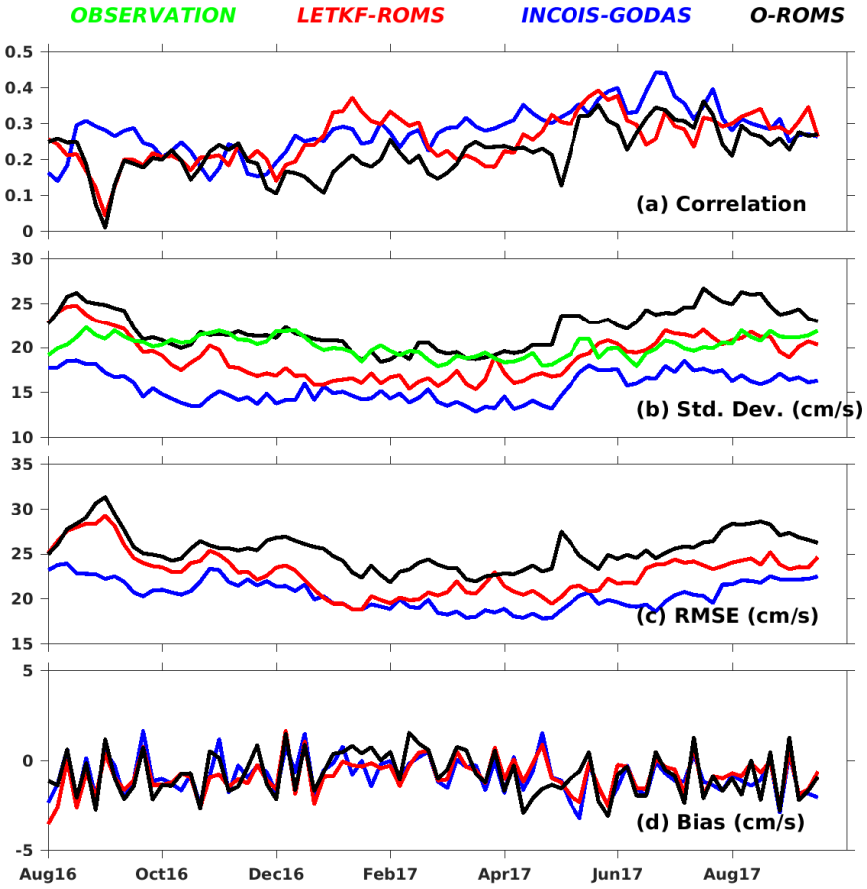

Figure 7.11: Temporal plot of (a) correlation, (b) standard deviation, (c) rmse and (d) bias in v from LETKF-ROMS (red), INCOIS-GODAS (blue) and O-ROMS (black). The standard deviation of v in OSCAR is shown in green.

7.3 Comparison with ADCP

We present here the comparison of horizontal components of current (u and v) from LETKF-ROMS, INCOIS-GODAS and O-ROMS with respect to observations from ADCP during August 2016 - September 2017. We show time-depth section of both u and v and also present statistics.

7.3.1 Deep Ocean

We first consider the comparison with respect to ADCPs located in relatively part of the ocean.

Bhatkal ADCP

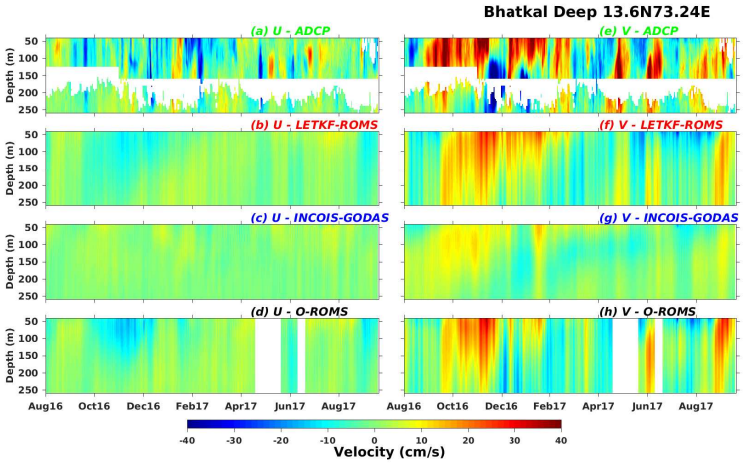

FIGURE 7.12: (a,e) u,v from ADCP (b,f) u,v from LETKF-ROMS. (c,g) u,v from INCOIS-GODAS. (d,h) u,v from O-ROMS at Bhatkal $(13.6°N, 73.24°E)$

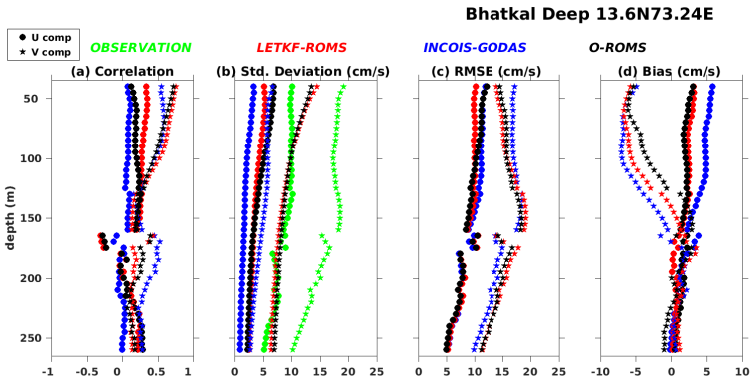

FIGURE 7.13: (a) Correlation of u(solid circle) and v(star) from LETKF-ROMS (red), INCOIS-GODAS(blue) and O-ROMS(black) with ADCP observations at Bhatkal. (b) Standard deviation of u(solid circle) and v(star) in LETKF-ROMS (red), INCOIS-GODAS(blue),O-ROMS(black) and ADCP(green). (c) rmse of u(solid circle) and v(star) from LETKF-ROMS (red), INCOIS-GODAS(blue) and O-ROMS(black) with respect to ADCP observations. (d) bias of u(solid circle) and v(star) from LETKF-ROMS (red), INCOIS-GODAS(blue) and O-ROMS(black) with respect to ADCP observations.

Goa ADCP

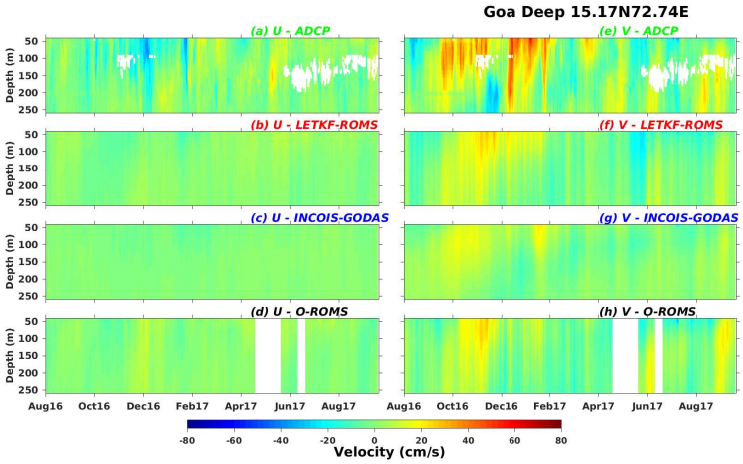

FIGURE 7.14: (a,e) u,v from ADCP (b,f) u,v from LETKF-ROMS. (c,g) u,v from INCOIS-GODAS. (d,h) u,v from O-ROMS at Goa $(15.17°N, 72.74°E)$

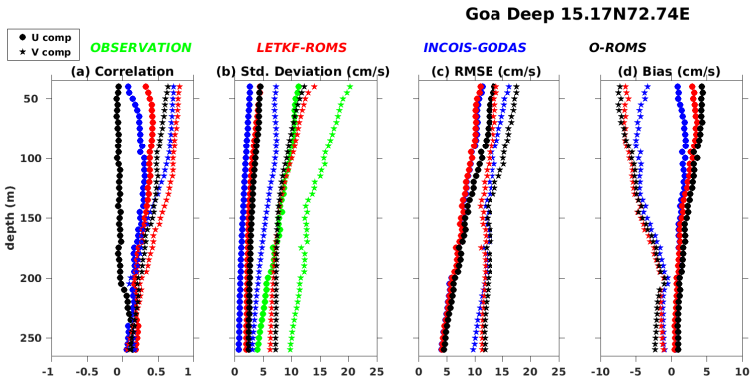

FIGURE 7.15: (a) Correlation of u(solid circle) and v(star) from LETKF-ROMS (red), INCOIS-GODAS(blue) and O-ROMS(black) with ADCP observations at Bhatkal. (b) Standard deviation of u(solid circle) and v(star) in LETKF-ROMS (red), INCOIS-GODAS(blue),O-ROMS(black) and ADCP(green). (c) rmse of u(solid circle) and v(star) from LETKF-ROMS (red), INCOIS-GODAS(blue) and O-ROMS(black) with respect to ADCP observations. (d) bias of u(solid circle) and v(star) from LETKF-ROMS (red), INCOIS-GODAS(blue) and O-ROMS(black) with respect to ADCP observations.

Kakinada ADCP

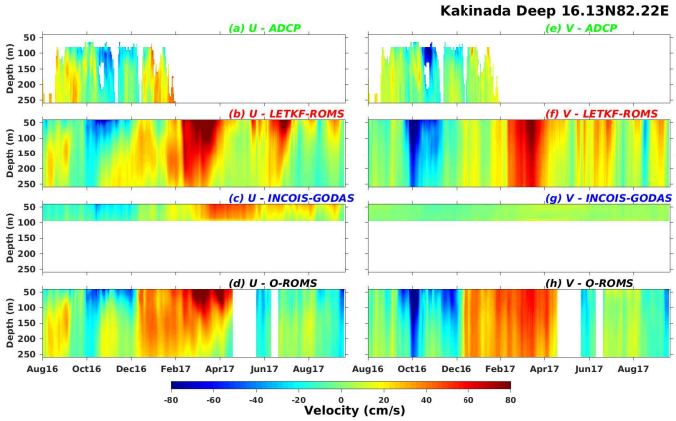

FIGURE 7.16: (a,e) u,v from ADCP (b,f) u,v from LETKF-ROMS. (c,g) u,v from INCOIS-GODAS. (d,h) u,v from O-ROMS at Kakinada $(16.13°N, 82.22°E)$

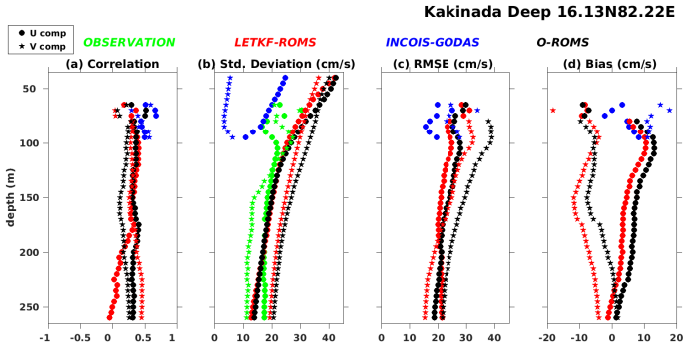

FIGURE 7.17: (a) Correlation of u(solid circle) and v(star) from LETKF-ROMS (red), INCOIS-GODAS(blue) and O-ROMS(black) with ADCP observations at Bhatkal. (b) Standard deviation of u(solid circle) and v(star) in LETKF-ROMS (red), INCOIS-GODAS(blue),O-ROMS(black) and ADCP(green). (c) rmse of u(solid circle) and v(star) from LETKF-ROMS (red), INCOIS-GODAS(blue) and O-ROMS(black) with respect to ADCP observations. (d) bias of u(solid circle) and v(star) from LETKF-ROMS (red), INCOIS-GODAS(blue) and O-ROMS(black) with respect to ADCP observations.

Vizag ADCP

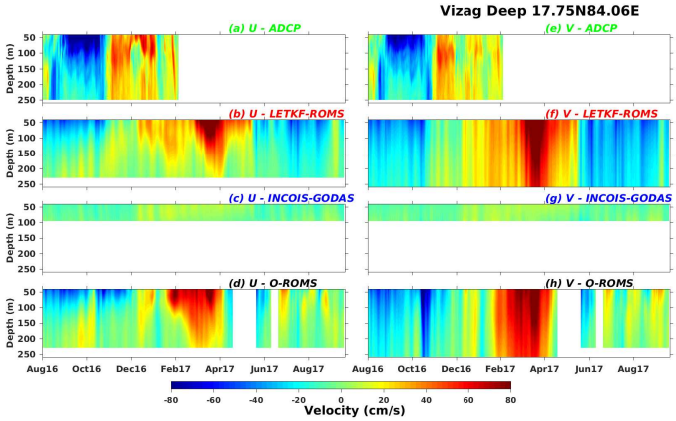

FIGURE 7.18: (a,e) u,v from ADCP (b,f) u,v from LETKF-ROMS. (c,g) u,v from INCOIS-GODAS. (d,h) u,v from O-ROMS at Vizag ($17.75°N, 84.06°E$)

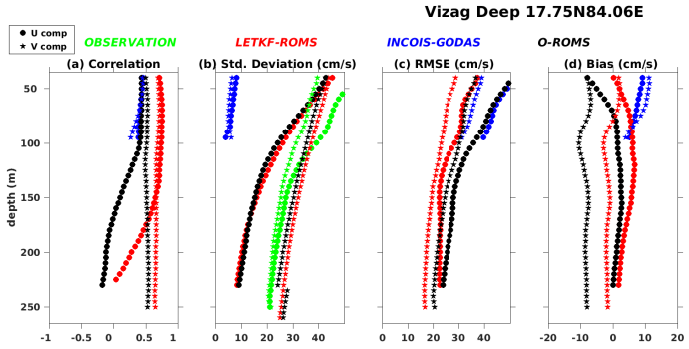

FIGURE 7.19: (a) Correlation of u(solid circle) and v(star) from LETKF-ROMS (red), INCOIS-GODAS(blue) and O-ROMS(black) with ADCP observations at Bhatkal. (b) Standard deviation of u(solid circle) and v(star) in LETKF-ROMS (red), INCOIS-GODAS(blue),O-ROMS(black) and ADCP(green). (c) rmse of u(solid circle) and v(star) from LETKF-ROMS (red), INCOIS-GODAS(blue) and O-ROMS(black) with respect to ADCP observations. (d) bias of u(solid circle) and v(star) from LETKF-ROMS (red), INCOIS-GODAS(blue) and O-ROMS(black) with respect to ADCP observations.

Paradeep ADCP

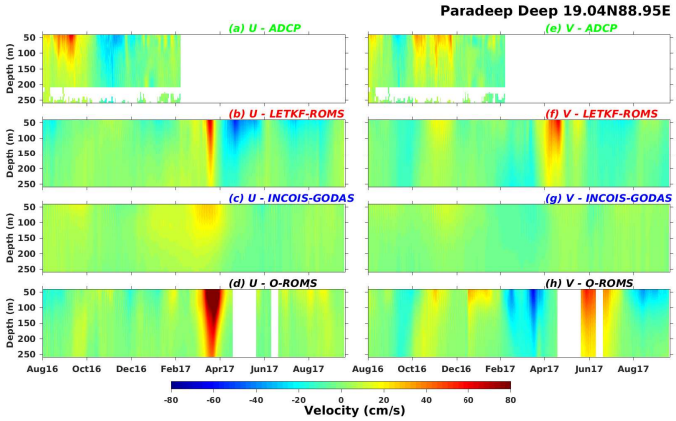

FIGURE 7.20: (a,e) u,v from ADCP (b,f) u,v from LETKF-ROMS. (c,g) u,v from INCOIS-GODAS. (d,h) u,v from O-ROMS at Paradeep $(19.04°N, 88.95°E)$

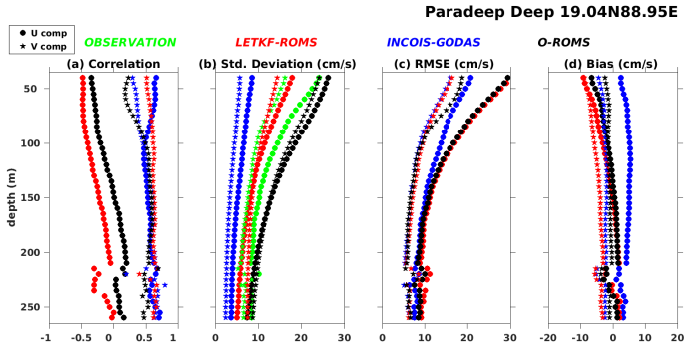

FIGURE 7.21: (a) Correlation of u(solid circle) and v(star) from LETKF-ROMS (red), INCOIS-GODAS(blue) and O-ROMS(black) with ADCP observations at Bhatkal. (b) Standard deviation of u(solid circle) and v(star) in LETKF-ROMS (red), INCOIS-GODAS(blue),O-ROMS(black) and ADCP(green). (c) rmse of u(solid circle) and v(star) from LETKF-ROMS (red), INCOIS-GODAS(blue) and O-ROMS(black) with respect to ADCP observations. (d) bias of u(solid circle) and v(star) from LETKF-ROMS (red), INCOIS-GODAS(blue) and O-ROMS(black) with respect to ADCP observations.

Mumbai ADCP

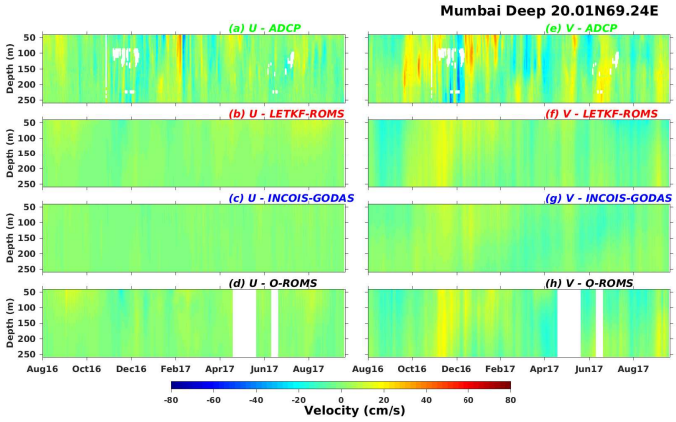

FIGURE 7.22: (a,e) u,v from ADCP (b,f) u,v from LETKF-ROMS. (c,g) u,v from INCOIS-GODAS. (d,h) u,v from O-ROMS at Mumbai $(20.01°N, 69.24°E)$

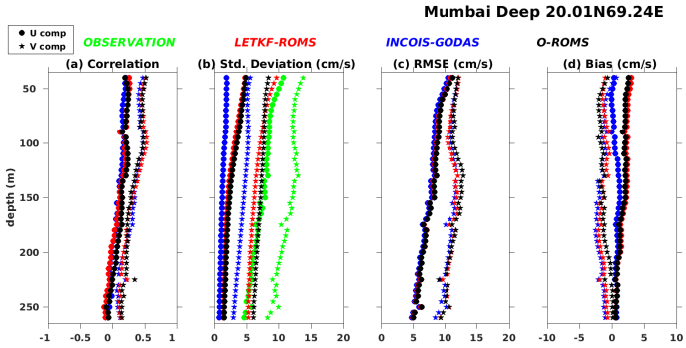

FIGURE 7.23: (a) Correlation of u(solid circle) and v(star) from LETKF-ROMS (red), INCOIS-GODAS(blue) and O-ROMS(black) with ADCP observations at Bhatkal. (b) Standard deviation of u(solid circle) and v(star) in LETKF-ROMS (red), INCOIS-GODAS(blue),O-ROMS(black) and ADCP(green). (c) rmse of u(solid circle) and v(star) from LETKF-ROMS (red), INCOIS-GODAS(blue) and O-ROMS(black) with respect to ADCP observations. (d) bias of u(solid circle) and v(star) from LETKF-ROMS (red), INCOIS-GODAS(blue) and O-ROMS(black) with respect to ADCP observations.

Kanyamumari ADCP

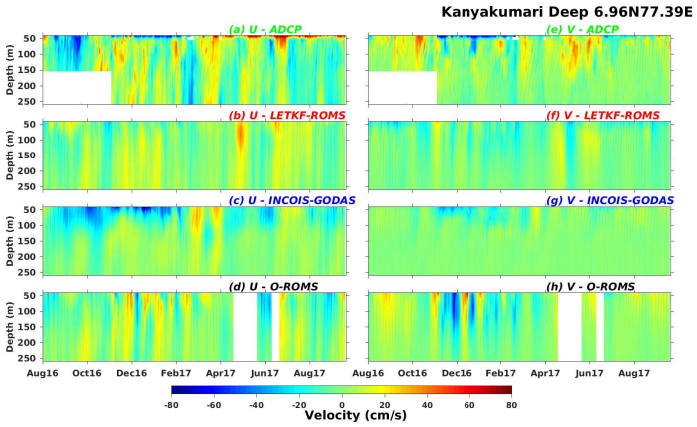

FIGURE 7.24: (a,e) u,v from ADCP (b,f) u,v from LETKF-ROMS. (c,g) u,v from INCOIS-GODAS. (d,h) u,v from O-ROMS at Kanyakumari $(6.96°N, 77.39°E)$

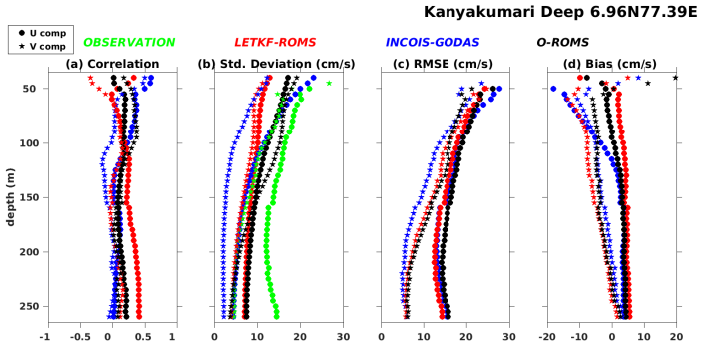

FIGURE 7.25: (a) Correlation of u(solid circle) and v(star) from LETKF-ROMS (red), INCOIS-GODAS(blue) and O-ROMS(black) with ADCP observations at Bhatkal. (b) Standard deviation of u(solid circle) and v(star) in LETKF-ROMS (red), INCOIS-GODAS(blue),O-ROMS(black) and ADCP(green). (c) rmse of u(solid circle) and v(star) from LETKF-ROMS (red), INCOIS-GODAS(blue) and O-ROMS(black) with respect to ADCP observations. (d) bias of u(solid circle) and v(star) from LETKF-ROMS (red), INCOIS-GODAS(blue) and O-ROMS(black) with respect to ADCP observations.

Kollam ADCP

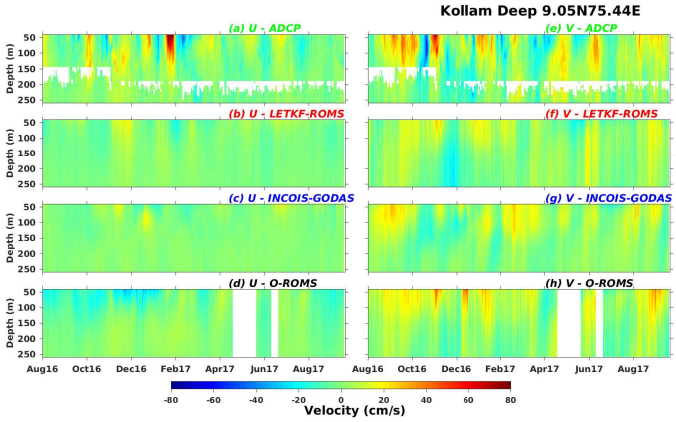

FIGURE 7.26: (a,e) u,v from ADCP (b,f) u,v from LETKF-ROMS. (c,g) u,v from INCOIS-GODAS. (d,h) u,v from O-ROMS at Kollam $(9.05°N, 75.44°E)$

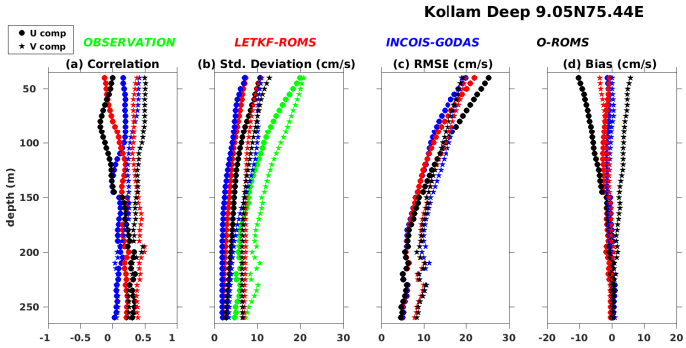

FIGURE 7.27: (a) Correlation of u(solid circle) and v(star) from LETKF-ROMS (red), INCOIS-GODAS(blue) and O-ROMS(black) with ADCP observations at Bhatkal. (b) Standard deviation of u(solid circle) and v(star) in LETKF-ROMS (red), INCOIS-GODAS(blue),O-ROMS(black) and ADCP(green). (c) rmse of u(solid circle) and v(star) from LETKF-ROMS (red), INCOIS-GODAS(blue) and O-ROMS(black) with respect to ADCP observations. (d) bias of u(solid circle) and v(star) from LETKF-ROMS (red), INCOIS-GODAS(blue) and O-ROMS(black) with respect to ADCP observations.

7.3.2 Shallow Ocean

We now consider the performance of LETKF-ROMS, INCOIS-GODAS and O-ROMS in the shallow ocean.

Bhatkal ADCP

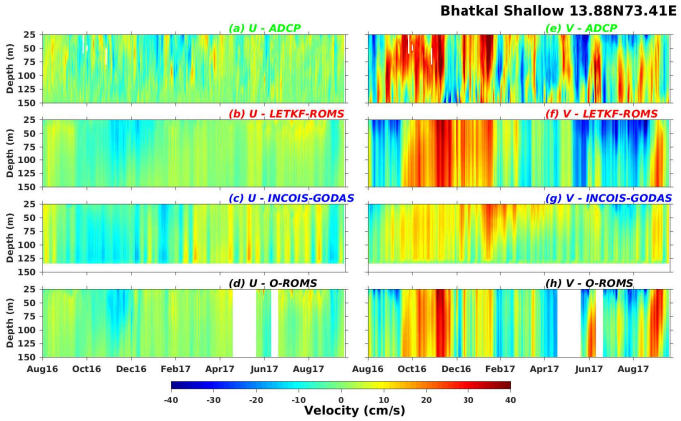

FIGURE 7.28: (a,e) u,v from ADCP (b,f) u,v from LETKF-ROMS. (c,g) u,v from INCOIS-GODAS. (d,h) u,v from O-ROMS at Bhatkal $(13.88°N, 73.41°E)$

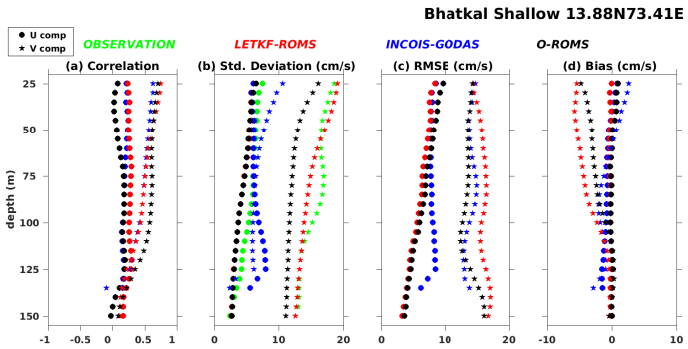

FIGURE 7.29: (a) Correlation of u(solid circle) and v(star) from LETKF-ROMS (red), INCOIS-GODAS(blue) and O-ROMS(black) with ADCP observations at Bhatkal. (b) Standard deviation of u(solid circle) and v(star) in LETKF-ROMS (red), INCOIS-GODAS(blue),O-ROMS(black) and ADCP(green). (c) rmse of u(solid circle) and v(star) from LETKF-ROMS (red), INCOIS-GODAS(blue) and O-ROMS(black) with respect to ADCP observations. (d) bias of u(solid circle) and v(star) from LETKF-ROMS (red), INCOIS-GODAS(blue) and O-ROMS(black) with respect to ADCP observations.

Goa ADCP

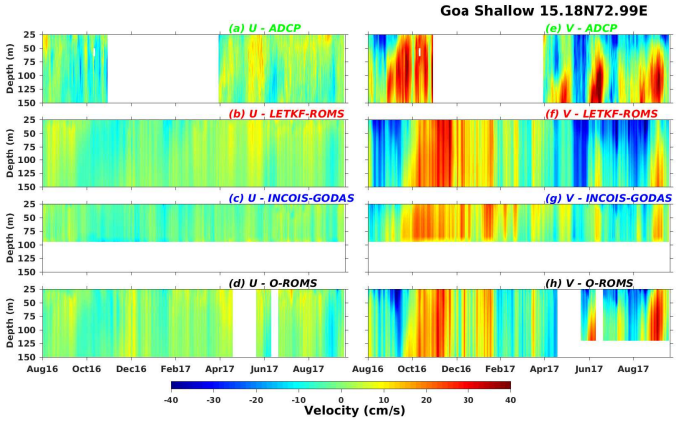

Figure 7.30: (a,e) u,v from ADCP (b,f) u,v from LETKF-ROMS. (c,g) u,v from INCOIS-GODAS. (d,h) u,v from O-ROMS at Goa $(17.06^{\circ}N, 83.06^{\circ}E)$

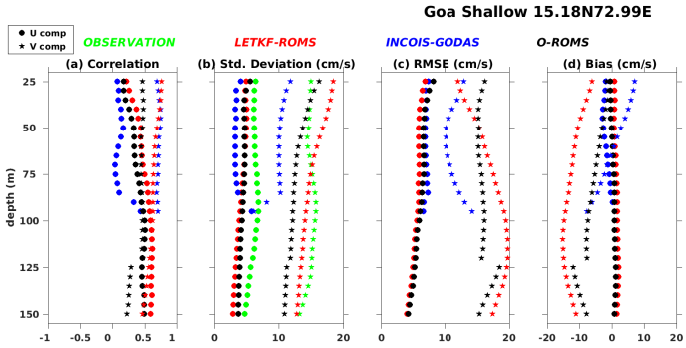

Figure 7.31: (a) Correlation of u(solid circle) and v(star) from LETKF-ROMS (red), INCOIS-GODAS(blue) and O-ROMS(black) with ADCP observations at Bhatkal. (b) Stardard deviation of u(solid circle) and v(star) in LETKF-ROMS (red), INCOIS-GODAS(blue),O-ROMS(black) and ADCP(green). (c) rmse of u(solid circle) and v(star) from LETKF-ROMS (red), INCOIS-GODAS(blue) and O-ROMS(black) with respect to ADCP observations. (d) bias of u(solid circle) and v(star) from LETKF-ROMS (red), INCOIS-GODAS(blue) and O-ROMS(black) with respect to ADCP observations.

Vizag ADCP

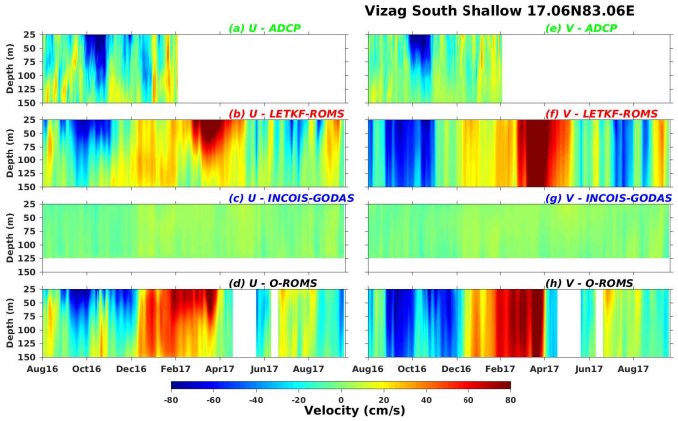

Figure 7.32: (a,e) u,v from ADCP (b,f) u,v from LETKF-ROMS. (c,g) u,v from INCOIS-GODAS. (d,h) u,v from O-ROMS at Kakinada ($18.59°N, 84.87°E$)

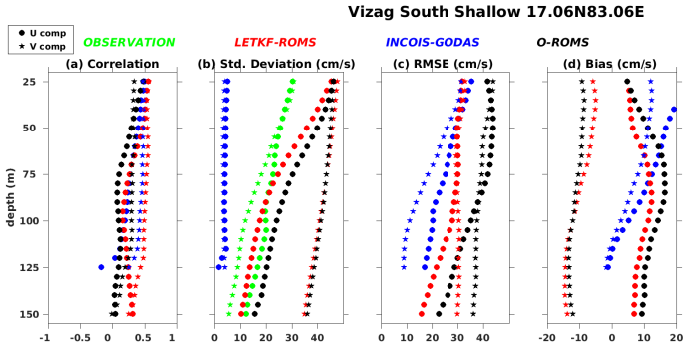

Figure 7.33: (a) Correlation of u(solid circle) and v(star) from LETKF-ROMS (red), INCOIS-GODAS(blue) and O-ROMS(black) with ADCP observations at Bhatkal. (b) Stardard deviation of u(solid circle) and v(star) in LETKF-ROMS (red), INCOIS-GODAS(blue),O-ROMS(black) and ADCP(green). (c) rmse of u(solid circle) and v(star) from LETKF-ROMS (red), INCOIS-GODAS(blue) and O-ROMS(black) with respect to ADCP observations. (d) bias of u(solid circle) and v(star) from LETKF-ROMS (red), INCOIS-GODAS(blue) and O-ROMS(black) with respect to ADCP observations.

7.4 Conclusion

We see a staggering improvement in estimating the components of horizontal velocity u and v in LETKF-ROMS over the present O-ROMS in the top layers of the ocean in most of the locations.

The improvements are as much as 8 cm/s in the u-component (Fig.7.6) and $2-3$ cm/s in the v-component (Fig.7.11) globally. LETKF-ROMS is better than INCOIS-GODAS in reproducing the equatorial current (Fig.7.4). However, INCOIS-GODAS shows less rmse in u-component of the current than either of the other two systems in the western coast of Africa. The bias observed in zonal current with respect to OSCAR is least in LETKF-ROMS (Fig.7.5). LETKF-ROMS manages to reproduce the global variability in the zonal current (Fig.7.6). Assimilation improves the correlation with currents obtained from ADCP and decreases the rmse. All these ADCPs are close to the coast (Fig. 1.1) that warrants large variability and hence large uncertainty. It should be kept in mind that INCOIS-GODAS has a much lower resolution compared to LETKF-ROMS and hence is expected to simulate coarser features of the current as is evident from its performance in Fig.7.6 and Fig.7.11. There are multiple locations where LETKF-ROMS is outperforming the other two systems in reproducing the currents - zonal component in particular. Any improvement in currents will aid in improving the search and rescue (SARAT) operations advised by INCOIS wherein currents are averaged over the top 15 m and fed into the SARAT system.

8 Discussion & Summary

We have developed an assimilation method, Local Ensemble Transform Kalman Filter (LETKF) that is interfaced (offline) with a similar set-up of present operational ROMS. This system assimilates all available in-situ temperatures and salinity profiles from RAMA moorings, NIOT buoys and Argo floats. It also assimilates satellite track (level 2) data of SST from AMSR-E. This report showcases results obtained for a 80 member system during the period Aug 2016 - Sep 2017. It is to be mentioned that the initial ensemble provided to the system is obtained from a perturbation of the initial condition from operational ROMS. The perturbations were along the growing modes of the model subjected to a different ensemble fluxes (NCEP) and hence is an approximate. The system is forced with 6-hourly ensemble fluxes provided by NCMRWF. Whenever there has been a gap in forcing, it has been interpolated to the previous nearest available fluxes. The system also uses Representation Error derived from a high resolution model. This representation error has spatio-temporal variabilities. Besides the ensemble atmospheric fluxes, a spread in the model state parameters like tracer diffusion coefficients and viscosity coefficient and a mix of vertical mixing scheme along with a 10% inflation ensures a stable model ensemble spread. A horizontal localization radius of 200 km keeps at bay remote spurious correlations due to assimilation. The observations are assimilated every 5 days.

We have compared the performance of our system, LETKF-ROMS, with the performance of two other systems - the high resolution operational set-up in INCOIS, O-ROMS and the coarser resolution global set-up INCOIS-GODAS which also assimilates temperature and salinity profiles. We have compared against the assimilated observations (dependent) and independent observations that includes SLA from AVISO and currents from ADCP and OSCAR. We have also compared the performance of LETKF-ROMS in estimating diagnostic variables like mixed layer depth and the 20° isotherm. It is to be noted that the daily ocean state obtained from LETKF-ROMS comprises of 4 days of unassimilated state and one day of assimilated state (analysis).

We have seen a significant improvement in SST from LETKF-ROMS in comparison to O-ROMS. The system-wide rmse in LETKF-ROMS is less than O-ROMS by about $0.2^\circ - 0.4^\circ$ C and the rmse averaged over the entire basin is always below 1° C. The average bias has been brought down to about 0.6° C from 0.8° C in O-ROMS. LETKF improves the basin-wide average

correlation and the correlation is very stable at more than 0.95. When compared against SST values obtained from in-situ measurements, LETKF-ROMS performs better than O-ROMS at all locations except at those moorings positioned in and around 67° E. The reason is still elusive and needs to be ascertained. The best system in reproducing SST is clearly INCOIS-GODAS. But it should be noted that SST is strongly relaxed to Reynolds SST (5-day relaxation time) in INCOIS-GODAS. This has its own potential hazard. Once the relaxation is turned off - as has to be done for forecasts - the system likely drifts away from reality in absence of any relaxation.

We see a notable improvement in the vertical temperature profile after assimilation at most of the locations. We have compared the performance against all RAMA and NIOT moorings which had a data availability of more than 50% during the period of our interest. We see that LETKF-ROMS is at par with or better than O-ROMS at most of the places. It improves the correlation vertically and decreases the rmse. When compared against Argo floats, we see a striking improvement in Arabian Sea, Bay of Bengal and Equatorial Indian Ocean - particularly up to $30 - 40$ m. The correlation is about 0.8 in the top layers and the rmse is less that 0.4° C. However, the features obtained from LETKF-ROMS are smooth compared to what we get in O-ROMS or INCOIS-GODAS. This is because the averaging of ensemble members smooths out the sharp features. In salinity, we see a significant improvement in Bay of Bengal due to assimilation when compared with Argo floats. This improvement extends up to 200 m in depth in both correlation, rmse and standard deviation. However, in majority of the locations, INCOIS-GODAS is best in reproducing most of the vertical temperature profile whereas LETKF-ROMS is better than the other two in simulating most of the salinity profiles. It should be kept in mind that SSS is relaxed to monthly SSS climatology in O-ROMS and LETKF-ROMS (30 day relaxation time).

We have also compared the performance of LETKF-ROMS in deriving salient diagnostic terms like mixed layer depth and 20° C isotherms. We have validated it against derived mld and D20 from multiple in-situ observations through Taylor Diagrams that estimates rmse, correlation and standard deviation. Time-series of these quantities were too noisy to be illustrated. We see that in most of the cases, there has been an improvement in estimating these quantities upon assimilation. It improves the mld and D20 by $5 - 10$ m at most of the location which is significant. The rmse has always been less than the standard deviation barring at one location (4° N, 90°E; Fig.5.12). INCOIS-GODAS reproduces better MLD at most of the locations whereas LETKF-ROMS is better at reproducing the depth of 20 degree isotherm (less rmse) at most of the locations.

The comparison of LETKF-ROMS, O-ROMS and INCOIS-GODAS with satellite observed AVISO daily gridded SLA (independent variable) is tricky. Whereas AVISO removes all barotropic

component of SLA inferior to 20-day period, there is no such filtering in either ROMS or MOM. The comparison makes sense only when the barotropic component of SLA (below 20-day period) is insignificant in the Indian Ocean. Also, there may be significant barotropic SLA in the Indian Ocean triggered from regions outside the operational domain ($30°E-120°E; 30°N-30°S$). Both O-ROMS and the ocean engine of LETKF-ROMS exchange information with INCOIS-GODAS at the boundaries on a daily scale and will therefore underestimate these barotropic SLA, if any, produced by fast moving barotropic waves that can traverse thousands of kilometers in hours. The presence of large-scale atmospheric fluctuations over tropical Oceans (MJO) can potentially trigger these barotropic waves which will remain a concern for regional models unless boundary exchanges are done more frequently. All the comparison with SLA should therefore be seen through a lens of speculation. We see a basin-wide averaged reduction in rmse by $4-5$ cm which, to be noted, is in the range of 4 cm error reported by AVISO. The correlation is higher than O-ROMS marginally. The spatial plot of RMSE from LETKF-ROMS shows improvement along the eastern coast of India compared to O-ROMS. Among all the three systems, LETKF-ROMS is best among the three systems in reproducing the variability.

The most striking improvements are in the currents due to assimilation. The basin-wide averaged rmse in u-current is brought down by 5 cm/s from 30 cm/s in O-ROMS. The correlation is about 0.5 compared to 0.4 in O-ROMS whereas the standard deviation is close to the standard deviation in u current in OSCAR. We see a better representation of u and v current in the eastern coast of India and the equatorial belt of the Indian Ocean. We see an identical improvement in v current as well when compared to OSCAR. We see a similar improvement when compared to ADCPs installed along the coast in India. The currents after assimilation show an improved correlation and a reduction in rmse. Even though the influence of assimilated observations does not reach the shallow ADCPS because of the 200 km localization radius, there are improvements in currents in shallow regions as well through multi-variate dynamical correlation.

We have extensively compared the performance of all the three systems against various kinds of observations. In Fig.8.1, we have tried to come up with an overview of statistics offered by Taylor diagrams from in-situ measurements in RAMA, NIOT buoys and ADCPs. We have compared in this table the performance of all the three systems with regard to SST, SSS, MLD, D20 and the currents. The first column shows the variable name and the number in parenthesis indicate the number of in-situ locations where performance of LETKF-ROMS, INCOIS-GODAS and O-ROMS is compared with the respective observations at those locations. For ex, there were 25 moored observations against which all the three systems were compared using Taylor diagrams that estimates statistics of rmse, correlation coefficient and standard deviation of SST and SSS. The SST row indicates that LETKF-ROMS outperforms INCOIS-GODAS at 11 locations (out of

25) in terms of rmse whereas INCOIS-GODAS outperforms LETKF-ROMS at 12 locations - one more than LETKF-ROMS. O-ROMS, in comparison, is better than the other two systems at only 2 locations in terms of rmse. Similarly, in terms of correlation, INCOIS-GODAS is better correlated with the observation at 12 locations in comparison to 11 locations in LETKF-ROMS and 2 locations in O-ROMS. Also INCOIS-GODAS manages to reproduce the standard deviation at 14 locations; better than the other two systems. Clearly, INCOIS-GODAS outperforms the other two systems in reproducing the SST and this is indicated at the last column of the table under the heading "verdict". Similarly, LETKF-ROMS outperforms the other two systems in reproducing the surface zonal current at both the shelf (shallow) and slope regions (deep); although this statistics is over a very limited sample size. Both LETKF-ROMS and INCOIS-GODAS is doing equally good in reproducing the surface meridional component of the current at the continental shelf - INCOIS-GODAS has less rmse whereas LETKF-ROMS is better correlated. Same is true for D20. In both these cases, we have refrained from coming up with a verdict.

Variable [No. of obs]	Letkf Roms			Godas			O-Roms			Verdict
	RMSE	CORR	STD	RMSE	CORR	STD	RMSE	CORR	STD	
SST [25]	11	11	9	**12**	**12**	**14**	2	2	2	**GODAS**
SSS [25]	**9**	**12**	10	**9**	7	**11**	7	5	4	**LETKF**
MLD [24]	10	10	**11**	**11**	**11**	5	3	3	8	**GODAS**
D20 [24]	**12**	9	**11**	11	**12**	9	1	3	4	
U(Deep) [7]	**4**	**4**	2	3	3	1			**4**	**LETKF**
V(Deep) [7]	**3**	**4**	**4**	2	1		2	2	3	**LETKF**
U(Shallow)[6]	**3**	**4**	2	1		2	2	2	2	**LETKF**
V(Shallow)[6]	1	**4**	2	**4**		2	1	2	2	

FIGURE 8.1: Comparison of the performance from only in-situ observation networkds of LETKF-ROMS, INCOIS-GODAS and O-ROMS from the Taylor diagrams for SST, SSS, MLD, D20 and the surface zonal and meridional currents. The red line demarcates the three systems - LETKF-ROMS, INCOIS-GODAS and O-ROMS.

Overall, LETKF-ROMS assimilation system significantly improves the ocean state analysis over

the present O-ROMS. Also the in-house developed LETKF-ROMS is as good as INCOIS-GODAS if not better even though the ensemble members were subjected to inaccurate initial conditions. The only drawback is that it consumes more computational resources, but within limits, than presently required. With 256 processors (for system specifications, see [27]), assimilation of observations ($\sim 10^4$ observations; see Fig.1.6) takes around 2 minutes in a 80 member ensemble.

References

[1] Song, Y. and D. B. Haidvogel, *A semi-implicit ocean circulation model using a generalized topography-following coordinate system*, J. Comp. Phys., 115 (1), 228-244 (1994).

[2] Haidvogel, D. B. and A. Beckmann, *Numerical Ocean Circulation Modeling. Series on Environmental Science and Management* Vol. **2**, Imperial College Press, 319 pp (2004).

[3] Haidvogel, D. B., H. G. Arango, K. Hedstrom, A. Beckmann, P. Malanotte-Rizzoli, and A. F. Shchepetkin, *Model evaluation experiments in the North Atlantic Basin: Simulations in nonlinear terrain-following coordinates*, Dyn. Atmos. Oceans, **32**, 239-281 (2000).

[4] Shchepetkin, A. F., and J. C. McWilliams *The Regional Ocean Modeling System: A split-explicit, free-surface, topography following coordinates ocean model*, Ocean Modelling, **9**, 347-404 (2005).

[5] P.A. Francis *et al*, *The Indian Ocean Forecast Syatem*, Current Science, **104**, 1354-1368 (2013).

[6] Hunt, Brian R., Eric J. Kostelich, and Istvan Szunyogh. **Efficient data assimilation for spatiotemporal chaos: A local ensemble transform Kalman filter.** Physica D: Nonlinear Phenomena **230(1-2)** 112-126. (2007)

[7] Penny, S. G., *Data assimilation of the Global Ocean using the 4D-local ensemble transform Kalman filter (4D-LETKF) and the Modular Ocean Model (MOM2).* Ph.D. dissertation, University of Maryland, 141 pp. [Available online at http://hdl.handle.net/1903/11716.] (2011).

[8] Etherton, B.J. and Bishop, C.H. *Resilience of hybrid ensemble/3DVAR analysis schemes to model error and ensemble covariance error.* Monthly weather review, **132(5)**, pp.1065-1080 (2004).

[9] M.J. Martin, M. Balmaseda, L. Bertino, P. Brasseur, G. Brassington, J. Cummings, Y. Fujii, D.J. Lea, J.-M. Lellouche, K. Mogensen, P.R. Oke, G.C. Smith, C.-E. Testut,

G.A. Waagb, J. Waters & A.T. Weaver. *Status and future of data assimilation in operational oceanography*, Journal of Operational Oceanography, **8**, (2015):sup1, s28-s48, DOI: 10.1080/1755876X.2015.1022055

[10] Sivareddy, S. A study on global ocean analysis from an ocean data assimilation system and its sensitivity to observations and forcing fields, Ph.D. thesis, Andhra University. Available at http://www.incois.gov.in/documents/PhDThesis_Sivareddy.pdf. (2015).

[11] Large, W. G., J. C. McWilliams, and S. C. Doney, *Oceanic vertical mixing: a review and a model with a nonlocal boundary layer parameterization*, Rev. Geophys., **32**, 363-403 (1994).

[12] Muschinski, Andreas. *A similarity theory of locally homogeneous and isotropic turbulence generated by a Smagorinsky-type LES*, Journal of Fluid Mechanics **325**, 239-260, (1996).

[13] Fairall, C. W., E. F. Bradley, D. P. Rogers, J. B. Edson and G. S. Young, *Bulk parameterization of air-sea fluxes for tropical ocean-global atmosphere Coupled-Ocean Atmosphere Response Experiment*, J. Geophys. Res., **101**, 3747-3764, (1996).

[14] Griffies, S.M. and R.W. Hallberg, *Biharmonic friction with a Smagorinsky-like viscosity for use in large-scale eddy-permitting ocean models,* Monthly Weather Rev., **128**, 8, 2935–2946 (2000) http://www.msm.cam.ac.uk/phase-trans/2000/C9/lectures45.pdf; http://cml.postech.ac.kr/2008/Steel_Microstructure/SM2.html

[15] Levitus, Sydney, et al. "World ocean atlas 2009." (2002)

[16] Levitus, Sydney, et al. *Global ocean heat content 19552008 in light of recently revealed instrumentation problems.* Geophysical Research Letters, **36**, 7, (2009).

[17] Fu, W. *On the Role of Temperature and Salinity Data Assimilation to Constrain a Coupled PhysicalBiogeochemical Model in the Baltic Sea*. J. Phys. Oceanogr., **46**, 713729, (2016). https://doi.org/10.1175/JPO-D-15-0027.1

[18] Ott, E., Hunt, B. R., Szunyogh, I., Zimin, A. V., Kostelich, E. J., Corazza, M., Yorke, J. A. *A local ensemble Kalman filter for atmospheric data assimilation.* Tellus A, **56(5)**, 415-428 (2004).

[19] Bishop, Craig H., Brian J. Etherton, and Sharanya J. Majumdar. *Adaptive sampling with the ensemble transform Kalman filter. Part I: Theoretical aspects.* Monthly weather review **129(3)**, 420-436, (2001).

[20] Mellor, G. L. and T. Yamada, *Developement of a turbulence closure model for geophysical fluid problems*. Rev. Geophys. Space Phys., **20**, 851-875. (1982).

[21] Kwon et al. *Effect of model error representation in the Yellow and East china sea modeling system based on the ensemble Kalman Filter*. Ocean Dynamics, **66**, 263-283. (2016).

[22] Luc Vandenbulcke & Alexander Barth. *A stochastic operational forecasting system of the Black Sea: Technique and validation*. Ocean Modelling, **93**, 7-21 (2015).

[23] The Ssalto/Duacs altimeter products were produced and distributed by the Copernicus Marine and Environment Monitoring Service (CMEMS) (http://www.marine.copernicus.eu).

[24] Dynamic atmospheric Corrections are produced by CLS Space Oceanography Division using the Mog2D model from Legos and distributed by Aviso, with support from Cnes (http://www.aviso.altimetry.fr/).

[25] Marshall, A. G. and Hendon, H. H. *Impacts of the MJO in the Indian Ocean and on the Western Australian coast*. Clim. Dyn. 42, 579-595 (2014).

[26] Piecuch, C.G. et al., *Vertical structure of ocean pressure variations with application to satellite-gravimetric observations*. Journal of Atmospheric and Oceanic Technology, **32(3)**, pp.603613 (2015).

[27] http://adityahpc.tropmet.res.in/Aaditya/Aaditya 800TF HPC system.html